How does the formation of a gel influence the dissolution of high molar mass polymers ?

Pauline Valois

THESE DE DOCTORAT DE
L'UNIVERSITE PIERRE ET MARIE CURIE

Spécialité

Physico-Chimie des Polymères
(Ecole doctorale de Physique et de Chimie des matériaux)

Présentée par

Pauline Valois

Pour obtenir le grade de

DOCTEUR de l'UNIVERSITÉ PIERRE ET MARIE CURIE

Sujet de la thèse :

Comment la formation d'un gel affecte-t-elle la dissolution des polymères de grande masse molaire ?

(How does the formation of a gel influence the dissolution of high molar mass polymers?)

soutenue le
devant le jury composé de :

M. Pierre LEVITZ	Président du jury
Mme. Catherine AMIEL	Rapporteur
Mme. Béatrice GUERRIER	Rapporteur
M. François LEQUEUX	Directeur de thèse
M. Jean-Philippe CARITEY	Invité
Mme Laurence TALINI	Invitée
Mme Emilie VERNEUIL	Invitée

Abstract

Keywords: high molar mass polyelectrolytes, dissolution, gel, swelling, erosion

Polymers of large molar mass are often used as fluids viscosifiers in the Oil and Gas industry. Ideally, the polymer powder must mix with water and totally dissolve as fast as possible before being pumped in the well. This study focuses on the understanding of the mechanisms at stake during the dissolution of a polyelectrolyte called GP. Even if they are hydrosoluble, GP grains exhibit a hydrophobic behavior when they are put in contact with water, which is responsible for a poor wetting. A viscoelastic gel layer forms and clogs the pores between GP grains, leading to the formation of lumps which increases the dissolution time. We demonstrate that the GP dissolution kinetics is controlled by the gel swelling kinetics. Gel swelling is a diffusive process governed by GP counter-ions osmotic pressure. Gel dissolution is not controlled by a reptation process but occurs when the polymer concentration inside the gel reaches c*, the overlap concentration of the GP. Dissolution is accelerated by stirring the polymer/water mix. The shear at the gel/solvent interface is responsible for the gel erosion. Erosion occurs when the polymer concentration inside the gel reaches the critical erosion concentration $c_{er} > c^*$, which increases with the mixing velocity ω. We demonstrate that GP dissolution kinetics is thus controlled by the erosion of the gel layer and that the dissolution time varies as ω to the power -1.2.

Mots-clefs : polyélectrolytes de grande masse molaire, dissolution, gel, gonflement, érosion

Les polymères de grande masse molaire sont couramment utilisés comme viscosifiants par l'industrie pétrolière. Ils peuvent se présenter sous la forme d'une poudre qui doit idéalement être dissoute dans l'eau le plus rapidement possible avant d'être pompée à l'intérieur du puits. Cette étude porte sur la compréhension des mécanismes qui entrent en jeu lors de la dissolution de la poudre d'un polyélectrolyte appelé GP. Bien qu'étant solubles dans l'eau, les grains de GP présentent un comportement hydrophobe lorsqu'ils sont mis en contact avec l'eau et le mouillage est défavorable. Une couche de gel viscoélastique gonfle et bouche les pores entre les grains, provoquant la formation de grumeaux qui augmentent le temps de dissolution. Nous avons montré que c'est la cinétique de gonflement du gel qui contrôle la cinétique de dissolution du GP. Le gonflement de ce gel est un processus diffusif gouverné par la pression osmotique due à la présence des contre-ions du GP dans la solution. La reptation ne joue aucun rôle dans le désenchevêtrement des chaines, qui survient uniquement lorsque la concentration en polymère dans le gel devient inférieure à la concentration critique de recouvrement c* du GP. La disparition du gel peut cependant être accélérée en imposant une vitesse d'agitation dans le mélange eau/GP qui génère un cisaillement à l'interface gel/solution. La couche de gel est alors érodée lorsque la concentration en polymère dans le gel devient inférieure, non plus à c*, mais à c_{er}, la concentration critique d'érosion, supérieure à c* et qui augmente avec la vitesse de mélange ω. Nous avons montré que la cinétique de dissolution du GP est alors contrôlée par l'érosion de la couche de gel et que le temps de dissolution varie comme ω à la puissance -1.2.

Remerciements

Je tiens tout d'abord à remercier mes encadrants de thèse au laboratoire SIMM, François Lequeux, Laurence Talini et Emilie Verneuil. Merci de m'avoir fait profiter de votre expérience et de vos conseils tout au long de ces trois années de thèse qui ont été pour moi une expérience très formatrice, tant sur le plan scientifique que sur le plan personnel.

Au laboratoire SIMM je voudrais aussi remercier Guylaine Ducouret, pour m'avoir encadrée lors de mon stage de master et avoir continué à me conseiller sur mes résultats de rhéologie tout au long de ma thèse. Merci aussi de m'avoir donné l'opportunité d'encadrer les travaux pratiques de rhéologie en deuxième année de thèse. Merci également à Ludovic Olanier pour la réalisation du montage permettant le suivi de la dissolution en rhéologie, à Bruno Bresson pour les mesures d'AFM, à Mohamed Hanafi pour son aide et ses conseils à propos de l'utilisation des équipements disponibles au laboratoire, et plus généralement à tous les membres du laboratoire qui m'ont apporté leur aide au cours de ces trois ans.

Un grand merci à tous les non-permanents du laboratoire pour tous les bons moments passés ensemble, au labo et en dehors et en particulier à mes co-bureaux, Hui Guo, Éric Lintingre et Marc Yonger pour toutes les fois où ils m'ont dépannée, supportée, encouragée, changé les idées, …

Je souhaite également remercier l'entreprise Schlumberger pour avoir financé mes travaux dans le cadre d'un contrat CIFRE et tout particulièrement Jean-Philippe Caritey, mon encadrant à Schlumberger. Son intérêt pour le sujet et sa participation constructive tout au long de la thèse au fil des réunions trimestrielles ont été déterminantes. Merci aussi Jean-Philippe de m'avoir intégrée à la vie de l'équipe et du service, malgré le peu de temps passé effectivement sur place. Et bien entendu un grand merci à tous les membres de SRWI pour leur accueil lors de mes peu fréquentes apparitions au centre Schlumberger de Clamart.

Mes remerciements vont également à tous les membres de mon jury de thèse pour le temps qu'ils ont consacré à l'examen de ma thèse et l'intérêt qu'ils y ont trouvé. Catherine Amiel et Béatrice Guerrier qui ont accepté de rapporter ma thèse et Pierre Levitz qui a présidé le jury.

Enfin, je remercie infiniment ma famille, mes amis et Raphaël, mon compagnon, sans qui je ne serais jamais arrivée jusque-là…

Résumé en français

Le contrôle de la rhéologie des fluides pétroliers est d'une importance cruciale, en particulier lors du forage et de la cimentation d'un puits de pétrole. Les boues de forage par exemple sont utilisées pour contrôler la pression hydrostatique à l'intérieur du puits lors du forage et éviter ainsi l'effondrement des parois et l'infiltration de fluides provenant de la formation rocheuse environnante. Elles sont également utilisées pour remonter les débris de forage à la surface. Pour cela, la boue doit être suffisamment fluide pour être pompée sans difficulté tout en possédant une contrainte seuil suffisamment élevée pour permettre de suspendre les débris provenant de la formation. L'industrie des services pétroliers utilise donc de nombreux fluides de formulations complexes comprenant en particulier des particules solides de différents types (agents alourdissants, ciment) nécessitant d'être maintenues en suspension. Elle développe pour cela différents additifs.

Cette étude porte sur la compréhension des mécanismes qui entrent en jeu lors de la dissolution de l'un de ces additifs, un polysaccharide de grande masse que nous appellerons GP (pour « Giant Polysaccharide ») pour des raisons de confidentialité. Le GP est un polyélectrolyte utilisé comme agent viscosifiant. Il se présente sous la forme d'une poudre qu'il faut dissoudre dans l'eau en compagnie d'autres additifs avant de pouvoir l'injecter dans le puit. Dissoudre 1 kg de poudre de GP dans 1 m^3 d'eau suffit à multiplier la viscosité de l'eau par plus de 1000. Lors de procédés de mélange en continu (« mix-on-the-fly »), où le fluide est préparé directement dans la cuve de pompage juste avant d'être pompé, la préparation doit être effectuée en 1 minute environ, ce qui laisse très peu de temps à la poudre pour se dissoudre et développer ainsi les propriétés attendues.
Cependant, lorsque la poudre de GP est mise en contact avec l'eau, une couche de gel se forme rapidement autour des grains, ce qui peut conduire à la formation de grumeaux qui mettent ensuite beaucoup plus de temps à se dissoudre que les grains isolés. L'objectif de l'étude est donc d'étudier la cinétique de formation et de disparition de ce gel afin de comprendre le rôle qu'il joue lors de la dissolution de la poudre et ainsi de tenter de minimiser la formation de grumeaux.

Le GP possède une fonction acide carboxylique par monomère, ce qui fait de lui un polyélectrolyte faible. À cause de sa masse molaire très élevée ($5 \cdot 10^6$ g/mol), sa concentration critique de recouvrement c* est très faible (0,15 g/L). La mesure des propriétés rhéologiques du GP permet d'estimer le temps de reptation des chaines de GP. Il s'agit du temps de relaxation le plus long des solutions enchevêtrées. La concentration c* étant très faible, les solutions de GP sont en fait des gels viscoélastiques sur une très large gamme de concentration. La dissolution de la poudre de GP va se révéler par la suite être contrôlée par l'existence de ce gel.

Classiquement, le processus de dissolution d'une poudre de polymère est décomposé en plusieurs étapes. La première est l'étape de mouillage, lorsque l'eau et le polymère entrent en contact.
Le mouillage dynamique d'un polymère par son solvant a été étudié par Tay et al puis par Dupas et al dans le cas de polysaccharides de masse molaire plus faible que celle du GP. Ils ont montré que la valeur de l'angle de contact est contrôlée par la fraction en eau dans la couche de polymère ϕ qui est

fixée par les différents mécanismes de transferts de la goutte d'eau vers la couche de polymère. Ils ont établi l'existence de différents régimes de mouillage en fonction de l'épaisseur e de la couche de polymère et de la vitesse d'avancée de la ligne de contact U. Le régime qui nous intéresse dans cette étude est le régime de couche mince où la fraction en eau ϕ et donc l'angle de contact θ dépendent de la vitesse et de l'épaisseur uniquement via le produit eU. Ce régime est atteint pour $e < D/U$ où D est le coefficient de diffusion mutuel de l'eau dans le polymère.

Des expériences de mouillage ont été réalisées en déposant des gouttes d'eau sur des couches de GP préalablement équilibrées dans une atmosphère dont l'humidité est contrôlée. Un exemple est présenté Figure 0-1.

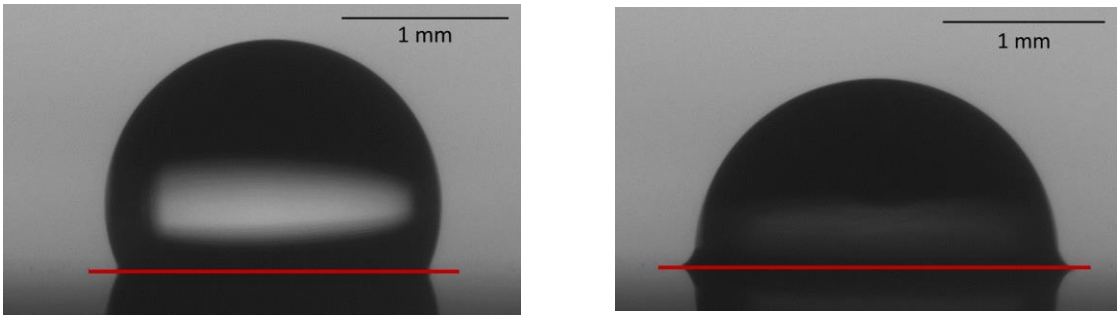

Figure 0-1: Vue de profil d'une goutte d'eau de 5 µL déposée sur une couche de GP de 3 µm d'épaisseur préalablement équilibrée à une humidité ambiante de 43%. Image de gauche: t = 1 s après dépôt – l'angle de contact est très élevé : ϑ = 110°. Image de droite : t = 50 s après dépôt – Apparition d'un pied de gel. La goutte s'est très peu étalée.

Bien que le GP soit soluble dans l'eau, il présente un comportement hydrophobe lorsqu'il est mis en contact avec celle-ci. Ce comportement hydrophobe est visible sur l'image de gauche où l'on constate que l'angle de contact entre la goutte d'eau et la couche de GP est très grand (environ 110°). Après quelques secondes de contact, le GP gonfle et un « pied » de gel apparaît à la ligne de contact (Figure 0-1 - image de droite). La formation de ce gel viscoélastique de GP ralentit fortement l'étalement de la goutte en accrochant la ligne de contact. Du fait de la masse molaire importante du GP, ce gel ne se dissout pas dans la goutte d'eau au cours de l'expérience.

Cependant, de manière surprenante, lorsque la goutte est alimentée en eau pour la forcer à s'étaler sur la couche de polymère, un comportement de mouillage classique sur couche mince est observé. L'angle de contact de la goutte varie comme le produit de la vitesse d'avancée U par l'épaisseur de la couche e uniquement.

Nous avons par ailleurs montré, en nous plaçant à l'échelle d'un grain de poudre, que la cinétique de dissolution d'un grain de GP est contrôlée par la cinétique de gonflement de la phase gel. L'étape de pénétration de l'eau dans le polymère vitreux n'est pas limitante car, bien que le coefficient de diffusion de l'eau dans le polymère vitreux soit normalement de plusieurs ordres de grandeur plus faible que celui dans la phase gel, la présence de nano-pores dans le grain permet à l'eau de pénétrer facilement jusqu'au cœur du grain.

Un dispositif expérimental que nous appellerons « de gonflement 1D » a été conçu pour étudier le gonflement du gel qui se forme lorsque l'eau et le GP entrent en contact. Dans le cas du dépôt d'une goutte d'eau sur une couche de polymère, la croissance du gel est limitée par la quantité d'eau disponible dans la goutte, tandis que dans des conditions réelles de dissolution d'une poudre dans un réservoir d'eau, le réservoir peut être considéré comme un milieu infini. C'est également le cas dans l'expérience de gonflement 1D où une couche mince de polymère de quelques microns à quelques dizaines de microns d'épaisseur sur une surface d'environ 2 cm^2 est placée dans un réservoir contenant environ un demi litre d'eau.
Nous avons ainsi mesuré les profils de concentration en polymère à l'intérieur du gel à différents temps. Un exemple est présenté sur la Figure 0-2.

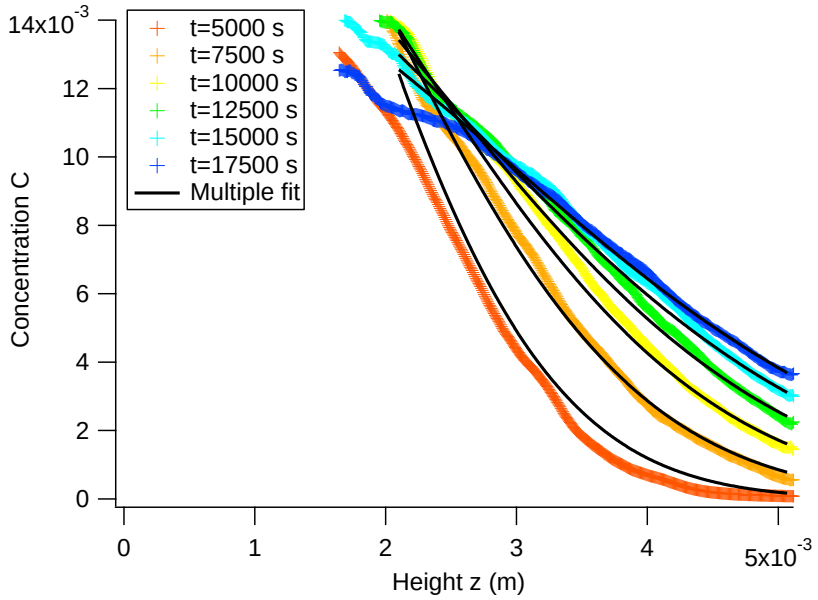

Figure 0-2: Profil de concentration à l'intérieur d'un gel de GP gonflant dans un réservoir d'eau distillée en fonction de la distance z à la couche de polymère. Chaque courbe correspond à un temps t après la mise en contact du polymère et de l'eau. L'épaisseur initiale de la couche est de 50 µm. Les données sont ajustées par un modèle de diffusion tenant compte des conditions aux limites et en ajustant la valeur du coefficient de diffusion.

Le gonflement d'un gel de GP est un processus diffusif. Aux temps courts, il peut être décrit par un coefficient de diffusion indépendant de la concentration. Aux temps longs, une description complète nécessiterait de considérer un coefficient de diffusion variable avec la concentration. On observe qualitativement que le coefficient de diffusion augmente lorsque la concentration en polymère diminue. Ce comportement est prédit par le calcul lorsqu'on considère la pression osmotique due à la présence des contres-ions comme étant le moteur du gonflement de ce polymère chargé.
Le comportement diffusif se retrouve sur des échelles de temps et de longueur qui varient de plus de trois ordres de grandeur, allant de temps très inférieurs au temps de reptation à des temps supérieurs, sans que le coefficient de diffusion ne soit modifié. La reptation ne joue donc aucun rôle dans la dissolution du gel.
D'autres expériences de gonflement 1D réalisées avec des couches de Polyéthylène Glycol (PEO) nous permettent également de conclure que la disparition du gel n'est pas contrôlée par la reptation des chaines. Ces expériences ont mis en évidence l'existence d'un temps critique t* à partir duquel les chaines de polymère sont transférées dans le solvant à une vitesse supérieure à la vitesse de

gonflement. Des expériences réalisées avec des PEO de différentes masses molaires ont permis de montrer que t* varie comme l'inverse de la concentration critique de recouvrement c* lorsque la masse molaire varie. Le mécanisme que nous proposons donc pour expliquer la disparition du gel est un gonflement coopératif du réseau de polymère jusqu'à ce que la concentration à l'intérieur du gel atteigne c*, concentration en deçà de laquelle les enchevêtrements disparaissent.

Le GP étant un polyélectrolyte, l'augmentation de la force ionique du solvant a une influence déterminante sur la cinétique de gonflement du gel. Le coefficient de diffusion diminue d'un facteur dix lorsqu'on remplace l'eau distillée par une solution de NaCl à 30 g/L (de l'ordre de grandeur de la concentration en sel dans l'eau de mer) pour atteindre des valeurs similaires à celles obtenues pour un polymère neutre comme le PEO. Ces expériences nous ont permis de conforter notre modèle pour lequel la pression osmotique des contre-ions contrôle le gonflement du GP.

Cependant, dans la situation réelle où une poudre de polymère est dissoute dans un réservoir de liquide, un autre paramètre est à prendre en compte. Il s'agit de l'agitation, qui permet bien évidemment de réduire la durée de la dissolution.
Un dispositif expérimental utilisant un rhéomètre pour imposer une vitesse de mélange et mesurer la concentration en polymère dissout via la mesure du couple a été conçu pour étudier l'influence de la vitesse de mélange sur la cinétique de dissolution de la poudre de GP. Le temps de dissolution $t_{1/2}$ est défini comme le temps nécessaire pour dissoudre 50% de la poudre. Plusieurs régimes ont été mis en évidence. La dépendance du temps de dissolution avec la vitesse de mélange en fonction des différents régimes est présentée sur la Figure 0-3.

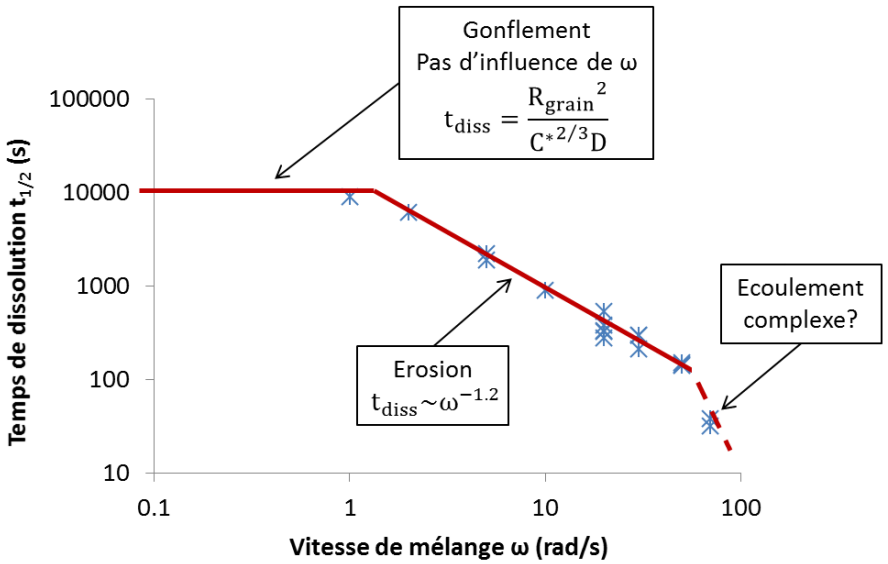

Figure 0-3: Evolution du temps de dissolution en fonction de la vitesse de mélange. Présentation des différents régimes.

À faible vitesse de mélange ω, le temps de dissolution est limité par le gonflement coopératif du gel jusqu'à la concentration critique de recouvrement c*.
Aux vitesses intermédiaires, le temps de dissolution varie comme la vitesse de mélange à la puissance -1.2. La dissolution du GP est contrôlée par l'érosion de la couche de gel. Un montage microfuidique composé d'un canal dont l'une des parois est une couche de GP et dans lequel de l'eau circule à une

vitesse contrôlée nous a permis d'observer l'érosion du gel en fonction de la vitesse de l'eau. L'eau qui circule dans le canal impose une contrainte de cisaillement qui dépend de sa vitesse. Le gel, lui, est érodé à un taux de cisaillement constant qui ne dépend pas de la vitesse de l'eau. La concentration à laquelle le polymère est érodé c_{er} varie donc avec la vitesse suivant une loi de puissance dont l'exposant est 0,6. À partir de cette observation, il est possible de prédire par un calcul en loi d'échelle le temps de dissolution d'un grain de polymère en fonction de la vitesse de l'eau. La loi expérimentale $t_{diss} \sim \omega^{-1.2}$ est en bon accord avec ce calcul.

Le régime à grande vitesse a été très peu étudié à cause de limitations dues à notre montage expérimental. Une explication possible à l'augmentation de l'exposant de la loi de puissance qui relie le temps de dissolution à la vitesse de mélange est l'apparition de turbulences dans l'écoulement.

Table of content

1 Introduction

Controlling the rheology and stability of complex fluids containing various solids to be kept suspended is of critical importance during the drilling and cementing of an oil well. A first example of such fluids is drilling muds. They are used to apply a hydrostatic pressure inside the well in order to prevent well collapse and fluids infiltration from the rock formation, and to suspend and carry out drill cuttings. The mud has thus to be fluid enough to be pumped in and out easily and in the same time it has to develop a high enough yield stress to carry the cuttings. Another type of fluids is the spacers. They are pumped inside the well after drilling and before well cementing to separate mud and cement. The aim is to avoid mixing which could lead to side reactions triggering the cement setting before it is in the right place. Spacers properties, such as viscosity and stability have thus to be very well controlled to properly displace the mud. Another example is cement slurries pumped to provide zonal isolation all along the well. This is achieved if the cement sheath around the casing develop the required properties, strongly dependent on fluid rheology and stability during both placement and setting phases.
Oilfield services industry develops many additives to control properties of such complex fluids[1]. For instance, hydrosoluble high molar mass polymers are often used as viscosifiers in order to adjust and control the rheology of those fluids. They are often available under solid powder form and they need to be dissolved in a solvent, generally fresh water or sea water, before being used. During the continuous mixing ("mix-on-the-fly") processes where the fluid is mixed directly in the pumping tank just before being pumped in the well, the polymer powder has to mix with water and dissolve totally in about 1 minute to meet the required pumping rate. It is a really short time to ensure a good dissolution of the powder and sometimes the polymer forms lumps which are very long lasting and prevent the onset of the expected rheological properties.
This study focuses on one of these polymers, called Giant Polysaccharide (GP). It is a very efficient viscosifier which increases the water viscosity by more than three orders of magnitude when 1 kg of powder is added to 1 m^3 of water. However, when put in contact with water, GP grains swell and a viscoelastic gel layer is formed at their surface. This gel is responsible for the formation of lumps which increases strongly the dissolution time.
The aim of this work is to study the mechanisms at stake during the formation and the disappearance of this gel in order to understand its role in powder dissolution and lumps formation.

Dissolution process of polymer powders is classically described as follows:
First, the powder grains are wetted by the solvent which penetrates by capillarity between the powder grains, leading to immersion of the powder. Then, the aggregates break up and the powder grains are progressively dissolved in the solvent. However, this description is quite simplistic because all those phenomena occur simultaneously and it is difficult to study them separately. Moreover, each step of the dissolution is governed by complex mechanisms, in particular because polymer properties may vary over several decades of magnitude when the solvent content increases. Polymer dissolution is thus only partially understood in the literature, especially the mechanisms limiting dissolution and the description of stirring effect on dissolution.

Results from the literature on polymer wetting by their solvent will be discussed in **Chapter 2**, along with more general phenomenological and theoretical studies on polymer powder dissolution and a few notions of polymer physics. We will see that there is no quantitative consensus on dissolution rate dependency with molar mass and powder granulometry.

In **Chapter 3**, the materials and methods used in this work will be described. We will present a complete characterization of GP properties that will be needed in the following chapters to explain GP behavior, such as for instance its molar mass, its granulometry, its sorption isotherm and ts rheological properties in solution. The preparation of polymer layers and their characterization will be explained.

In **Chapter 4**, the wetting of GP by water will be discussed. Preliminary experiments performed on polymer powder beds will be presented. Then we will focus on the wetting of GP layers by water droplets. The contact angle will be measured for different layer thicknesses and contact line velocities and the results will be compared with Dupas et al observations for polysaccharides of smaller molar masses than GP. The onset of a gel layer will be evidenced.

In **Chapter 5**, swelling of the gel without convection will be studied. A home-made 1D swelling experimental set-up will be detailed which has enabled us to demonstrate that gel swelling follows a diffusive behavior. Gel disappearance will be linked to the overlap concentration of the polymer solution.

Finally in **Chapter 6**, the influence of erosion on the polymer dissolution will be studied using both a macroscopic and a microscopic dissolution experiment with a convective flux of solvent. Several dissolution regimes will be evidenced.

2 State of the art

2.1 Polymer physics

Polymers are macromolecules in the form of long chains made of elementary units called monomers which are connected by covalent bonds. In this first paragraph, we will present simple models of polymer chains and polymer solutions and we will introduce several physical quantities characteristic of polymers that will be used in the following chapters to describe GP and to model GP swelling.

2.1.1 Single chain

Chains with no interactions between monomers that are far apart along the chain, even if they approach each other in space are called ideal chains.
For an ideal chain made of n+1 backbone atoms A_i ($0 \leq i \leq n$) connected by n bonds of length l with a tetrahedral angle between neighboring monomers θ, the largest end-to-end distance is:

$$R_{max} = nl\ cos\frac{\theta}{2}$$

R_{max} is called the contour length.
r_i is the bond vector going from atom A_{i-1} to atom A_i.

$$\vec{r_i}.\vec{r_j} = l^2 \cos\theta_{ij}$$

The end-to-end vector is:

$$\overrightarrow{R_n} = \sum_{i=1}^{n} \vec{r_i}$$

The average end-to-end vector $\langle\overrightarrow{R_n}\rangle$ is equal to 0 for an isotropic collection of flexible chains. The simplest non-zero average is the mean-square end-to-end distance:

$$\langle R^2\rangle = \langle\overrightarrow{R_n}^2\rangle = \sum_{i=1}^{n}\sum_{j=1}^{n}\langle\vec{r_i}.\vec{r_j}\rangle = l^2\sum_{i=1}^{n}\sum_{j=1}^{n}\langle\cos\theta_{ij}\rangle = C_n n l^2$$

C_n is the Flory's characteristic ratio.
For a long-enough polymer chain ($n \to \infty$)

$$\langle R^2\rangle \cong C_\infty n l^2$$

A simplest description valid for all ideal polymers is the equivalent freely jointed chain model.
The equivalent freely jointed chain as the same maximum end-to-end distance and the same mean-square end-to-end distance as the actual chain but it has N freely jointed monomers of length b called Kuhn monomers. b is the Kuhn length.
For freely jointed monomers,

$$\cos\theta_{ij} = \delta_{ij} \leftrightarrow C_n = 1$$

And so:

$$\langle R^2\rangle = Nb^2$$

$$R_{max} = Nb$$

The root-mean-square end-to-end distance R_0 is:

$$R_0 = bN^{1/2}$$

The equivalent freely jointed model will always be used in the following to describe polymers unless specified otherwise.

For real chains, interactions between monomers lead to an excluded volume. In good solvent where the chain swells, the excluded volume is positive.
Conformation of a real chain in good solvent can be described by Flory theory. According to this theory, the chain conformation is set by the polymer free energy. It is a balance between repulsive energy between monomers that tends to swell the chain and entropy loss due to the chain deformation.
The real chain optimum size in Flory theory R_F minimizes the free energy of the chain.

$$R_F = bN^{3/5}$$

To describe their conformations under any external circumstances, polymer chains can be subdivided into "blobs". The thermal blob is defined by excluded volume interactions. On length scales smaller than the thermal blob length, excluded volume interactions are weaker than thermal energy and the chain conformation is nearly ideal. On the contrary, on length scales larger than the thermal blob length, chains are swollen and they can be described by Flory theory.
For semi-dilute solutions, another length scale will be introduced in the following paragraph: the correlation length.

2.1.2 Polymer solution

Polymer chains can be solubilized in solvent.
At very low concentration, polymer chains are isolated coils in the solvent without interactions with each other. They behave as single real chains, following the Flory behavior.

Increasing concentration, a point is reached where the solution total volume becomes smaller than the sum of every chain coil volume and chains begin to overlap. This critical volume fraction is called the overlap concentration.
Above the overlap concentration, solution properties are mostly determined by overlapping chains even if they occupied a very small volume compared to the solvent. In that case, polymer solutions are called "semi-dilute".
In semi-dilute solutions, a critical correlation length[2,3] ξ appears. Below this length, a monomer is surrounded mostly by solvent and by a few other monomers belonging to the same chain. Conformation of a chain section of length ξ containing g monomers is then very similar to those of a single chain in good solvent predicted by Flory theory because there is no interactions with other chains. On length scales larger than the correlation length, excluded volume interactions are screened by the overlapping chains and polymer chain is then an ideal random walk of elementary units of size ξ called correlation blobs.

The correlation length in a semi-dilute solution decreases with increasing concentration[4] as:

$$\xi \sim \Phi^{-0,76}$$

When the correlation length reaches the size of a thermal blob, the intermediate swollen regime disappears. Polymer solutions are in the concentrated regime. In this regime, chains have nearly ideal conformations at all length scales.

In real networks made of long linear polymers, network chains impose topological constraints on each other because they cannot cross. These topological constraints are called entanglements.

De Gennes proposed a model for the motion of linear entangled polymers called the reptation model[5]. In this model, the polymer chain motion is restricted to a tube of diameter ξ created by the surrounding chains called the Edwards tube. The chain diffuses along this tube with a curvilinear diffusion coefficient D_c.

$$D_c = \frac{kT}{N\zeta}$$

N is the number of monomers and ζ is the friction coefficient of a monomer.
L is the polymer chain contour length.
The time needed by the chain to diffuse out of its original tube of length L is the reptation time τ_{rep}.

$$\tau_{rep} = \frac{L^2}{D_c} \sim N^3$$

The reptation time is predicted to be proportional to the cube of the monomer number. However, the experimentally measured scaling exponent is:

$$\tau_{rep} \sim N^{3.4}$$

The reptation time determines the polymer rheological behavior (see Annex 8).

Chains entanglement occurs at a critical concentration[6] c_e which is slightly above the overlap concentration c*. It is characterized by an abrupt change in the power law exponent for the viscosity dependence on concentration[7].

2.1.3 The case of polyelectrolytes

Polyelectrolytes are polymers whose monomers have ionizable or ionic groups. Those groups can be carboxylic acids. In that case, the polymer is called a weak polyelectrolyte because the carboxylic function is only partially ionized in water and its pK_a is around 4 – 5.
The ionization ratio α is defined as the number ratio between ionized monomers and all monomers.
To ensure the neutrality of the polymer solution, the polymer backbone charge is equilibrated by free ions in the solution. Those ions are called counter-ions.

In the case of enough charged polyelectrolytes, a portion of the counter-ions remains close to the polymer backbone to reduce its effective charge. This phenomenon is called Manning condensation[8,9]. It occurs when the distance between charges is equal to the Bjerrum length which is 0.7 nm in water.

Below the condensation threshold (when the distance between charges is above the Bjerrum length), the counter-ions number is equal to the number of ionized sites. Above it, it is constant.

The conformation of a polyelectrolyte chain is stretched compared to the one of a neutral polymer.[10] This is due to electrostatic repulsions between charged monomers. In a diluted solution of polyelectrolytes without salt, the mean square end-to-end distance of the chain is proportional to the number of monomers N. In a semi-dilute solution, the chain is a random walk of correlation blobs.

For a polyelectrolyte solution, the osmotic pressure is mainly due to the mixing entropy of the counter-ions liberated by the chains[11]. Its expression will be detailed in paragraph 5.2.3.4.

GP is a polyelectrolyte. In this study, it will be considered in good solvent and its Kuhn length will be considered equal to its monomer length.

2.2 Wetting

In this study we will be interested in the dissolution process of polymer powders, i.e. the transition between a solid glassy state and a polymer solution.
First step in the dissolving process is the contact between polymer and water. It is called the wetting step. Imbibition of the powder grains is ensured by the advance of the water contact line on grain and inside the grain pores. Affinity between polymer and solvent is critical to ensure a good wetting. It is usually characterized by measuring the equilibrium contact angle of a solvent droplet deposited onto a polymer layer. Dynamic wetting experiments are also used to mimic water penetration by capillarity into the porous structure of the powder.

2.2.1 Equilibrium contact angle: Young's relation

The equilibrium state for a liquid droplet deposited on a solid smooth and homogeneous surface in a vapor atmosphere is determined by the surface tensions between the three phases: the surface energy of the solid γ_S, the liquid surface tension γ and the solid/liquid interfacial energy γ_{SL}.
If $\gamma_S > \gamma + \gamma_{SL}$, the system free energy is minimized by a "total wetting" situation where the liquid spread all over the solid surface.
If $\gamma_S < \gamma + \gamma_{SL}$, the system free energy is minimized by a "partial wetting" situation with a droplet having a finite contact angle as presented in Figure 2-1.

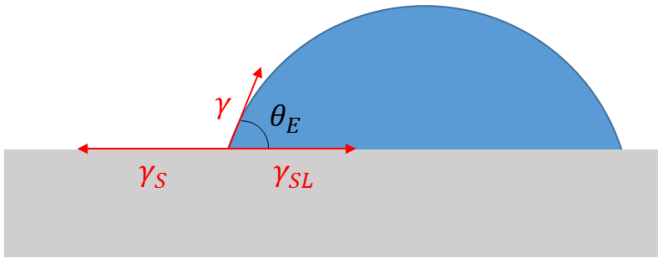

Figure 2-1: Partial wetting situation: energy parameters for the Young's relation

The equilibrium contact angle between the droplet and the solid substrate θ_E is given by the Young's relation[12]:

$$\gamma_S - \gamma_{SL} = \gamma * \cos\theta_E$$

If $\theta_E < 90°$, the liquid is said to be "mostly wetting". In that situation, if the liquid is water, the substrate is said to be "hydrophilic". If $\theta_E > 90°$, the liquid is said to be "mostly non wetting" and for water, the substrate is said to be "hydrophobic".

2.2.2 Spreading dynamics

2.2.2.1 Of a non-volatile droplet on a non-soluble surface

A classical description of the spreading of a non-volatile liquid droplet onto a non-soluble solid surface has been given by Cox and Voinov[13,14]. The dynamic contact angle is different from the equilibrium contact angle and it depends on the contact line velocity U. Hydrodynamic approach is used to calculate this angle. The equation obtained by balancing interfacial forces and viscous dissipation diverges near the contact line, and a microscopic cut-off length L_m has to be introduced. Reynolds number $\frac{\rho UL}{\eta}$ have to be small (η is the fluid viscosity, ρ its density and L is a characteristic length of the problem).

In that case, the Cox-Voinov law relates the dynamic contact angle θ_D to the contact line velocity U:

$$\theta_D{}^3 = \theta_m{}^3 + \mathrm{Ca}\ln\left(\frac{L}{L_m}\right)$$

θ_m is the microscopic contact angle, usually taken equal to θ_E and Ca is the capillary number equal to $9\eta U/\gamma$. For pure water droplets, $Ca = U/U^*$ with U* = 7 m/s.

This law is well verified experimentally for the spreading of a non-volatile liquid droplet onto a non-soluble solid surface with $\ln(L/L_m)$ being an adjustable parameter. Taking L as the droplet size and L_m as 1 nm is reasonable. However, for Ca << 1, the spreading is quasi-static and $\theta_D = \theta_E$. In this study it will always be the case because the contact line velocity U never exceeds a few millimeters per second, i.e. U << U*.

Contact angle variations with the contact line velocity are thus not accounted for by this hydrodynamic approach. They are related to the fact that, by working with polysaccharides and water, we are looking at a soluble substrate and a volatile solvent. Hydration occurs and modifies the substrate energy.

2.2.2.2 Wetting on soft substrates

In Young equation, the vertical component of the liquid surface tension γ is not taken into account. However, it has been shown by Shanahan et al[15] that this component γ sin θ induces strain in the wetted solid leading to the formation of a "wetting ridge". The height of this wetting ridge is γ/G, where G is the elastic modulus of the substrate. For a water droplet on a soft viscoelastic substrate, γ =70 mN/m and G is typically of the order of 1 kPa. The height of the wetting ridge is thus significant, typically a hundred micrometers. When the droplet moves at a velocity U, the displacement of the ridge is dissipative if the substrate is viscoelastic. This dissipation is thus responsible for the observed braking of a moving drop[16].

2.2.2.3 *Wetting of a volatile solvent on a soluble substrate*

Halperin and De Gennes[17] theoretically predicted that the contact angle between a polymer and its solvent should be zero. However, this is in contradiction with earlier experiments[18]. For hydrophilic polymers, the existence of a finite equilibrium contact angle could be attributed to a reorientation of the polymer chains during layer preparation in order to place the most hydrophobic parts of the chains at the air/layer interface[19].

During their PhD works, A. Tay and J. Dupas designed and improved an experimental set-up to study the wetting dynamics of volatile solvent on a soluble substrate.
A silicon wafer coated with a thin layer of polymer is placed in a controlled atmosphere chamber and a water droplet is deposited onto it. The wetting is then studied by measuring the contact angle between solvent and polymer θ and the contact line velocity U during droplet spreading. Experimentally, when the droplet spreads, they observed that θ and U decreased with time. The larger the contact angle is, the poorer the solvent is wetting the polymer.

Three mass transfers are at stake during the spreading of a solvent droplet onto a soluble polymer layer substrate: dissolution of the polymer layer in the droplet, direct water diffusion from the droplet to the layer and evaporation of water from the droplet followed by recondensation of this water on the polymer layer. Those mechanisms are represented on Figure 2-2. In Tay et al papers[20,21], hydration of the polymer layer by direct diffusion is assumed to be negligible behind hydration by evaporation/recondensation because the diffusion coefficient of water in polymer is much smaller than the one in air.

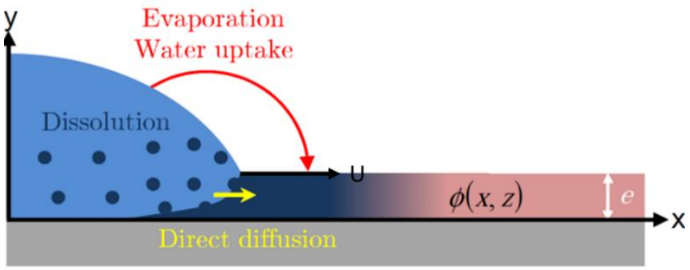

Figure 2-2: Mass transfers at stake during spreading of a water droplet onto a soluble polymer substrate (adapted from J. Dupas PhD manuscript)

They show that wetting by a droplet of a volatile solvent on a soluble polymer substrate strongly depends on the degree of hydration of the polymer close to the contact line[19] induced by evaporation/recondensation mechanism, and that a dry layer can be poorly wetted by water even though the polymer is soluble in it.
The larger the velocity U of the droplet and the thickness e of the layer are, the dryer the layer close to the contact line is and so the larger the contact angle is (see Figure 2-3).
There are different regimes for the dependency of the contact angle on the layer thickness e and the contact line velocity U, depending on the efficiency of the different solvent transfer mechanisms.

In the thin film regime, the water diffuses through the entire layer thickness fast enough to ensure that there is no vertical water content gradient in the polymer layer. This regime is observed when the diffusion coefficient D verifies D > eU. In that case, the wetting contact angle is a function of the product eU only (see insert on Figure 2-3) The maximum value of eU for which the contact angle is a function of eU only is thus a good indicator of the diffusion coefficient value.
For thick polymer layers, the wetting contact angle becomes independent of the thickness e, being only a function of the velocity of the contact line.

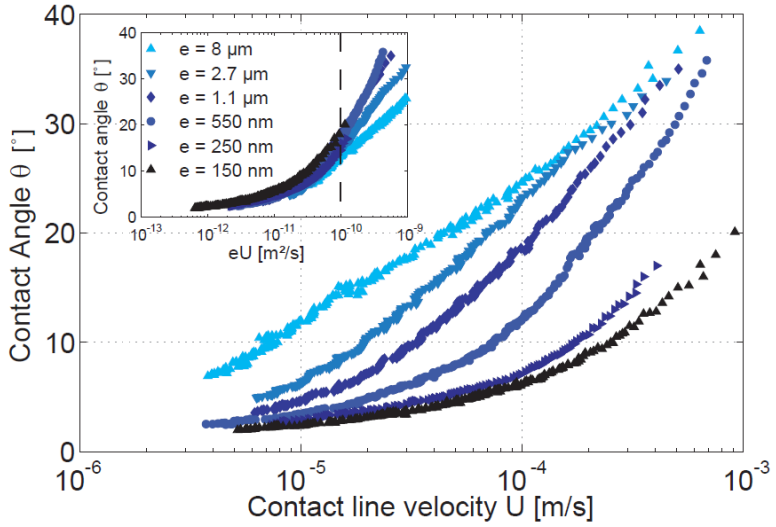

Figure 2-3: Contact angle ϑ versus contact line speed U for droplets of water spreading on Maltodextrin films of varied thicknesses e. Insert: Same data, Contact angle collapses on a single curve when plotted versus the product eU as long as eU<10^{-10} m^2/s (dashed line) (adapted from Dupas et al[22])

In addition, another phenomenon, namely the crossing of the glass transition due to water uptake in the polymer layer, can modify the wetting dynamics. Indeed, amorphous polymers undergo a glass transition in water content when the water volume fraction inside the polymer ϕ increases above a value ϕ_G. This is due to the fact that the glass transition temperature of a polymer decrease with its water content and becomes smaller than the room temperature for $\phi = \phi_G$. Thus, at $\phi < \phi_G$, the polymer is glassy, its elastic modulus is high and the diffusion coefficient of water in the polymer D is small. In that case, the substrate will not significantly deforms at the contact line. At $\phi > \phi_G$, the polymer is viscoelastic, its elastic modulus decreases strongly with increasing water content and D is large. In this case, the polymer substrate strongly deforms at the contact line due to the action of the vertical component of the capillary force and the viscoelastic dissipation that occurs in the deformed zone slows down the droplet.
In a wetting experiment in which a polymer is wetted by its solvent, the water content at the contact line increases during the experiment and an initially glassy polymer can thus turned into a melt during spreading.
Glass transition in water content at the contact line during droplet spreading is thus responsible for a sudden change in the contact angle dependency with water velocity[23].

2.2.2.4 Wetting of a polymer layer: Influence of the molar mass

Otherwise, molar mass is expected to affect solvent wetting dynamics since solvent sorption, but also the solvent volume fraction at which glass transition occurs, depends on molar mass. Indeed, ϕ_G increases with molar mass before reaching a plateau.

An increase of the contact angle value with the molar mass of the coated polymer was observed by J. Dupas on the same experimental set-up with polymer substrates equilibrated at $\phi>\phi_G$ (see Figure 2-4).

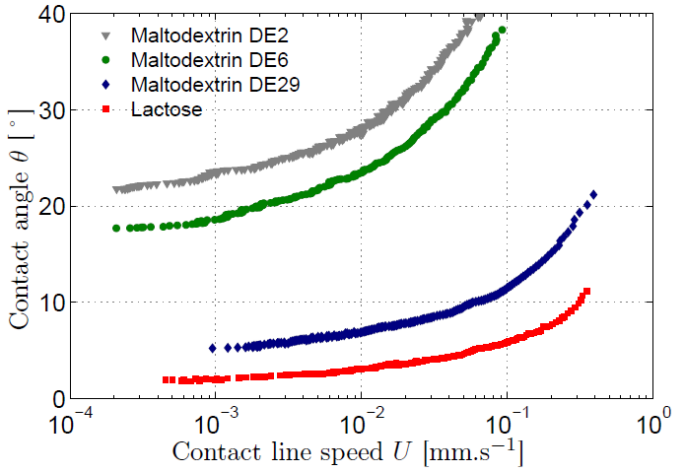

Figure 2-4: Effect of the molar mass on the wetting dynamics for 4 carbohydrate samples of increasing molar masses. Molar masses increase from Lactose to Maltodextrin DE2 (adapted from Dupas phD manuscript[24])

The increase on the contact angle with the polymer molar mass results from the influence of chain ends on the hydrophilicity of the polymer layer surface. The monomers at chain ends being more mobile than the monomers in the bulk, they are expected to reorient more easily at the interface. Therefore, the hydrophobic parts being initially exposed at the interface with air, as the polymer is hydrated, the exposure of more hydrophilic parts is faster for small chains, ensuring a better wetting. Wetting of water is thus poorer on high molar mass polymers.

2.2.2.5 Wetting on a rough substrate

Roughness of a surface modifies its wetting properties.

Johnson and Dettre[25] measured the contact angle of water droplets deposited on wax substrate of roughness controlled by successive annealing. They observed that the advancing and receding contact angles increase with surface roughness.

Two limit cases can be considered for the wetting or a rough surface: (a) the liquid perfectly follows the surface shape (Figure 2-5 (a)), or (b) air bubbles are trapped between the liquid droplet and the solid surface (Figure 2-5 (b)).

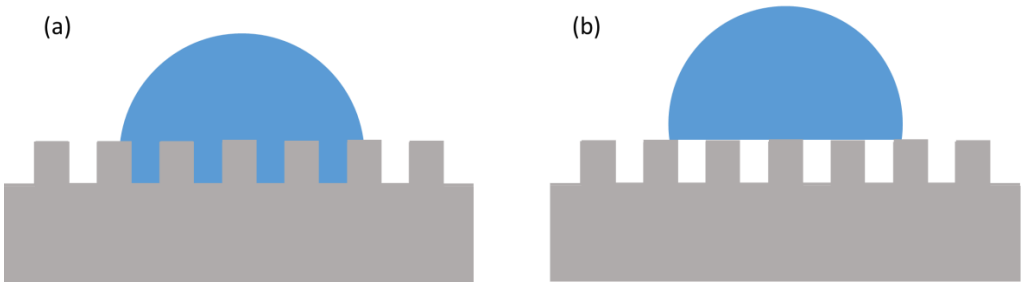

Figure 2-5: Schematic representation of a droplet deposited on a rough substrate: (a) Wenzel situation and (b) Cassie-Baxter situation

Wenzel[26] proposed an expression for the contact angle of a pinned droplet in the case (a).

$$\cos\theta^* = r\cos\theta_{eq}$$

Where r is the surface roughness, defined as the ratio between the real surface area and the projected surface area (r>1) and θ_{eq} is the equilibrium contact angle given by the Young relation for the equivalent flat surface.

According to this equation, roughness enhances the hydrophilic/hydrophobic property of the surface.

Another possible model is the Cassie-Baxter model[27] which describes the wetting of a flat but chemically heterogeneous surface. Case (b) corresponds to this situation with air bubbles being considered as chemical heterogeneities on the surface.

For a surface made of two different materials, the macroscopic contact angle is

$$\cos\theta^* = \phi_1\cos\theta_1 + \phi_2\cos\theta_2$$

Where ϕ_1 and ϕ_2 are the surface fractions of the two materials and θ_1 and θ_2 are the respective equilibrium contact angles defined by the Young relation.

The contact angle on case (b) is then

$$\cos\theta^* = \phi_S\cos\theta_{eq} - (1-\phi_S)$$

because the contact angle of water on air θ_2 is 180°.

Polymer layer roughness can be difficult to control, especially for layers of high molar mass polymers prepared by scraping a polymer solution. Altogether, the substrate roughness modifies the static contact angle of a droplet. Depending on whether the droplet is pinned or sat on the top of the roughness, the contact angle can be larger or smaller. Besides, substrate roughness also changes the dynamics of an advancing droplet. It pins the contact line[28], resulting on larger advancing contact angles on rough surfaces than on flat surfaces.

To conclude, it was demonstrated that wetting dynamics of a polymer wetted by its solvent is ruled by solvent transfer from the droplet into the polymer substrate. The huge change in the polymer properties at the glass transition is thus responsible for a modification of the wetting dynamics. Molar mass of the polymer also have an influence on the wetting properties. The apparent hydrophobicity of the polymer layer surface increases with the molar mass. Finally, the substrate roughness also plays a role in the wetting dynamics, preventing the solvent spreading by pinning the contact line.

2.3 Powdered Polymer Dissolution

Dissolution of polymer powders is a key step in many industrial processes, because a lot of materials are conditioned in a powder form and need to be rehydrated before being used[29,30]. Understanding the influence of the physico-chemical parameters on the dissolution kinetics is thus a critical need to ensure a fast, lump free dissolution of the powders. To do that, several studies have been performed: some phenomenological observations have been reported in the literature and some theoretical models have been proposed which are presented in the following paragraphs.

2.3.1 Phenomenological observations

2.3.1.1 Dissolution in the absence of lumps

Dissolution of a dry grain of polymer powder in water is a complex phenomenon which has been partially described in the literature.
Due to complexity of theoretical calculations, phenomenological laws based on observations have been developed by Kravtchenko et al[31], Parker et al[32] or Wang et al[33,34,35].

Kravtchenko et al[31] studied the dissolution of pectin powder using a modified rotational viscometer to record the macroscopic changes in torque caused by dissolution. They fitted their dissolution measurements with an empirical equation proposed by Mitchell et al[36].
This equation is of the form:

$$m = m_{\infty}\left(1 - exp(-kt)\right) \qquad \textit{(Eq 2-1)}$$

Where m is the mass of polymer dissolved at time t and m_{∞} is the final polymer mass dissolved. The fitting parameter k quantifies the dissolution rate of the polymer.
They ensured good dispersing conditions by dry-mixing the pectin powder with a large excess (18 g for 1 g of pectin) of ground sucrose of roughly the same grain size before dissolution.
A typical dissolution curve of a pectin powder under dispersing conditions is shown on Figure 2-6.

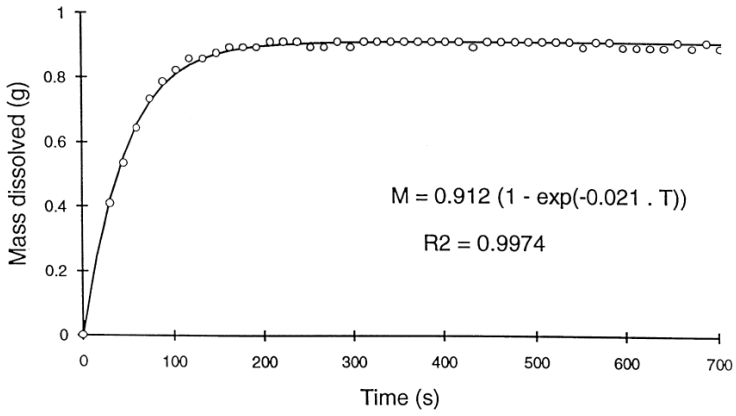

Figure 2-6: Dissolution kinetics of pectin under dispersing conditions (adapted from Kravtchenko et al)

In a more recent paper, Parker et al[32], using the same experimental set-up as Kravtchenko et al, describe dissolution in terms of constant surface flux of dissolving polymer, neglecting the capillary imbibition phase. The concentration of dissolved polymer C_p as a function of time is then:

$$C_p(t) = C_0[1 - (1 - kt/R_0)^3], \qquad kt \leq R_0$$

Where C_0 is the initial mass concentration of grains in the solution, R_0 is the initial radius of a spherical grain of density ρ_0 and $k=J/\rho_0$ is the volume flux where J is the mass flux, defined as the mass of polymer chains shed per unit surface area per unit time.

From this law, a single number characterizing dissolution process can be defined. It is v_{in}, the reduced initial dissolution velocity, given by

$$v_{in} \equiv \frac{1}{C_0}\left(\frac{dC_p(t)}{dt}\right)_{t=0} = \frac{3k}{R_0}$$

This law can be extrapolated to polydisperse grains populations by integration over the size distribution.

This kind of empirical laws is very well adapted to characterize dissolution and hence to study the effect of different parameters such as grain size or molar mass of the polymer on dissolution time.

Parker et al performed their dissolution experiments on sieved fractions of different molar mass polysaccharides. They showed that dissolution velocity is inversely proportional to grain size for all the polymers studied and that the proportionality coefficient depends on the polymer molecular mass (see Figure 2-7).

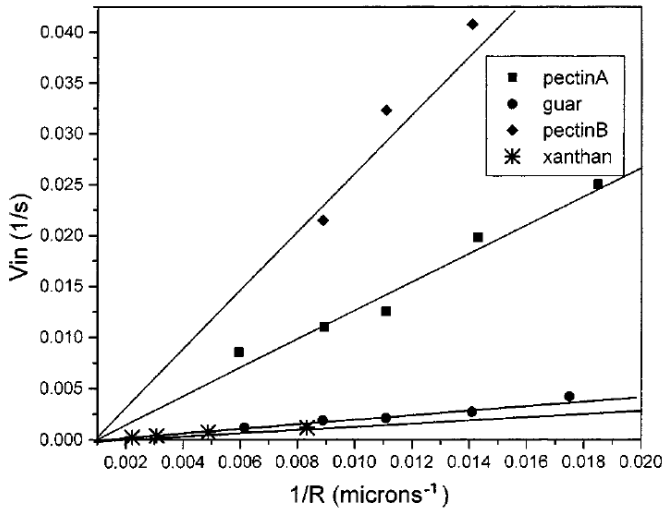

Figure 2-7: Initial dissolution velocity of a grain v_{in} for 4 different molar mass polysaccharides under dispersing conditions. The molecular mass are ranked as follow: Pectin A < Pectin B < Guar < Xanthan (adapted from Parker et al)

Wang et al[33,34,35] studied the dissolution of guar gums by mixing them with water and measuring the viscosity of the supernatant at different times. In a first paper[33], they proposed three different models for an empirical dissolution law: first-order kinetics, logarithmic model and Weibull function. In all those models, solution viscosity η_t is used to quantify polymer dissolution as a function of time. From their experimental results, they concluded that the most suitable model was the logarithmic one.

It reads

$$\ln\left(1-\frac{\eta_t}{\eta_\infty}\right)=k\ln[a(t+t_0)] \qquad \textit{(Eq 2-2)}$$

Using this model, the effect of molar mass on dissolution rate, characterized by the hydration index $t_{0.8}$, was investigated[34]. $t_{0.8}$ is defined as the time needed for the viscosity of the dispersion to reach 80% of its final value. The hydration index was found to be inversely proportional to the polymer molar mass (see Figure 2-8).

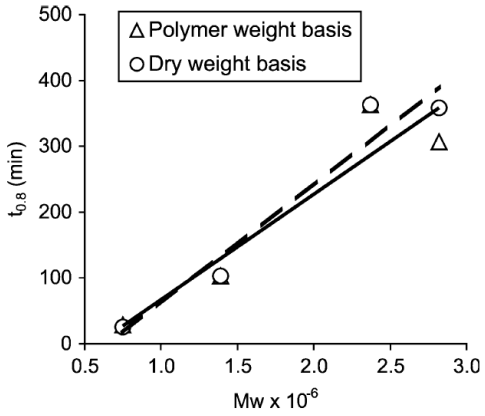

Figure 2-8: Hydration index versus molar mass of guar gum flour (adapted from Wang et al)

In a third paper[35], the effect of the grain size on dissolution rate was also investigated. Six samples of the same polymer with different grain sizes ranging from 80 µm to 500 µm were used. The size distribution is presented on Figure 2-9.

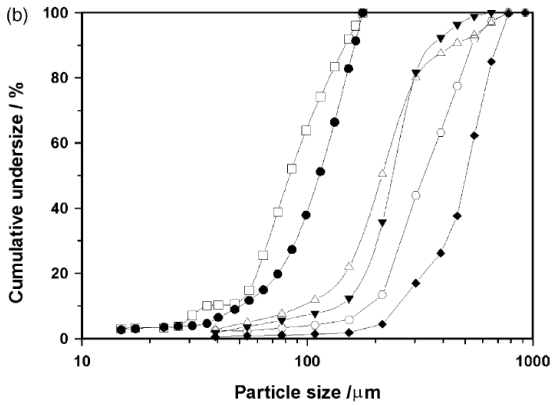

Figure 2-9: Particle size cumulative percentage curves for polymer samples 1 to 6 (adapted from Wang et al)

Dissolution curves for those samples are presented on Figure 2-10 (a) where supernatant viscosity is plotted as a function of time. The logarithmic model found in their previous studies is suitable for guar gum powders where the mean particle size is about 50 µm to 70 µm but it is not applicable for larger particles (> 80 µm). However, by using an arbitrary factor to shift data along the time scale, a unique master plot where all dissolution curves are superimposed appears (see Figure 2-10 (b)).

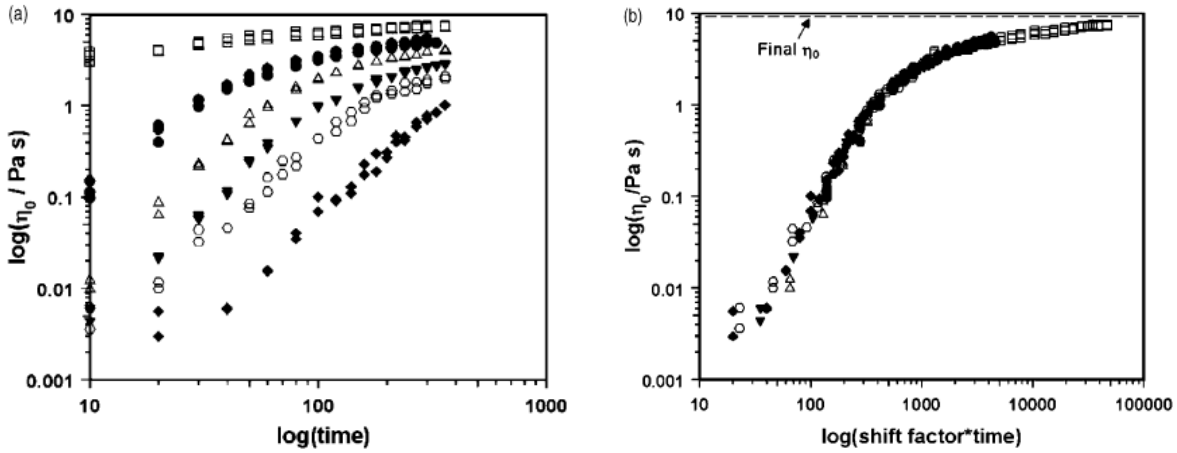

Figure 2-10: (a): Zero shear viscosity plotted against hydration time for the six grain sizes presented in Figure 2-9. Top curve to bottom curve: 80 µm to 500 µm. (b): Corresponding master curve of viscosity versus time produced from the (a) data by applying a time shift-factor (adapted from Wang et al)

This shift factor can be directly related to particle size by an empirical power law. The dissolution rate is expected to depend on grain surface for homogeneously spherical geometries and on volume for tessellated and complex geometries, which gives an exponent between 2 and 3. Indeed, the exponent of this law determined thanks to Figure 2-11 is 2.5 ± 0.3.
The increase of the dissolution rate with the grain size is in agreement with Parker et al results but the exponent of the power law is not the same.

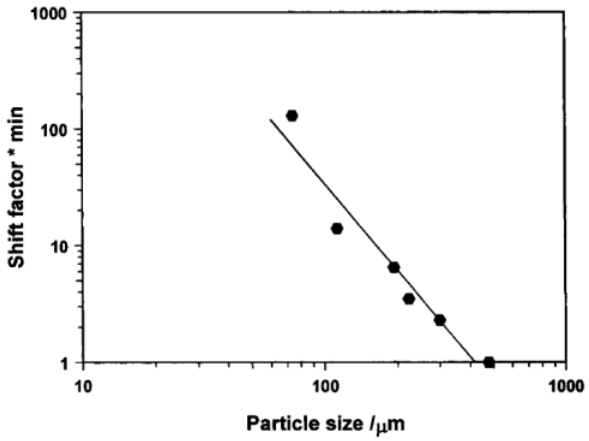

Figure 2-11: Time shift factor used in Fig 7b plotted versus particle size (adapted from Wang et al)

For all those experiments, the authors claim that the mixing velocity is chosen very high in order to neglect the impact on dissolution of the diffusion of the polymer in solution. However, in industrial processes, it is often impossible to increase too much the mixing velocity and the influence of diffusion has therefore to be investigated.

Devotta et al[37] also demonstrated that, for an high mixing velocities, the dissolution time decreases almost linearly with the particle size until a critical particle size under which the dissolution time becomes constant. They conducted dissolution experiments for various mixing velocities and they

observed that the dissolution time decreases with increasing velocity but also that the critical particle size increases with the rate of stirring (see Figure 2-12).

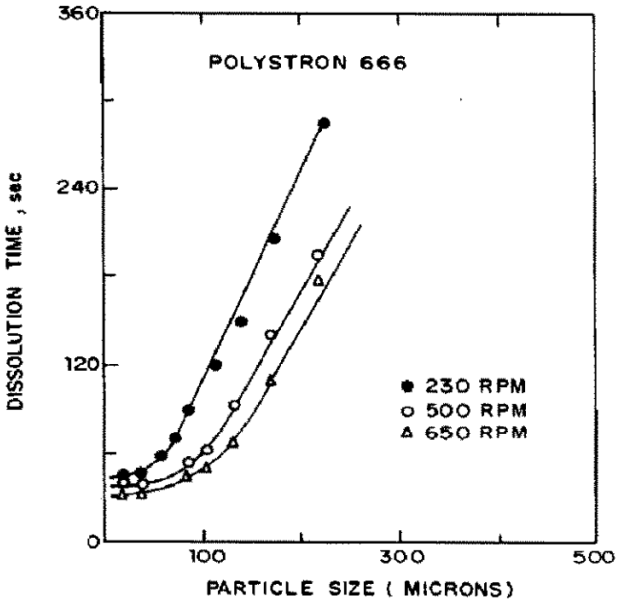

Figure 2-12: Dissolution time as a function of the average particle size of polystyrene particles ($1.6 \cdot 10^5$ g/mol) in cyclohexane at different stirring speeds (T=35°C)

Studies on polymer dissolution have also been conducted on polymer pieces of different geometries instead of grains. For instance, the effect of molar mass on the dissolution rate was investigated for polymer thin films. Papanu et al[38], observed that the dissolution rate in inversely proportional to the polymer molar mass, as for Wang and al. Pekan et al[39] made the same observation on glassy polymer disks.
Manjkow et al[40] observed that the dissolution rate is not only dependent on the polymer molar mass but also on its polydispersity. They found that a polydisperse polymer can be dissolved almost twice as fast as a monodisperse one.

To sum-up, there have been several experimental studies on polymer dissolution that have demonstrated phenomenologically that the dissolution is faster for small particle size and small polymer molar mass. Those studies have been conducted in the particular case of dispersing conditions (no lumps formation) and high mixing velocities. In those studies, the description of the dissolution kinetics is done with empirical laws and no theoretical models are proposed.

2.3.1.2 Dissolution with lump formation

Under non-dispersing conditions, i.e. when no particular efforts are done to ensure a perfect dispersion of the powder in the solvent and thus a single grain by single grain dissolution, a part of polymer grains are involved in lumps formation, which considerably slows down dissolution and increases characteristic dissolution time.

Kravtchenko et al[31] show that in this case, a single exponential (Eq 2-1) is no longer enough to describe the variation with time of the mass that is dissolved.
To take into account this phenomenon, another equation is developed with a sum of two exponentials:

$$m = A\left(1 - exp(-k_a t)\right) + B\left(1 - exp(-k_b t)\right) \qquad \textit{(Eq 2-3)}$$

Where $k_a > k_b$ and $A+B=m_{tot}$.

As we can see on Figure 2-13 below, the new equation fits quite well the data.

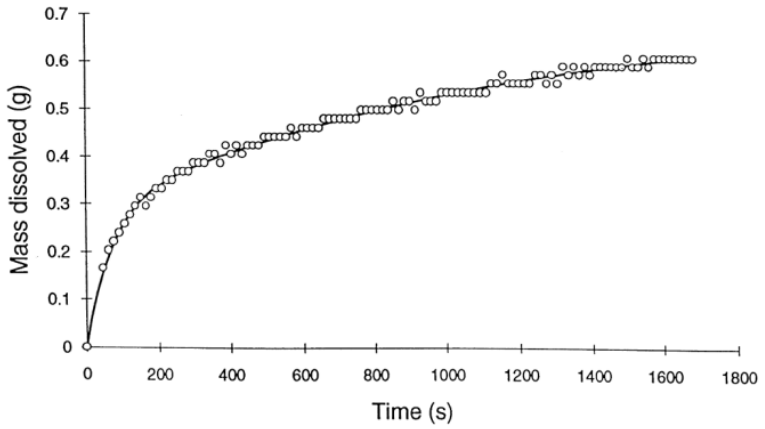

Figure 2-13: Dissolution kinetics of pectin under non-dispersing conditions (adapted from Kravtchenko et al)

The intuitive explanation for these two independent processes with different rates is that the fast one corresponds to dissolution of well dispersed individual grains and the slow one to dissolution of lumps. Experimentally they found that the value of k_a is close to the value of k, determined under dispersing conditions (see Figure 2-6), which means without lump formation. This observation evidences that the fast process is actually dissolution of individual grains.
Then, the prefactors A and B in (Eq 2-3) should correspond to the initial mass of grains involved respectively in individual dissolution and in lump formation, allowing the authors to define A as an index of polymer dispersibility (ID). The experiments show very reproducible values of this ID, which can thus be used to characterize a polymer tendency to form lumps.

Parker et al[32] also extrapolate their model equation (Eq 2-2) to take lumps formation into account. They used a bimodal approximation describing polymer powder in solution as the sum of two polydisperse populations, one composed by grains that dissolve individually and the other, much larger, by lumps.

Lump formation is due to grains swelling, which induces the apparition of a sticky, low permeability layer around grains blocking the pores between them before they can separate to dissolve individually. This phenomenon is most likely to occur with small particles. Experiments show that formation of lumps for polydisperse grains population is limited by the smallest grain size in the sample (see Figure 2-14 where unfractionated sample behaves similarly to fractions of smallest grain sizes).

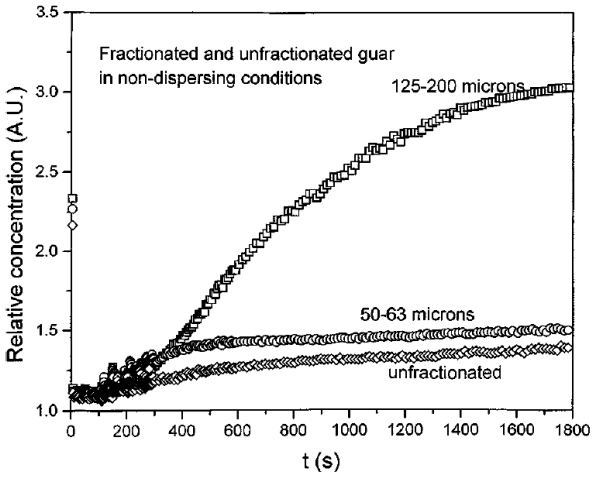

Figure 2-14: Sieved and non-sieved data for guar under non-dispersing conditions (adapted from Parker et al)

2.3.2 Theoretical approach of the dissolution mechanism

Even though dissolution mechanism of a polymer powder is really complex, some theoretical approaches have been done in the literature at grain scale. They are summarized in Miller-Chou et al review[41].

The complexity of the mechanism results from the fact that there are many different steps in the process which are impossible to separate. At the beginning of a dissolution experiment, polymer in the grains is in a glassy state. Water uptake induces a transition to a gel state. This gel is swollen by solvent. Polymer chains disentangle from the surface of the gel layer and finally migrate to the bulk through a boundary layer.

The positions of the glassy polymer/gel and gel/solution interfaces are described on Figure 2-15. They depend on different experimental parameters, as depends on those parameters the speed of each step.

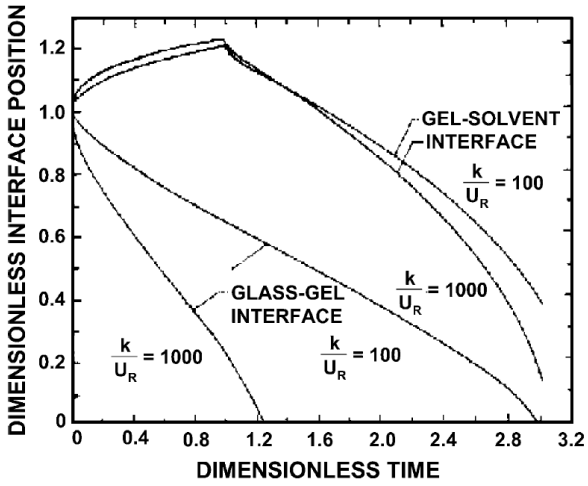

Figure 2-15: Movement of glass-gel and gel-solvent interfaces during the dissolution process (adapted from Ranade et al)

The disentanglement step of polymers in the rubbery state has been described by Brochard and De Gennes[42]. The theoretical situation studied is a droplet of semi-dilute polymer solution at a concentration c_0 with an initial radius r_0 immersed in a pure solvent.

In this case, dissolution process is divided in two steps, controlled by two different diffusion coefficients. The first one is the polymer gel swelling, where all polymer chains swell simultaneously from concentrated regions to less concentrated ones. It is controlled by the cooperative diffusion coefficient D_{coop}. During this step, the chains are stretched. Once the chains are stretched, the swelling slows down and the second step occurs. It consists in the viscous yielding of the polymer swollen network due to reptation of polymer chains from the network to the solvent bulk. It is controlled by a diffusion constant D_{rep} which is much smaller than D_{coop} because it is related to the diffusion of one polymer chain among the others during the reptation process. It is related to the reptation time τ_{rep} and the size of polymer coil.
Brochard and De Gennes define a characteristic length l corresponding to a critical value of r_0 at which what limits disentanglement changes of nature. The limiting step for disentanglement is not the same for $r_0 < l$ and $r_0 > l$.

$$l = [D_{coop}(c_0)T_{rep}(c_0)]^{1/2}$$

When the initial radius r_0 is smaller than the characteristic length l, swelling is fast and the limiting step is the viscous yield of polymer network. In this case, the overall dissolution time is equal to τ_{rep}. On the other hand, when r_0 is larger than l, the swelling process is the rate-limiting step. The overall dissolution time is then equal to r_0^2/D_{coop}. These conclusions are represented on Figure 2-16.

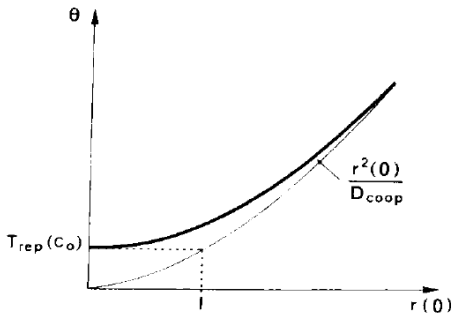

Figure 2-16: Dilution time ϑ versus the original droplet radius r_0 (adapted from Brochard and De Gennes)

Brochard and De Gennes results are limited to the case of semi-dilute polymer solutions in good solvents. Thus, they do not take into account glass transition which occurs in a polymer grain before the semi-dilute step.
More generally, there are no general theoretical models to describe the complete dissolution of dry polymer grains in a solvent.

In the literature, dissolution rate is always found experimentally to follow a law of the type

$$\tau \backsim \frac{1}{R^{\alpha}}$$

Where R is the grains radius, but the value of the exponent α is different in all the studies.
Experimentally, Kravtchenko et al obtain α=1 (see Fig 2) whereas Wang et al calculate α=2.5 (see Fig 6). The theoretical prediction of Brochard and De Gennes is α=2 (see Figure 2-16), which can be considered not so far from Wang et al experimental value. However, Brochard and De Gennes are not taking into account glass transition and, in the case where it is indeed the limiting step, water

penetration at a constant velocity in the polymer during this phase should set the coefficient α at the value α=1. This corresponds to Kravtchenko et al observations.
Moreover, Brochard and De Gennes have predicted no dependence between dissolution rate and molar mass but Wang et al have observed that they are inversely proportional to each other.
The contradictions between all those results show how complex is the problem of polymer powder dissolution and how difficult it is to elaborate a complete theory of it, especially if it has also to integrate the capillary imbibition.

3 Materials and Methods

3.1 Materials

3.1.1 Giant Polysaccharide (GP)

For confidentiality reasons, the polymer mainly studied in this manuscript will be called GP, for Giant Polysaccharide.

GP is a biopolymer produced by a naturally-occurring bacterial strain. It is a polysaccharide with an average molar mass of $5 \cdot 10^6$ g/mol. This value is given by the supplier and will be confirmed in paragraph 3.2.2. Its polydispersity index is unknown.

The GP monomer is presented in Figure 3-1. Its molar mass is around 1036 g/mol and its length is $3 \cdot 10^{-9}$ m.

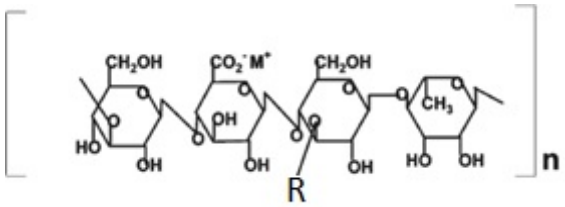

Figure 3-1: GP

According to the structural formula, GP is a polyelectrolyte with one counter-ion per monomer.

An elementary analysis was performed by the CNRS Analysis Central Service. For the cations, Sodium, Calcium, Potassium, Magnesium and Ammonium were found at the following mass fractions in gram per gram of sample:

Sodium	3942 ppm
Potassium	13400 ppm
Calcium	564 ppm
Ammonium	4420 ppm
Magnesium	293 ppm

For the anions, Acetate, Chlorure, Nitrate, Sulfate were found at the following mass fractions in gram per gram of sample:

Acetate	4762 ppm
Chlorure	566 ppm
Nitrate	68 ppm
Sulfate	205 ppm

A part of the cations are present in GP powder to compensate the anions charges and the other part are the counter-ions of the GP monomers. The number of cations available for compensate the GP monomer charges corresponds to 0,84 counter-ion per monomer. It means that 84% of the monomers are in basic form and 16% of the monomers are in acid form (see paragraph 3.2.3 for conductimetry measurements). Moreover, for one mole of GP monomers, there is about 0.1 mol of free cations and anions.

GP extensive characterization will be presented in paragraph 3.2.

3.1.2 Maltodextrin

Maltodextrin is a polysaccharide produced from starch by partial hydrolysis. It consists in glucose monosaccharide units connected in chains of variable length by glycosidic bonds (see Figure 3-2). Chains length is related to Dextrose Equivalence (DE) of maltodextrin which is roughly the fraction of glycosidic bonds in the starch that have been broken during hydrolysis. The higher the DE value is, the shorter the glucose chains are and the higher the solubility is.

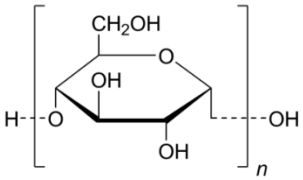

Figure 3-2: Maltodextrin

In this study, DE1, DE6 and DE29 maltodextrins were used. Their molar masses are as follow:
Maltodextrin DE29: about $2.5 \cdot 10^3$ g/mol
Maltodextrin DE6: about $8 \cdot 10^4$ g/mol
Maltodextrin DE1: about $5 \cdot 10^5$ g/mol

3.1.3 Polyethylene oxide

Polyethylene oxide (PEO) is a synthetic neutral semi-crystalline polymer (see Figure 3-3). Its molar mass may vary from a few hundreds to several million grams per mole.

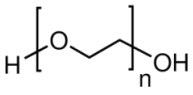

Figure 3-3: Polyethylene oxide

In this study, four PEO with different molar masses M_w were used. They are shortened as follow:

- PEO_0.3M for $0.3 \cdot 10^6$ g/mol PEO
- PEO_0.6M for $0.6 \cdot 10^6$ g/mol PEO
- PEO_1M for $1 \cdot 10^6$ g/mol PEO

- PEO_8M for $8 \cdot 10^6$ g/mol PEO

The overlap concentration of PEO (see paragraph 2.1.2) will be needed in the following chapters. It was calculated from the radius of gyration values obtained with a formula established for PEO by Devanand and Selser[43]:

$$R_g = 0.215 {M_w}^{0.583} \text{ (Å)}$$

Knowing that the hydrodynamic radius $R_h = 0.72 R_g$ ([4]) and the volume of a single chain in dilute solution $V_{chain} = \frac{4}{3}\pi {R_h}^3$ we have

$$C^* = \frac{M_w}{N_a \frac{4}{3}\pi {R_h}^3}$$

$N_a = 6.02 \cdot 10^{23} mol^{-1}$ is the Avogadro number.

The overlap concentration values are summarized in the following table.

Polymer name	C^*
PEO_0.3M	9.5 g/L
PEO_0.6M	5.7 g/L
PEO_1M	3.9 g/L
PEO_8M	0.8 g/L

This study focused mainly on GP but Maltodextrin and PEO were also studied for comparison.

3.2 Materials characterization

3.2.1 GP powder

GP is found on the market in powder form at different grades obtained by sieving the samples with controlled-size mesh. In this study, a powder with a cut-off size of the mesh and grain size of 74µm is always used unless otherwise specified in the protocol. In the industry, the granulometry is often given in mesh, which is a unity related to the inverse of sieves mesh size. The cut-off size of 74 µm correspond to a granulometry of 200 mesh.

Particle Size Distribution measurements realized on a Malvern Mastersizer using a non solvent, ethanol, as a carrier liquid and ultrasounds to disperse particles revealed a Gaussian size distribution between 1 µm and 100 µm instead of a cut-off at 74 µm as expected. This is due to the particles non-spherical shape: its smallest dimension allows the particle to pass through the sieve even if its equivalent diameter is above cut-off size.
The polydispersity and the non-spherical shape of the grains were confirmed by Scanning Electron Microscopy (SEM) pictures such as the one presented in Figure 3-4 where the grains are found to have an elongated shape and a wide polydispersity in size.

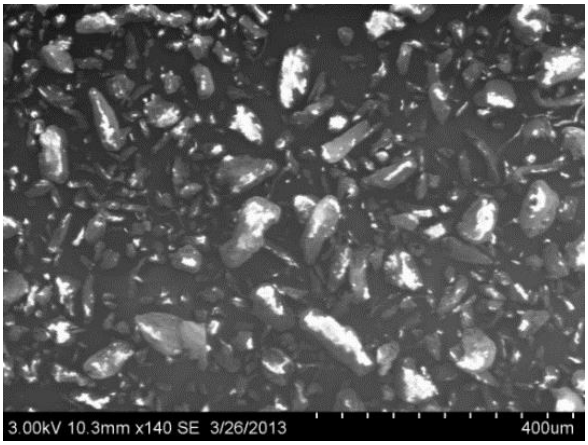

Figure 3-4: SEM picture of GP particles

A powder is a porous media with two porosity scales: mesoscopic porosity due to large pores between agglomerated particles (usually measuring a few tenth of the grains diameter) and microscopic porosity inside the particles. Mercury intrusion porosimetry was used to determine the pore diameter distribution as presented on Figure 3-5 where the cumulative pore volume and its derivative are represented as a function of the pore diameter (a reverse x-axis is used for the pore diameter).

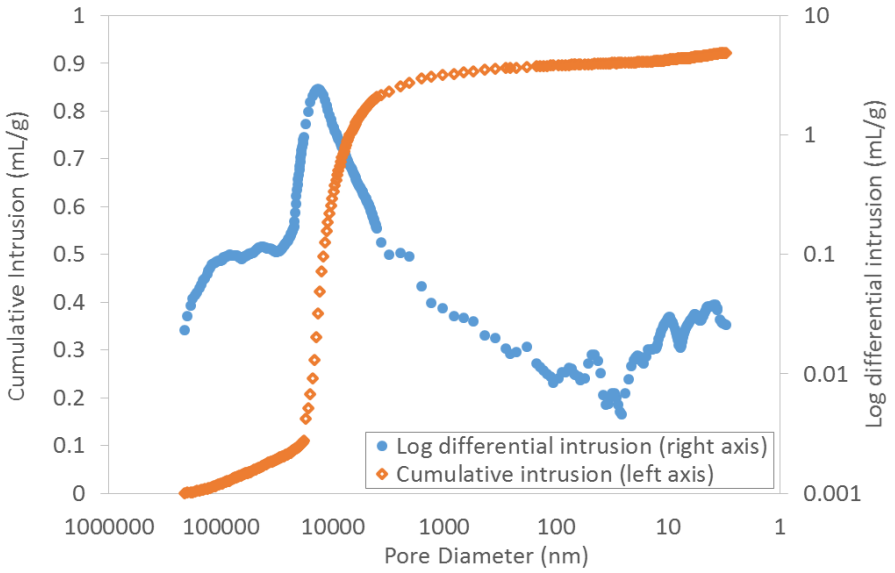

Figure 3-5: Mercury porosimetry on a sample of GP 200 mesh

The first peak around 10 µm on the differential intrusion curve (blue circles) corresponds to the mesoscopic porosity for an average grain diameter of 40 µm. It is consistent with the granulometry measurements. A second smaller peak seems to appear between 10 nm and 3 nm. It is attributed to the porosity inside the grains.

According to the literature[44], GP anhydrous density is 1.5.

3.2.2 GP chains

In the literature[45], GP molar mass is said to be around $5 \cdot 10^6$ g/mol. Direct confirmation of this value by Gas Permeation Chromatography (GPC) is impossible for such a high molar mass. However, it can be calculated thanks to a measurement of GP hydrodynamic radius and overlap concentration because

$$C^* = \frac{M_w}{N_a V_{chain}}$$

And

$$V_{chain} = \frac{4}{3}\pi {R_h}^3$$

So

$$M_w = \frac{4}{3}\pi {R_h}^3 N_a C^*$$

Measurements of GP overlap concentration C* will be presented in paragraph 3.2.5. The value obtained from this measurement is 0.15 g/L. It will be used to evaluate GP molar mass.

The hydrodynamic radius was measured by Dynamic light scattering (DLS). In this technique, a polymer solution below the overlap concentration is used. It is lit by a monochromatic laser. Each polymer chain is isolated and scatters the laser light. The scattered light intensity fluctuations are related to the polymer whole chain motion. The scattering signal autocorrelation decreases in time depending on the particles motion. The thermal motion is set by the diffusion coefficient which itself is related to the particle size.
DLS measurements were conducted at a scattering angle of 90° at room temperature. Results for GP dissolved in deionized water were not very satisfying because polyelectrolyte chains does not adopt a spherical coil configuration due to charge repulsions. A DLS measurement was performed with a salted GP solution ([NaCl]=$2 \cdot 10^{-2}$ mol/L) because the presence of salt screens the interactions and the chains are allowed to form spherical coils. GP hydrodynamic radius was thus roughly estimated as R_H=220 nm.

The calculated molar mass is then M=$4 \cdot 10^6$ g/mol. Considering the important variability of the DLS measurement and the fact that the molar mass varies as the cube of the hydrodynamic radius, this result is consistent with the value of $5 \cdot 10^6$ g/mol which will be used in the following for the molar mass.

3.2.3 GP solution properties

Surface tension measurements were realized on a GP solution. The surface tension was found to be equal to water surface tension measured in the same conditions, meaning that GP is not a surfactant.

pH and conductimetry measurements were realized on a 0.1%wt GP solution. pH was found to be equal to 5.5 ± 0.1 and conductivity to 100 µS/cm ± 2 µS/cm.
Knowing that in a GP solution 84% of the monomers are in the basic form and 16% are in the acid form, GP pK_a is calculated.

$$pK_a = pH - \log\left(\frac{base}{acid}\right) = 4.8$$

This is a consistent value for a carboxylic acid and it is in good agreement with the value of 4.6 obtained by acido-basic titration.

3.2.4 Sorption isotherm

GP is a hydrophilic and hygroscopic polymer. When exposed to water vapor, is absorbs water at a given mass fraction ϕ so as to be in equilibrium with the ambient atmosphere. More precisely, equilibrium is obtained when absorbed water and vapor have the same water activity.
Water activity a_w is defined as the ratio of p, the vapor partial pressure of water at equilibrium, to p_o, the saturated vapor pressure of water at the same temperature. In the case of the atmosphere, which is an air/water system, a_w is equal to the relative humidity RH.
GP powder equilibrates with the atmosphere. Water content in GP is directly related to water activity (a_w) of the atmosphere by the sorption isotherm.

In order to determine this isotherm, few amounts of powder were placed in desiccators with saturated salt solutions setting the water activity at different levels, and left during weeks. They are weighted once a week. When the weight does not vary any more, they are considered as having reached the equilibrium point.
The precise rate of absorbed water is determined by Thermo Gravimetric Analysis (TGA). It is a precision balance placed in a furnace where the temperature is precisely known and controlled. The powder weight loss measured after 30 minutes in the furnace at 110°C in an N_2 atmosphere corresponds to the initial water content in the sample. Results are presented in Figure 3-6 where water content is the mass fraction of water ϕ in the GP powder and water activity is taken as the RH at with GP was equilibrated.

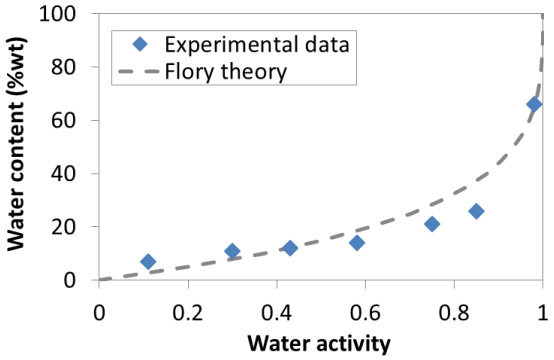

Figure 3-6: GP sorption isotherm determined by TGA. The dotted line correspond to the Flory-Huggins expression with χ=0.5

The Flory-Huggins theory is often used to describe the sorption isotherm of polymers. It gives the following expression for water activity a_w as a function of the water fraction ϕ:

$$a_w = \phi \exp\left((1-\phi) + \chi(1-\phi)^2\right)$$

where χ quantify the affinity between the polymer and the solvent. In our case, we take χ=0.5.

a_w^g, the water activity at which glass transition occurs, is roughly estimated by observing the aspect of the powder samples equilibrated at different a_w. For $a_w \geq 85\%$, the powder is sticky and looks melted whereas for $a_w \leq 75\%$, the powder is dry. a_w^g is thus approximately equal to 80%.

3.2.5 Rheological behavior

3.2.5.1 Material and methods

The rheological behavior of aqueous solutions of GP has been studied on an AR1000 and an ARG2 rheometer (TA Instrument). Both are rotational rheometers which apply a controlled shear stress and measure the induce shear rate. The geometry used to perform viscosity and modulus measurement on pre-prepared solutions is a steel cone and plate sample cell. The plate radius is 40 mm, the cone angle is 2° and the gap between the cone and the plate is set to 56 µm.
For the most diluted solutions, measurements were performed on a Low-Shear rheometer using a Couette geometry to apply a controlled shear rate.

For steady viscosity measurement, a logarithmic ramp of shear stress ranging from 0.01 Pa to 50 Pa is applied to the sample at 25°C. For each point, the measurement lasts 10 seconds and is repeated until the sample is at equilibrium (defined when the error percentage between two measurements lays below 5%) within a limit of one minute.
For linear viscoelasticity measurements, the sample is submitted to a frequency sweep between 0.1 and 100 Hz at 5 Pa at 25°C. A previous stress sweep test has shown that at this stress, rheological properties of the sample are in the linear range.

3.2.5.2 Flow measurements: viscosity

Flow measurements were performed on several solutions at different concentrations between 0.025%wt and 0.9%wt of GP. Results are presented in Figure 3-7 where the viscosity η is plotted as a function of the shear rate $\dot{\gamma}$.

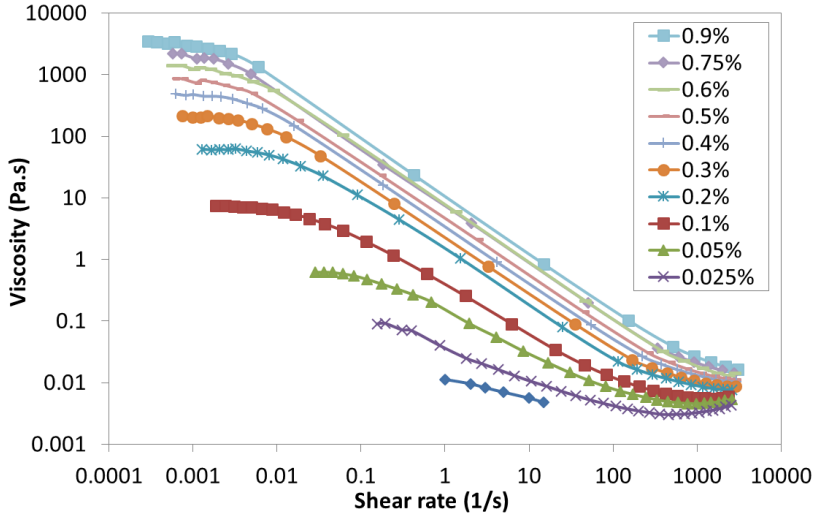

Figure 3-7: GP rheological behavior under continuous shear at different concentrations

We observe that at a given concentration and for low shear rates ($\dot{\gamma} \leq 1/\tau$ where τ is the characteristic time of the solution), GP structure is not affected by the shear so GP viscosity does not depend on shear rate. It is the first Newtonian plateau. At higher shear rates ($\dot{\gamma} \geq 1/\tau$), the flow is responsible for a modification of the polymer structure, namely polymer chains disentanglement and GP viscosity decreases along with shear rate while shear stress remains constant. Finally, at very high frequencies, viscosity reaches a second Newtonian plateau. The polymer chains are completely disentangled by the flow and stretched in the flow direction. GP solutions viscosity tends towards solvent (water) viscosity. This is the characteristic behavior of a shear-thinning polymer.

The viscosity of a GP solution increases along with polymer concentration. Due to the shear-thinning behavior of GP, the increasing law depends on the measurement shear rate.

Viscosity of a GP solution at the Newtonian plateau is presented in Figure 3-8 as a function of the polymer mass fraction ϕ.

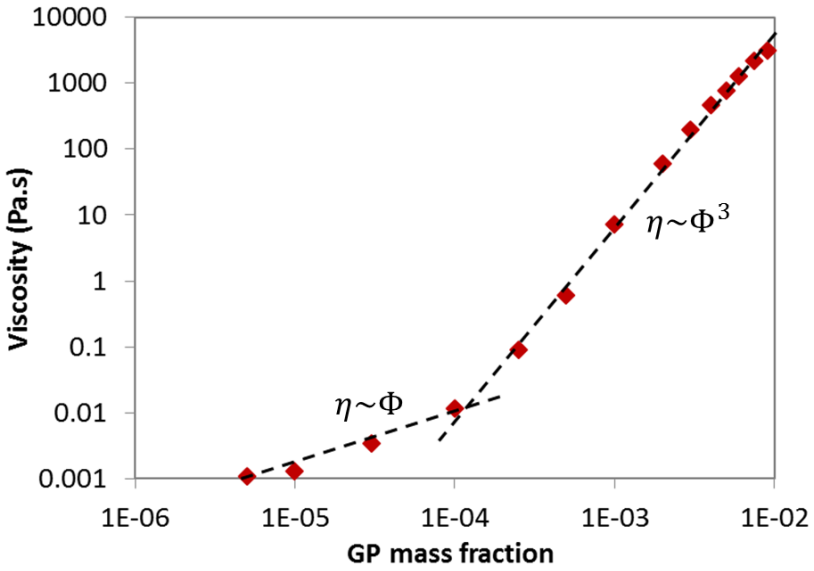

Figure 3-8: Effect of the concentration on GP viscosity at the Newtonian plateau

For semi-dilute solutions ($\phi > 10^{-4}$) and vanishing shear rates, the plateau viscosity varies with the concentration to the power 3. For dilute solution ($\phi < 10^{-4}$), the viscosity measurements were performed with the Low-Shear rheometer. The viscosity is independent of the shear rate all along the range accessible with the Low-Shear rheometer (Newtonian behavior) and the viscosity is linear in concentration.

The overlap concentration is determined experimentally as the concentration at which a change in the slope of the viscosity versus concentration curve is observed. We find $\phi^* = 1.5 \cdot 10^{-4}\, g/g \pm 0.5 \cdot 10^{-4}\, g/g$ which i.e. C^*= 0.15 g/L ± 0.05 g/L. It is in good agreement with the value of 0.2 g/L found in the literature[44].

3.2.5.3 Oscillatory measurements: storage and loss moduli

Oscillatory measurements were performed on several solutions at different concentrations between 0.1%wt and 3%wt of GP. The storage modulus G' characterizes the fluid elastic response and the loss modulus G'' characterizes the fluid viscous response. Both of them are plotted as a function of the frequency on Figure 3-9. G' is represented by diamonds and G'' is represented by circles.

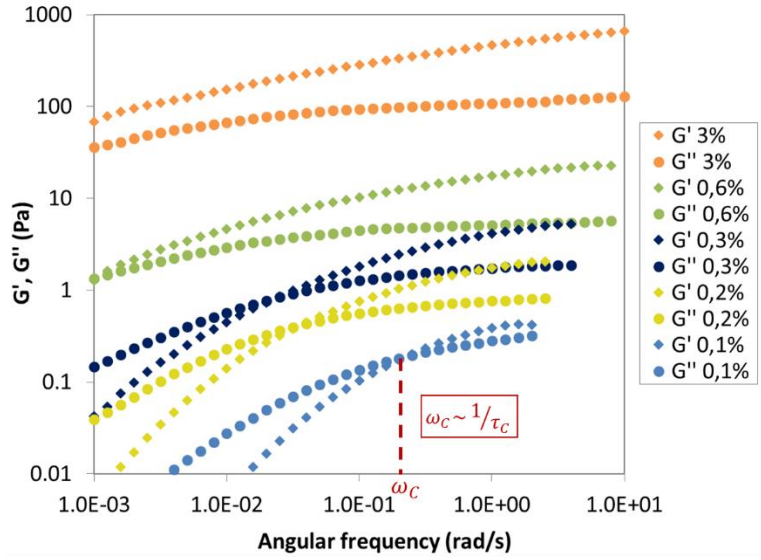

Figure 3-9: Storage and loss modulus for GP gel at different concentrations

GP has a viscoelastic behavior (see Annex 8). At low frequencies the loss modulus is larger than the storage modulus. GP solution behaves like a viscous fluid. On the contrary at high frequencies the loss modulus is lower than the storage modulus. GP solution behaves like an elastic solid. The limit between those two behaviors is given by the intersection between the two moduli. The intersection frequency ω_c decreases when the concentration increases.

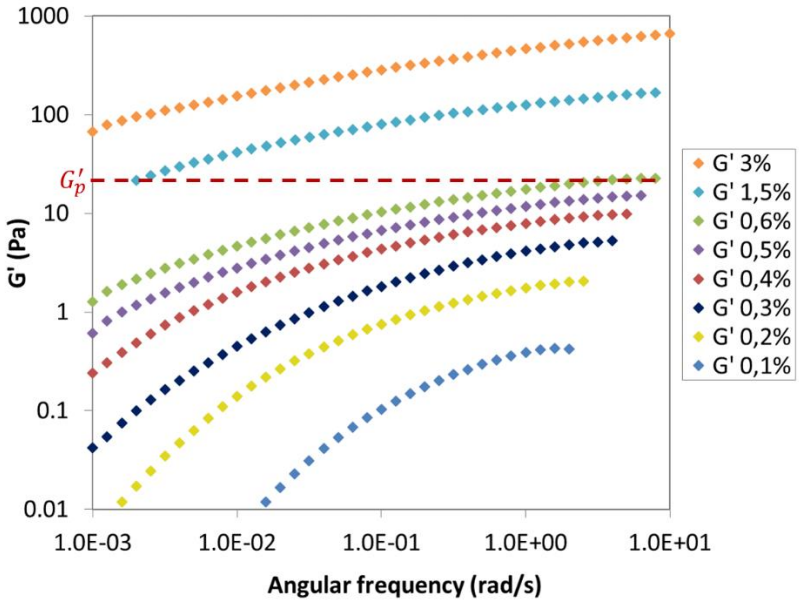

Figure 3-10: Storage modulus for GP gel at different concentrations

At high frequencies, the storage modulus reaches a plateau. The value of the plateau modulus G'_p increases with the concentration (see Figure 3-10). The variation law will be presented in the next paragraph.

3.2.5.4 Rheological behavior of a GP solution: Reptation time

De Gennes suggested a model for the motion of linear entangled polymer called the reptation model. In this model, the polymer chain motion is restricted to a tube created by the surrounding chains (Edwards tube).The time needed by the chain to diffuse out of the original tube of length L is the reptation time τ_{rep}.

As presented in Annex 8, the reptation time can be estimated as the inverse of the intersection frequency ω_c. The reptation time can also be estimated in flow, where it corresponds to the reciprocal of the shear rate at which viscosity begins to decrease, called $\dot{\gamma}_c$. It is related with the fact that, at this point, when disentanglement occurs, entanglements do not have time to be created again in the flow. Doi Edwards model for semi-dilute solutions predicted a power law dependency between reptation time and concentration[46]:

$$\tau_{rep} \sim \varphi^{3/2} \qquad \textit{(Eq 3-1)}$$

As explained in Annex 8, Doi-Edwards model also predicted the following relationship between plateau modulus G'_p and polymer concentration.

$$G'_p \sim \varphi^{9/4} \qquad \textit{(Eq 3-2)}$$

As shown on Figure 3-11, this law is verified by experimental data taken from the oscillatory measurements of GP solutions shown in Figure 3-10.

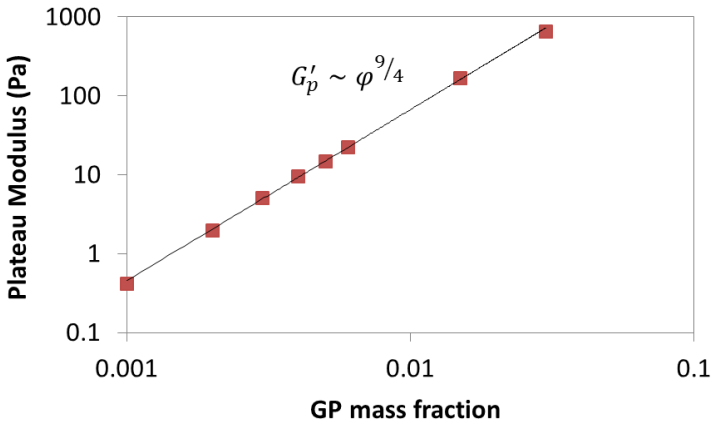

Figure 3-11: Plateau modulus versus concentration for GP solutions

Another way to evaluate the reptation time from the plateau modulus G'_p is

$$\tau = \frac{\eta}{G'_p}$$

where η is taken from the flow measurements at the low shear Newtonian plateau.

Experimental data are presented in Figure 3-12 where the characteristic time $\tau = 1/\omega_c$ measured by oscillatory measurements, the characteristic time $\tau = 1/\dot{\gamma}_c$ measured in flow experiments and the characteristic time $\tau = \eta/G'_p$ calculated from both types of experiments are plotted as a function of GP mass fraction.

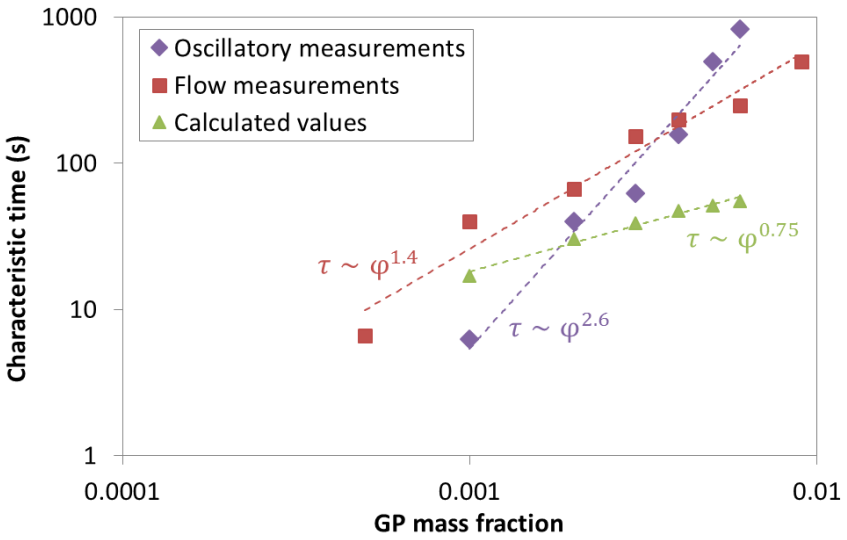

Figure 3-12: Characteristic time versus concentration for GP solutions obtained by three different techniques

Measurements of the characteristic time obtained by flow experiments can be fit to a power law with exponent 1.4. They are in good agreement with (Eq 3-1).
Data obtained by oscillatory measurements fit to a power law with exponent 2.6 and are not in good agreement with (Eq 3-1). Data obtained from both experiments by calculating $\tau = \eta/G'_p$ fit to a power law with an exponent 0.75. They are not in good agreement with (Eq 3-1) either.
Those discrepancies can be attributed to several factors. First, the frequency range that can be explored with the rheometer for oscillatory measurements is limited and a power law fit over less than one decade in concentration is not very reliable.
Second, the definition of a single reptation time is correct when the Maxwell model is well verified by the polymer rheological behavior. For GP, the definition of a single reptation time is an approximation because of the polydispersity of chains length. Its rheological behavior would be better explained with a distribution of reptation times.
In particular, the $\tau = \eta/G'_p$ law is only valid for polymer verifying the Maxwell model. For GP, knowing that $\eta \sim \varphi^3$ (according to Figure 3-8) and $G'_p \sim \varphi^{9/4}$ (according to Figure 3-11), the expected scaling law will be $\tau \sim \varphi^{3/4}$, which is verified experimentally (see Figure 3-12).

In the following chapters we will use the power law obtained from the flow experiments because it is in good agreement with the simple Doi-Edwards model. Reptation time can thus be extrapolated at any concentration using the following law:

$$\tau_{rep} = 6 \cdot 10^5 \cdot \varphi^{3/2} \qquad \textit{(Eq 3-3)}$$

3.3 Polymer layers preparation

We have conducted different experiments which required polymer layers of different thicknesses deposited onto solid substrates. In the following, the methods used to prepare those layers will be described.

All polymer layers were prepared from polymers solutions which were stirred for at least 24 hours before being used. To preserve the polymer after dissolution and avoid rotting, a few milligrams per liter of NaN_3 were added to each solution.

For wetting experiments, silicon wafers were used as substrates for polymer coating. They were oxidized using H_2O plasma treatment (30 seconds of exposure) or UV-ozone treatment (15 minutes of exposure) and coated with polymer solution within the ten following minutes. Plasma / UV-ozone treatments were made to control the wafers surface properties. Thanks to that treatment, wafer affinity for water was increased and contact angle was reduced to almost 0°, facilitating polymer solution spreading.
Thin layers were produced using a spin-coating method (see Figure 3-13). By adjusting polymer solution concentration, acceleration and spinning velocity, thickness of the deposited films can be precisely controlled. However, preparation of homogeneous layers is limited by the very high viscosity of GP solutions even at low concentrations. Indeed, a satisfactory spreading of the solution on the wafer requires a small enough viscosity. The use of a very small acceleration velocity made it possible to obtain quasi-homogeneous layers. The best compromise was achieved with GP solution at 0.4%wt, acceleration of 30 rpm/s and rotation at 3000 rpm during 180 s. Layers of a few tens of nanometers thickness were obtained with this protocol.

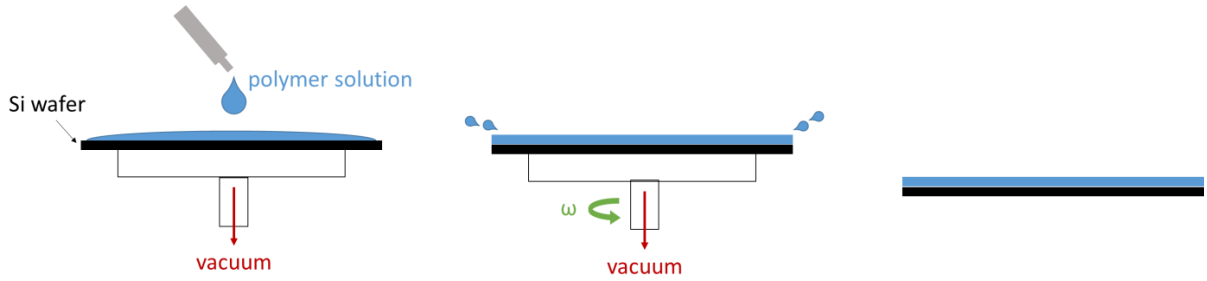

Figure 3-13: Schematic representation of the spin-coating process

Layers of larger thickness could not be produced by spin-coating. In that case, GP solution at 0.75%wt was deposited onto oxidized wafers with a pipette and the solution excess was removed with a controlled-thickness scraper. Then wafers were left to dry at room temperature. Viscosity of a GP solution at 0.75%wt is large enough to allow the scraper technique because the polymer solution dries before flowing. Two different scrapers (75 µm and 500 µm) were used, leading to two different layer thicknesses (around 500 nm and around 3 µm).
A few layers were also made by precipitation in alcohol instead of air drying. GP solution was deposited onto an oxidized wafer inside a Petri box in order to cover the whole wafer surface. Ethanol was added

above the polymer solution and left a few minutes to let water diffuse in it. The operation is repeated several times before letting the layer dry.

For swelling experiments, much thicker layers were required. Glass slides were used as solid substrates and 7-mm-high, 1-cm-large and 2-cm-long PDMS molds were used to hold back polymer solutions (see Figure 3-14). The layer thickness is determined by the mold size and the solution concentration. For most of the samples, 3%wt GP solution was employed. Part of the solution always dried on the mold walls and was removed after complete drying. The remaining layer thickness was around 50 µm, depending on the amount of dried polymer on the walls.

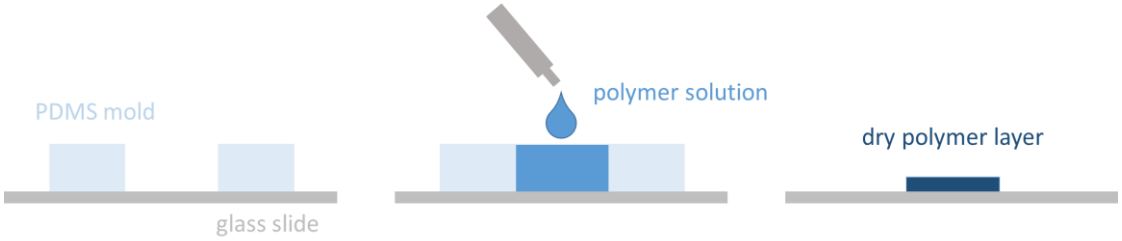

Figure 3-14: Preparation of GP thick layers

3.4 Polymer layers characterization

For thin enough layers, the thickness can be measured by ellipsometry. It is an optical method where the complex reflectance of a polarized laser beam illuminating the layer is measured. A model analysis, which takes into account this measurement, the layer refractive index and the estimated thickness of the layer, is then performed.
This method is suitable for thicknesses ranging between a few nanometers and one micrometer. It was used to characterize spin-coated layers. GP refractive index was supposed to be close to maltodextrin index and an index of 1.56 was taken. An incident angle of 70° for the laser beam was chosen. The measured thickness was 41 nm ± 2 nm, depending on where the measurement was performed on the layer. No roughness could be detected.

For scraper layers, the thickness measurements were performed using an Atomic Force Microscope. Atomic force microscopy (AFM) is a type of scanning probe microscopy with a very high-resolution, typically of the order of a few angstroms. The atomic force microscope consists in a cantilever with a sharp tip called the probe which is used to scan the sample surface. When it is brought close to the surface, interactions lead to the deflection of the cantilever. It is related to the relative height of the sample zone below the probe.
A notch was carved on the layer down to the wafer and the layer thickness was measured by difference. Topography of the layer was obtained by scanning the surface around the notch. For layers obtained with the 500 µm scraper, measured thickness was between 1.5 µm and 3.5 µm depending on where the notch was done. Roughness was about 500 nm (see Figure 3-15). For those obtained with the 75 µm scraper, measured thickness was around 400 nm with a roughness around 200 nm.

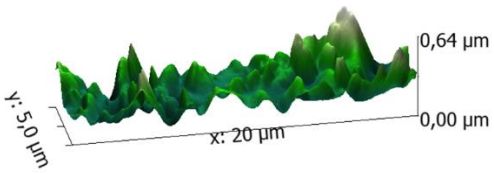

Figure 3-15: GP layer roughness (3D AFM plot)

For molded layers, thickness was measured by homemade mechanical sensor. Precision is around a micrometer. Layers thicknesses were between 10 µm and 80 µm, depending on preparation concentration and drying. Thickness also varied by several micrometers across the same layer. Roughness was under a micrometer.

3.5 Conclusion

Studies presented in the following chapters were mainly conducted with GP, which extensive characterization was presented in this chapter.
GP is a weak polyelectrolyte with less than one counter-ion per monomer. It has a molar mass of several millions gram per mole, which is extremely high for a polymer. Consequently, viscosity of a GP solution is much larger than water viscosity, even at very small concentrations. For instance at 0.1%wt, which is the concentration used in the industrial application, viscosity at the Newtonian plateau is already ten thousand times the water viscosity! Due to the large chain length, the overlap concentration is small (0.2 g/L) and above it, entanglements are responsible for the viscoelastic behavior of GP solutions. Reptation time of a GP chain can be determined as a transition time between an elastic behavior due to polymer network persistence and a viscous behavior where the polymer flows. It is also very large, reaching almost 10^3 s for a 1%wt GP solution, and increases with the concentration to the power 3/2.
All those characteristics made the elaboration of smooth reproducible films for dissolution experiments very challenging.

Other polymers were also studied as comparison. Maltodextrins are polysaccharide like GP which were extensively used by J. Dupas during its phD thesis to study the wetting of soluble polymers by their solvents. They are available with different molar masses. In this study, they were used to investigate the effect of molar mass on wetting and capillary imbibition. Polyethylene oxide is a neutral polymer often used as a model polymer in the literature[47]. It is available with different molar masses. It was used to investigate the influence of charges and molar mass on polymer dissolution.

4 Wetting

In this chapter we will focus on the first step of the dissolving process which is the onset of the contact between polymer and water. We will study the behavior of a water droplet deposited on a polymer substrate. First we will describe a simple qualitative experiment made to evidence the specific hydrophobic behavior of GP. Then we will study the spreading of a water droplet on a GP layer and compare it with the results obtained by Dupas et al on small molar mass polysaccharides.

4.1 Preliminary experiment: Water droplet deposited on polymer powder

Water droplets of controlled volumes were deposited onto reproducibly packed polymer beds and left at ambient atmosphere until full evaporation of water. A series of Maltodextrins powders of different molar masses and GP were used to investigate the effect of molar mass for a given granulometry. Droplets were deposited on the edge of the powder bed and pictures from the side were taken through the transparent wall of the dish containing the powder. A series of such side pictures taken after 1 s are presented in Figure 4-1 and corresponds to an increasing molar mass from left to right.

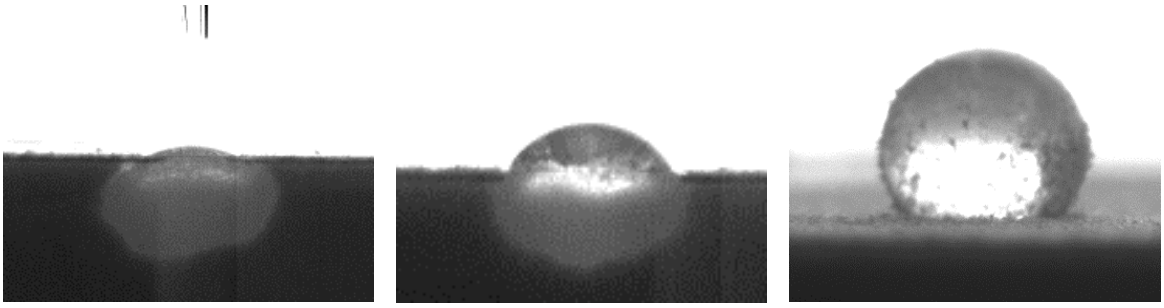

Maltodextrin DE29 Maltodextrin DE1 GP

Figure 4-1: Deposit of a 10 µL deionized water droplet onto a compact polymer bed. Left: Maltodextrin DE29; Middle: Maltodextrin DE1. Right: GP. All 3 images were taken 1 s after the droplet deposition.

The droplet behavior strongly depends on the polymer molar mass. For Maltodextrin DE29 powder (smallest molar mass), the droplet rapidly imbibed the powder, completely penetrating inside the bed in around 1 s (see Figure 4-1-Left). On the contrary for GP (highest molar mass), the water droplet stayed on top of the powder bed and never imbibed the grains, nor spread onto the powder bed (see Figure 4-1-Right). The macroscopic contact angle observed is large, close to 120°. It is characteristic of poor wetting conditions. Moreover, as soon as the droplet reached the powder, grains began to migrate from the powder bed to the droplet surface and finally recovered it. This phenomenon was previously described in the literature by Aussillous and Quéré[48,49] and McEleney et al[50] for non-soluble hydrophobic particles. The obtained decorated droplets were named “liquid marbles”. We thus observe that dry GP powder behaves as a hydrophobic powder although it is a hydrosoluble polymer. It is consistent with the large contact angle of water droplets observed. For Maltodextrins of intermediate molar mass, the imbibition was slower than for Maltodextrin DE29 but the water finally penetrated inside the powder bed and no hydrophobic behavior was observed (see Figure 4-1-center).

Figure 4-2: Maltodextrin DE29 pancakes obtained after evaporation of several droplets of different sizes deposited on the same powder bed

After total evaporation of water, a hard polymer "pancake" due to polymer dissolution in the droplet and/or grains aggregation remained on the powder bed (see Figure 4-2). It was easily separated from the intact polymer powder and weighted. This experiment was performed on the three Maltodextrins of different molar masses and on GP for different droplet volumes and repeated three times for each configuration. The results are highly reproducible. They are summarized on the graph presented on Figure 4-3.

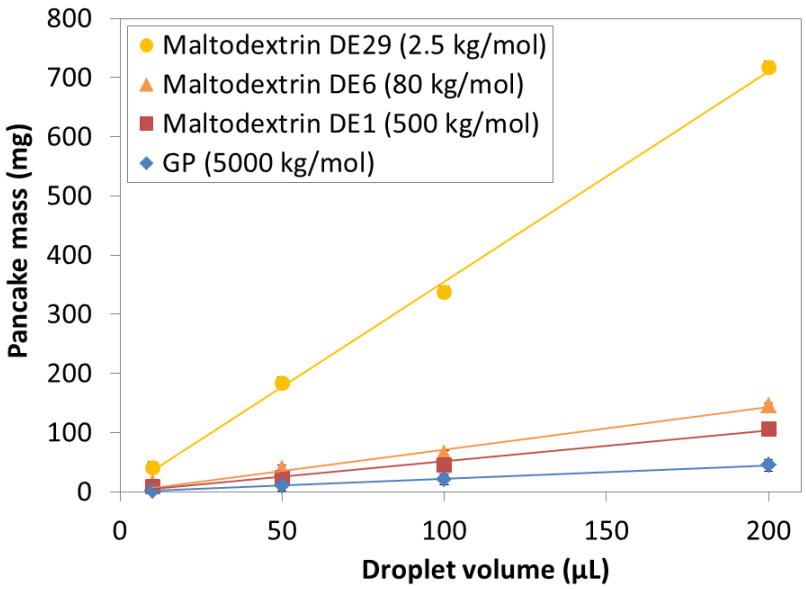

Figure 4-3: Influence of the droplet volume on the mass of the polymer pancakes obtained by deposit of a water droplet onto a polymer bed

The "pancake" mass represents the mass of polymer dissolved or incorporated in the water droplet before drying. For each polymer, it varies linearly with the droplet volume. This indicates that the maximum value of polymer concentration before drying is the same whatever the volume of the droplet is. This value, denoted α_{max}, is measured through the slope of the pancake mass versus droplet volume curves for every polymer. Results are reported in the following table.

Polymer	α_{max} (g/g)
GP	0.23
Maltodextrin DE1	0.52
Maltodextrin DE6	0.69
Maltodextrin DE29	3.55

Those mass fractions α_{max} are much higher than the concentrations that can be reached for homogeneous solutions obtained by mixing the polymer powder with water in a vial with a magnetic stirrer. For instance, the maximum mass fraction that was prepared for GP solutions is 0.03. At this concentration the elastic modulus is much higher than the viscous modulus and the solution does not flow. It means that most of the polymer grains incorporated in the pancake are probably not properly dissolved.

As presented in Figure 4-4, α_{max} decreases with the polymer molar mass.

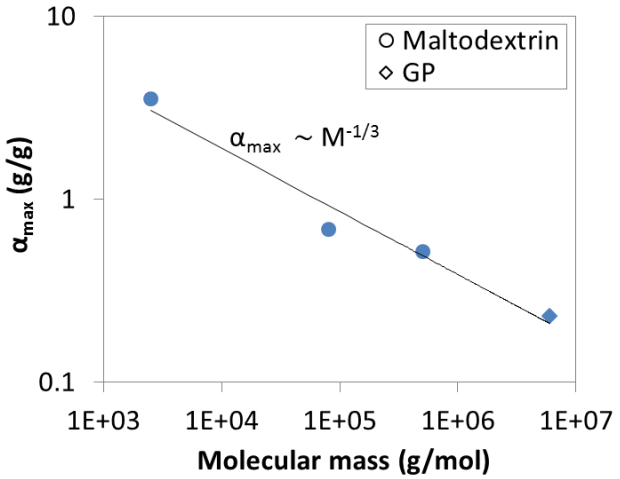

Figure 4-4: Influence of the molar mass on the coefficient α_{max}

The same experiments were realized with three granulometries of GP. Results are presented in the following table. We find that α depends on the powder granulometry decreases with the grain size.

GP	α_{max} (g/g)
80 mesh (< 200 µm)	0.14
200 mesh (< 70 µm)	0.23
750 mesh (< 20 µm)	0.45

This simple test combines in fact various aspects of dissolution. First, water advance on the polymer is controlled by wetting. But rapidly the polymer forms a gel that also hinders water penetration inside the powder. Surprisingly, the maximum mass fraction of polymer dissolved in a water droplet α_{max} is independent of the droplet size. However, owing to the coupling between different phenomena, this test is difficult to interpret.

A possible explanation of these results is that this maximum value α_{max} corresponds to an elastic modulus of the gel G' for which the droplet cannot deform enough anymore to penetrate further inside the powder bed. A characteristic length for this problem is the elasto-capillary length. It compares surface energy and elastic energy resulting from a deformation and writes as

$$l_{ec} = \frac{\gamma}{G'}$$

γ is the liquid surface tension and G' is the elastic modulus of the GP gel.

G' increases with GP concentration and surface tension of GP solutions is equal to water surface tension and does not depend on the GP concentration. l_{ec} thus decreases when the gel mass fraction increases.

For a water droplet on a GP gel at 23%wt it is

$$l_{ec} = \frac{\gamma}{G'} = \frac{7 \cdot 10^{-2}}{6 \cdot 10^{4}} \sim 1\ \mu m$$

Where G' is the elastic modulus of a GP gel at 23%wt extrapolated from (Eq 3-2).

1 µm is the order of magnitude of the smallest grains in 200 mesh GP powder.

Therefore, when the elasto-capillary length reaches the grain size, it becomes impossible to incorporate more powder grains and the maximum mass fraction α is reached.

It is clear that GP in contact with water presents a hydrophobic behavior leading to a poor imbibition of the GP powder by water.

The wetting behavior will be more quantitatively studied with water droplets deposited on GP homogeneous layers. Experimental methods and results are presented in the next paragraph.

4.2 Wetting experiments on polymer layers

Decoupling the different phenomena at stake during GP dissolution is interesting to understand the dissolution process. To dissociate as much as possible wetting from swelling, wetting experiments were performed on flat and well controlled polymer layers. In practice, both spontaneous and forced spreading experiments of sessile droplets were performed.

4.2.1 Experimental set-up

Coated wafers used for the wetting experiments were prepared as presented in paragraph 3.3. Then they were placed in a home-made transparent PMMA chamber tightly closed at the top by a removable lid which was made hermetic by vaseline (see Figure 4-5). In its bottom part, the box contains a drawer filled with a saturated salt solution which sets humidity inside the chamber. Humidity and temperature inside the box were measured continuously with a Rotronic HC2-C04 sensor.

Four different salts were used:

- LiCl sets the humidity to RH=11%
- K_2CO_3 sets the humidity to RH=43%
- NaCl sets the humidity to RH=75%
- K_2SO_4 sets the humidity to RH=97%.

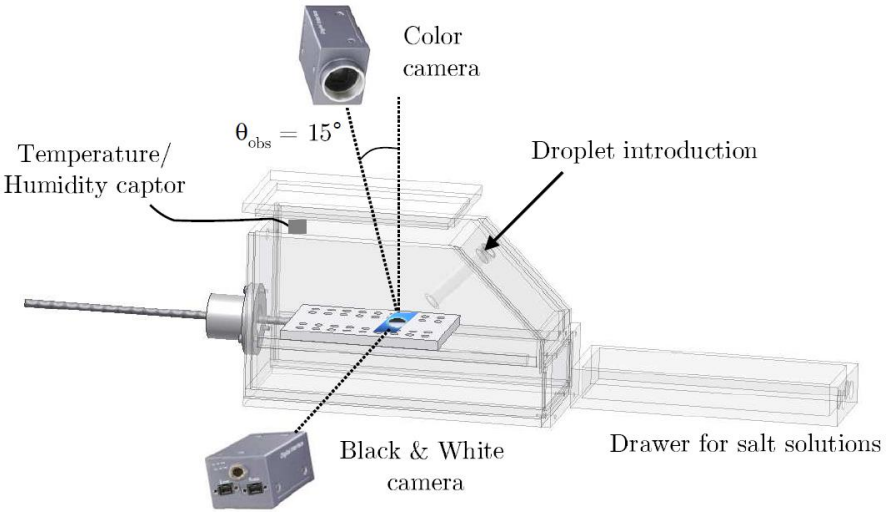

Figure 4-5: Experimental set-up for spreading experiments made by Dupas et al (adapted from Dupas et al[51])

Before any measurement, the wafer coated with the polymer layer was left in a hermetic recipient containing the same salt as the box during at least 24 hours for equilibration. Then it was placed in the chamber and left another 20 min with the lid tightly closed for atmosphere equilibration before deposing the droplet.

Deionized water was always used for wetting experiments.

For sessile droplets experiments, a 5 µL droplet was deposited on the polymer layer with a micro-pipette. For swollen droplets experiments, a syringe pump was used to feed the droplet and control the contact line velocity. The droplet was inflated at a constant volume rate varying from 2 µL/min to 200 µL/min. Droplets were filmed both from the side and the top. The top view was used to verify that the droplet shape remained circular during the spreading and contact angle measurements were performed on the side views.

Side views were binarized using ImageJ. A Matlab program was written to extract the value of the contact line velocity and the contact angle from each of those pictures. The contact line is presicely determined as the droplet reflects on the silicon wafer (see Figure 4-6) and the contact angle is calculated from the intersection between the contact line and a circular fit of the droplet contour.

Experimental results obtained with this set-up are presented in the following paragraphs.

4.2.2 Spreading dynamics

Deionized water droplet were deposited onto GP layers of different thicknesses equilibrated at different water activities. Figure 4-6 presents a typical result obtained at the beginning of the experiment.

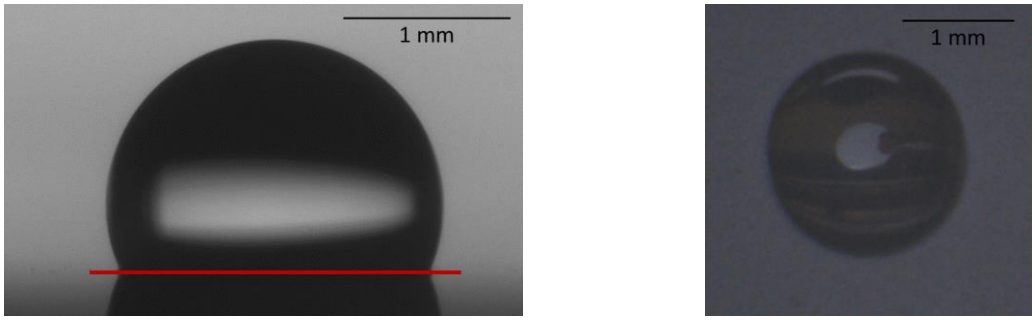

Figure 4-6: Side and top view of a 5µL sessile droplet deposited on a 3 µm GP layer equilibrated at a_w=43% - t = 1 s after deposit

The droplet is spherical and the contact angle between GP and water is large (close to 110°). Dupas et al predicted high values of the contact angle for thick layers of high molar mass polymers (see paragraph 2.2.2.3), but the values obtained with GP layers are larger than expected. Qualitatively, the same poor wetting and hydrophobic behavior as on GP powder (see paragraph 4.1) is observed.

Experiments conducted with sessile droplets were not reproducible. Indeed, the layer roughness is responsible for the pinning of the contact line and it modifies the spreading dynamics. (see paragraph 2.2.2.5).

To obtain reproducible spreading dynamics, the droplet spreading was forced by feeding the droplet with water at a controlled rate during the experiment.
Swollen droplet experiments were conducted on GP layers of variable thicknesses (between 30 nm and 3 µm) at different water activities. The results are presented on Figure 4-7.

Dupas and al shown that the wetting dynamic depends on the initial water content in the polymer layer. The more hydrated the polymer, the smaller the contact angle and the contact line velocity. They also shown that it depends on the layer thickness because the water content in the layer is related to the layer thickness. The thinner the layer, the smaller the contact angle.

For all the experiments presented on Figure 4-7, the contact angle increases with the contact line velocity. At a given contact line velocity, it increases with the layer thickness. Those results are in good agreement with Dupas et al theoretical predictions and observations (see Paragraph 2.2.2.3). They confirms the fact that water condensates ahead of the contact line and diffuses quickly across the polymer thickness. The amount of water is thus governed by the product eU.
Indeed, Dupas et al have predicted that in the case of a polymer layer homogeneously hydrated along the vertical direction i.e. for thin enough layer with thickness $e < D/U$, the contact angle, which is a direct function of water content in the polymer, only depends on the product eU.
Contact angle as a function of the product eU is plotted in the right column of Figure 4-7 for all the experiments. All the data for the different layer thicknesses collapse on a single master curve for eU values ranging between $10^{-15}\ m^2/s$ and $10^{-10}\ m^2/s$. This rescaling is predicted to be valid for $eU < D$, which means that the mutual diffusion coefficient of water in polymer is such as

$$D > 10^{-10}\ m^2/s$$

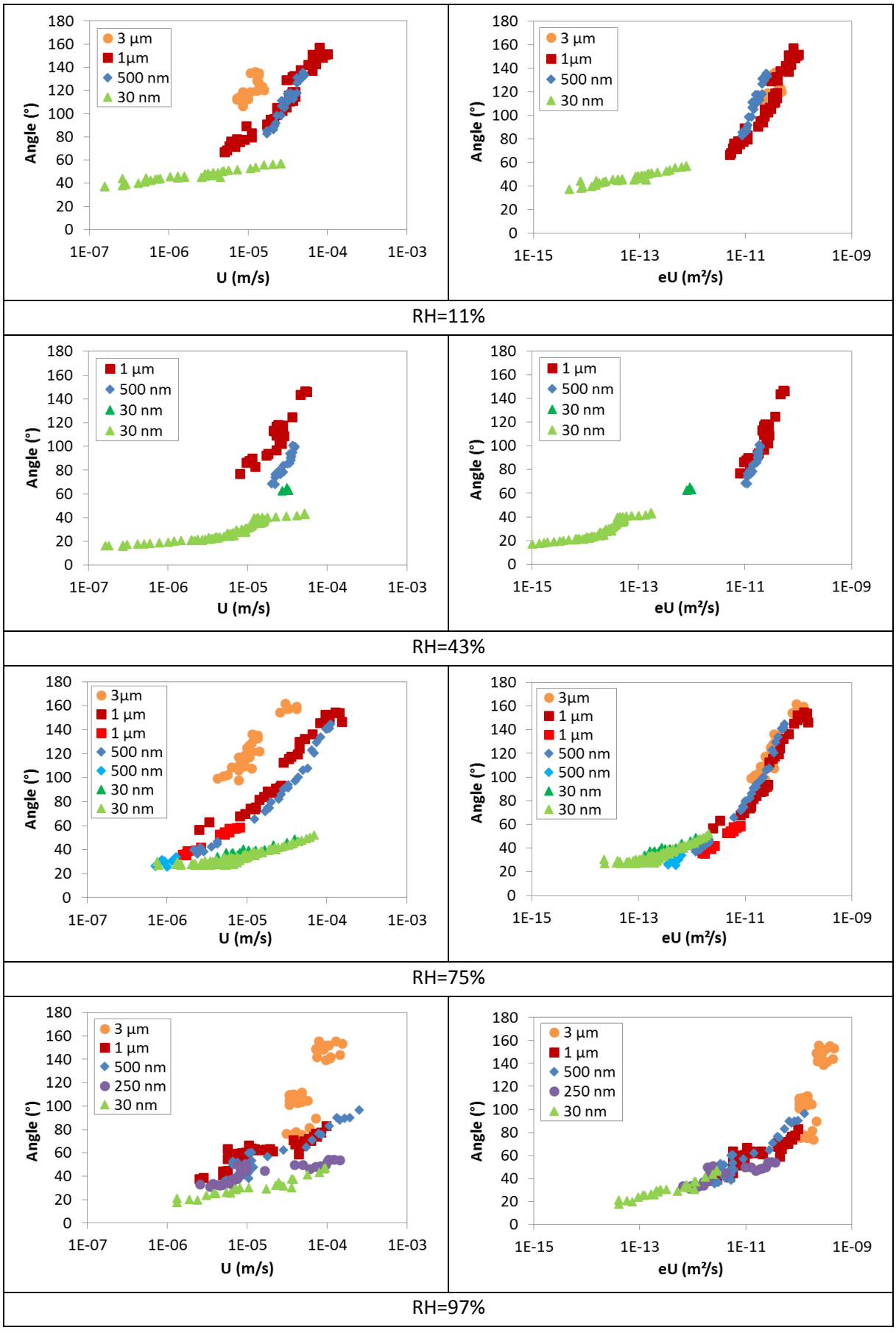

Figure 4-7: Contact angle versus velocity and rescaling as a function of eU for 4 humidities

Dupas et al also predicted an influence of humidity on the value of the contact angle. Indeed, ambient humidity sets the initial water content of the polymer layer and this water fraction sets the value of the substrate interfacial energy and thus the contact angle. Results presented in the right column of Figure 4-7 for different water activities are plotted altogether on Figure 4-8. Each color corresponds to a different humidity and the different marker types correspond to the different layer thicknesses for each humidity.

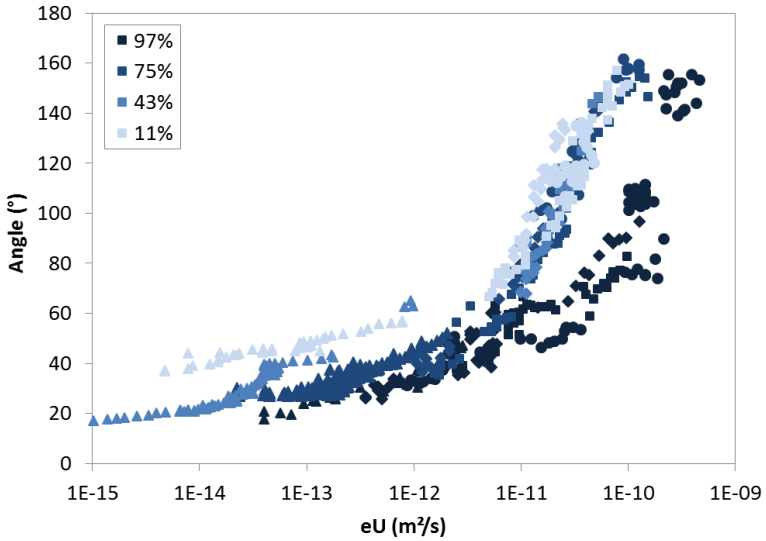

Figure 4-8: Contact angle versus eU for GP layers at different ambient humidities

Surprisingly, the contact angle is independent of the ambient humidity for RH $\leq$ 75%, except at very small eU i.e. for experiments performed on very thin GP layers. This is different from Dupas et al observations on Maltodextrin DE29. On Maltodextrin DE29, the contact angle decreases with water activity on the whole water activity range (0% to 75%). On the other hand, for GP equilibrated at RH = 97%, the contact angle at a given eU is smaller than for the other water activities. This evolution is consistent with Dupas et al observations and can be interpreted as follows:

At RH < 75%, GP is glassy. On the contrary, at RH = 97%, GP is in a melt state. This can be accounted for by considering that the polymer/solvent mixture undergoes a glass transition in water content at ambient temperature. The wetting behavior is not the same on a glassy and on a molten polymer because the substrate properties are different: in particular, the diffusion coefficient of water in polymer is much larger and the elastic modulus is much smaller for a molten polymer than for a glassy one. A molten polymer layer hydrates faster and dissipates more than a glassy polymer layer so the contact angle at a given eU is smaller.

4.2.3 Formation of a gel layer

For a sessile droplet of constant volume deposited on a GP layer, a change in the droplet shape was observed after the first seconds of spreading. A foot appeared at the edge of the droplet (see Figure 4-9).

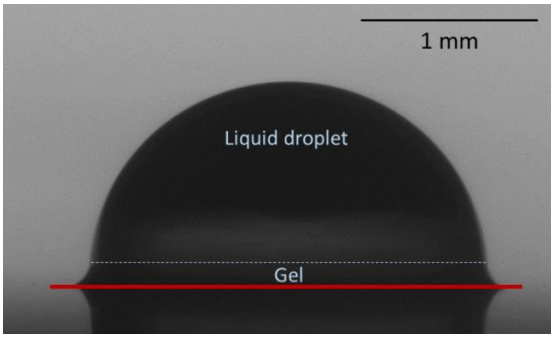

Figure 4-9: Side view of the Figure 4 6 droplet at t = 50 s – Apparition of a gel foot

Foot apparition can be explained by the formation of a viscoelastic gel layer below and beyond the droplet due to the swelling of the polymer in contact with water. Once the gel is formed, the droplet cannot spread anymore because the apparent contact line is strongly pinned by the gel.
It is no longer possible to measure a solid/liquid contact angle because the shape of the droplet is no longer spherical. Indeed, the water/gel contact line is not clearly defined because there is a gradient of concentration between the liquid droplet and the solid layer.

Moreover, it appears that the polymer gel layer is very long lasting. Indeed, similar experiments with low molecular mass polymers like Maltodextrins were conducted by Tay and al[52]. In those experiments, the polymer layer is completely dissolved in the water droplet during the experiment and the zone where the droplet was deposited is polymer free. The polymer has been transported to the contact line (see Figure 4-10 right). But, for a GP layer, after complete droplet drying (which takes between 30 min and 2 h depending on the water activity inside the chamber), almost all the polymer is still at its initial location (see Figure 4-10 left).

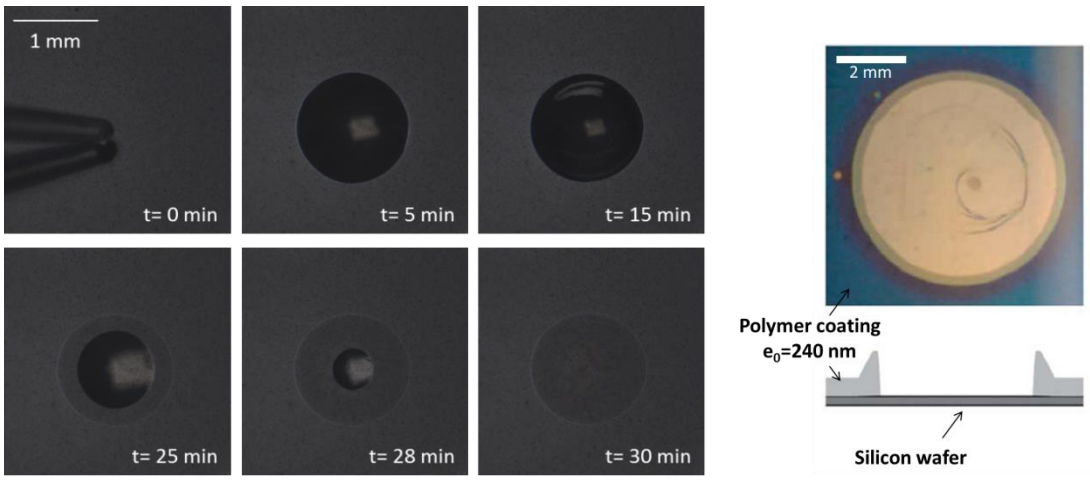

Figure 4-10: Left: Top view of a 5 µl droplet deposited onto a 3 µm thick GP layer equilibrated at a_w=11%. After 15 min, the droplet dries and contact line recedes. It is visible on images at t=25 min, t=28 min and t=30 min that no polymer is transported during swelling and drying. Right: Photograph of the deposit left by a water drop deposited onto a cationic polymer after complete water evaporation and corresponding height profile (adapted from Tay et al[52]). The naked wafer appears inside the circle left by the initial contact line because most of the polymer has left the substrate during the experiment.

There is almost no polymer transport during the experiment. The polymer layer swells in presence of water but is not dissolved. We will come back to this point in the following paragraph.

4.3 Conclusion

Altough hydrosoluble, when GP is put in contact with water it exhibits a hydrophobic behavior. This phenomenon is responsible for a poor wetting and consequently a limited spreading of water droplets on the polymer.

When in contact with water, the polymer swells and a viscoelastic gel of a few hundreds micrometers thickness appears. This gel phase remains longer than the experiment duration, which is limited by the droplet drying. During this time, almost no polymer is dissolved. Indeed, the only chains that are able to move during the experiment are the dissolved ones and it was observed that there is almost no polymer transportation during the experiment. This is consistent with the reptation time measurements for GP solutions. Indeed, the minimum concentration in the gel is roughly equal to the ratio between the dry layer initial thickness and the gel final thickness, which is around 3 µm / 100 µm = 3%. At this concentration, the extrapolated reptation time is around 1 h. Consequently, during these wetting experiments, reptation does not have enough time to occur. In contrast, the reptation times of Maltodextrins are much smaller.
The slow advance of water onto the polymer can also be explained by the fact that the contact line is pinned on this long lasting gel layer.

However, when the spreading is forced by feeding the droplet with water during the experiment, the wetting dynamics is similar as for other polysaccharides, with the contact angle θ being a function of the product thickness times velocity eU for $e < D/U$.
The observed rescaling of the wetting curves for eU < 10^{-10} m²/s means that the mutual diffusion coefficient of water in polymer is larger than 10^{-10} m²/s. We will see in the following chapter that this is consistent with the results obtained in the gel swelling without convection experiments.

Another point is that we were not able to modify the polymer layer initial roughness. This roughness is likely to also play a role in the slow spreading and the high contact angle values observed for sessile droplets on GP layers because it can pin the contact line. But, when the contact line is forced to advance, the eU scaling is conserved despite this roughness, showing how contact line dynamics remains set by the polymer hydration even on rough viscoelastic substrate.

An apparent contact angle can be defined for the sessile droplet even after gel swelling (close to 80° on Figure 4-9). We could expect this contact angle to be close to an extrapolated zero-speed contact angle from the swollen droplet experiments (around 30°) because the contact line advance on the gel is very slow. But this is not the case. A possible explanation is that at small velocities the contact line exhibits a stick-slip motion (the contact line is pinned and the contact angle increases until a critical value at which the contact line slips forward to a certain distance) whereas at large velocities, the contact line motion is continuous. This behavior was described by Kajiya et al[53] for viscoelastic cross-linked gels. In their case, the stick-slip motion occurs in an intermediate regime where the elastic

deformation of the gel at the contact line relaxes and pins the contact line like a “surface defect”. If this stick-slip motion occurs in our case, it could be responsible for the higher than expected values of the contact angle at vanishing velocities for sessile droplets.

During the imbibition step of the dissolution process of a polymer powder, the pores are wetted by water. In this situation, gel swelling can be responsible for pore clogging and thus lead to macroscopic lumps formation.
In the following chapter, we focus on the swelling kinetics of this gel.

5 Swelling without convection

In this chapter, swelling of the gel phase without convection will be studied. In the wetting experiments presented on the previous chapter, gel swelling could not be quantitatively studied because it was limited by the finite amount of water in the droplet. On the contrary, the experiments presented in the present chapter were conducted in a semi-infinite water reservoir.
First, we will present small scale experiments conducted on polymer pieces of different size (grains and pancakes) put in contact with water. Observing their dissolution will provide us with qualitative information on the phenomena at stake. Swelling of the polymer gel will be evidenced as the limiting step in the dissolution process without convection. Then we will describe an experimental set-up designed to study precisely the gel swelling and we will present several quantitative results.
Investigating GP swelling with those different experiments allows us to probe length scales and timescales spanning more than three order of magnitude. This is relevant because powder dissolution involves multiple scales behavior and different regimes can be expected depending on the relative values of reptation times and experimental times[42].

5.1 Small scale experiments

In order to identify the different steps of the dissolution mechanism, dissolution experiments were conducted onto polymer pieces of size spanning a large range, from grains of a few tens of micrometers to polymer pancakes of a few millimeters.

Dissolution of single GP grains was observed with an optical microscope. The grain was placed between a glass slide and a cover glass slide and a deionized water droplet was deposited at the edge of the cover glass. It penetrated between the two slides by capillarity. The grain dissolution was captured by a Giga-Ethernet video camera at an acquisition frequency of 150 Hz. A typical image sequence is presented in Figure 5-1.

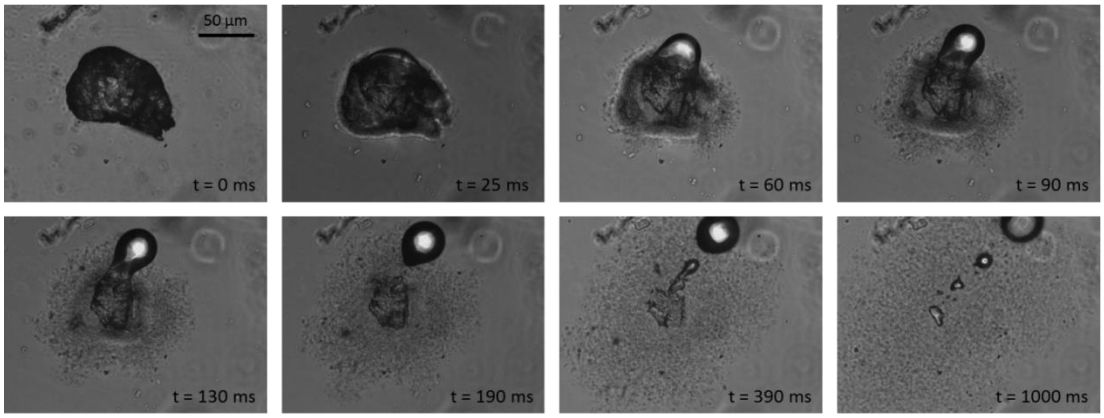

Figure 5-1: Dissolution of a GP grain (80 µm diameter) in deionized water

A few milliseconds after grain / water contact, an interface appeared between a dry and a wet phase. The dry phase decreased and disappeared in less than one second while the gel phase swelled, going out of the camera window in a few seconds. Then, the gel phase disappearance by dissolution was very long, taking several minutes. The grain diameter during the first seconds of swelling was measured. The swollen grain radius minus the initial grain radius is called “gel thickness”. A plot of it versus time is presented in Figure 5-2.

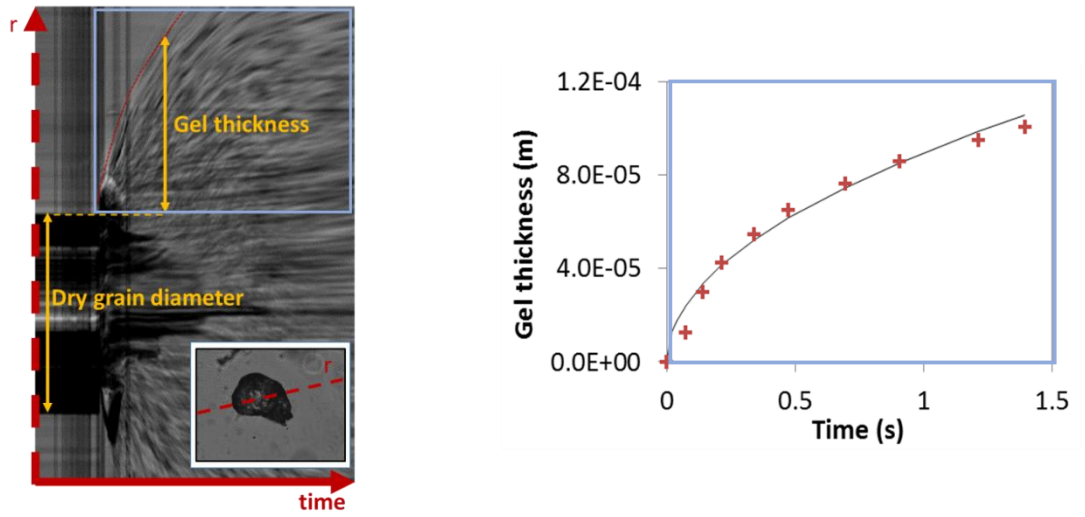

Figure 5-2: Evolution of the gel thickness during the dissolution of a GP grain. Left: Space-time diagram obtained from slicing the Figure 5-1 pictures along the red dotted line plotted on the insert picture. Right: Gel thickness as defined on the space-time diagram versus time

The gel/water interface is visible owing to a sharp variation in the intensity of transmitted light. However, the exact location of the interface depends on arbitrary chosen optical criteria. In the 1D swelling experiment presented on the next paragraph, quantitative polymer concentration measurements have been performed to locate the interface.

Gel thickness varies as the square root of time. It is characteristic of a diffusive behavior $h = \sqrt{Dt}$. In the present experiment, the diffusion coefficient D is $8 \cdot 10^{-9}$ m²/s.

The same experiment was conducted with dry polymer pancakes prepared as described in paragraph 4.1 instead of polymer grains. The polymer pancake dissolution was recorded with an acquisition frequency of 1 Hz. A typical image sequence is presented in Figure 5-3.

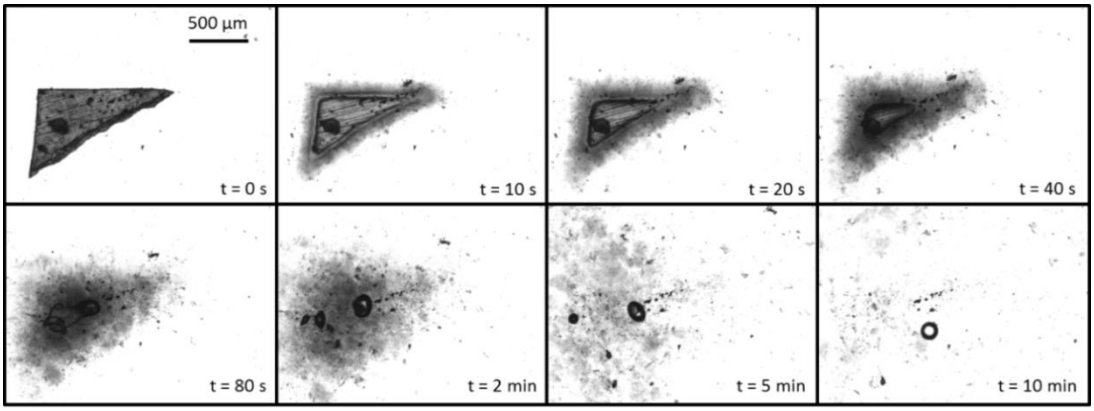

Figure 5-3: Dissolution of a GP pancake (1 mm diameter) in deionized water

As for GP grains, an interface between a dry, glassy phase and a hydrated swollen phase appeared. The dry phase quickly disappeared while the gel phase expanded and slowly dissolved. The gel thickness is defined as for GP grains. It is represented versus time on Figure 5-4.

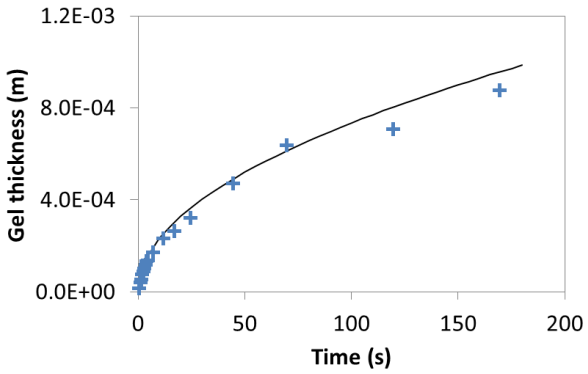

Figure 5-4: Evolution of the gel thickness during the dissolution of a GP pancake

We find again that gel swelling is a diffusive process with $h = \sqrt{Dt}$. Size and time scales are larger than those for the dissolution of a GP grain but the value of the diffusion coefficient D is close ($D = 5 \cdot 10^{-9}$ m²/s). The diffusion kinetics is independent of the time and size scales.

The gel swelling kinetics will be quantitatively studied in the following paragraph thanks to a homemade set-up.

5.2 1D swelling experiment

A few studies on gel swelling diffusive kinetics have been performed in the literature using different techniques such as interferometry[54] or neutron radiography[47]. In order to measure the variations of diffusion coefficient with polymer volume fraction, we designed an experiment where the quasi-one-dimension swelling of a polymer layer is measured in a quasi-semi-infinite geometry by light scattering. The set-up allows one to change the polymer and/or the solvent salt content. This experiment will be referred to as “1D swelling experiment”.

5.2.1 Experimental set-up

Polymer layers of controlled thickness prepared as described in paragraph 3.3 were used for the 1D swelling experiments. The glass slide supporting the polymer layer was placed in a 15-cm-long, 10-cm-large, 5-cm-high tank and enlighten with a laser sheet (λ=514 nm, P=10 mW, thickness~0.5 mm). The laser sheet was placed on the middle of the polymer layer and focalized on the dry layer substrate as shown in Figure 5-5.

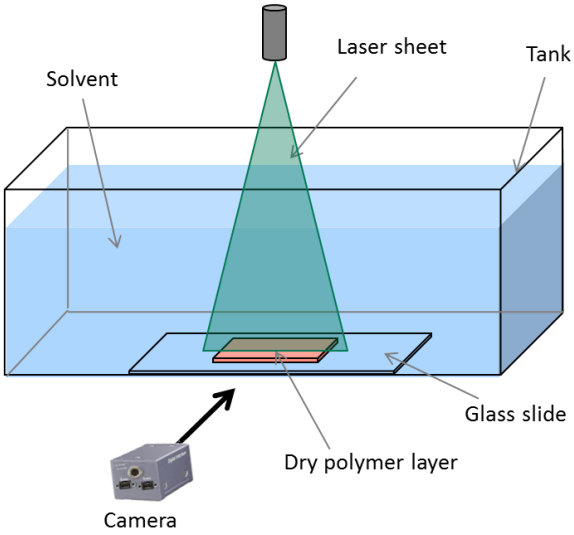

Figure 5-5: Schematic representation of the swelling experimental set-up

At the beginning of the experiment, the tank was filled with solvent. Solvent was deionized water or NaCl solutions. The gel swelling was recorded by a SONY XCD-U100 black and white camera placed perpendicularly to the laser sheet. Laser light is diffused by the gel and the gel evolution can thus be measured from the resulting speckle figure (see Figure 5-6).

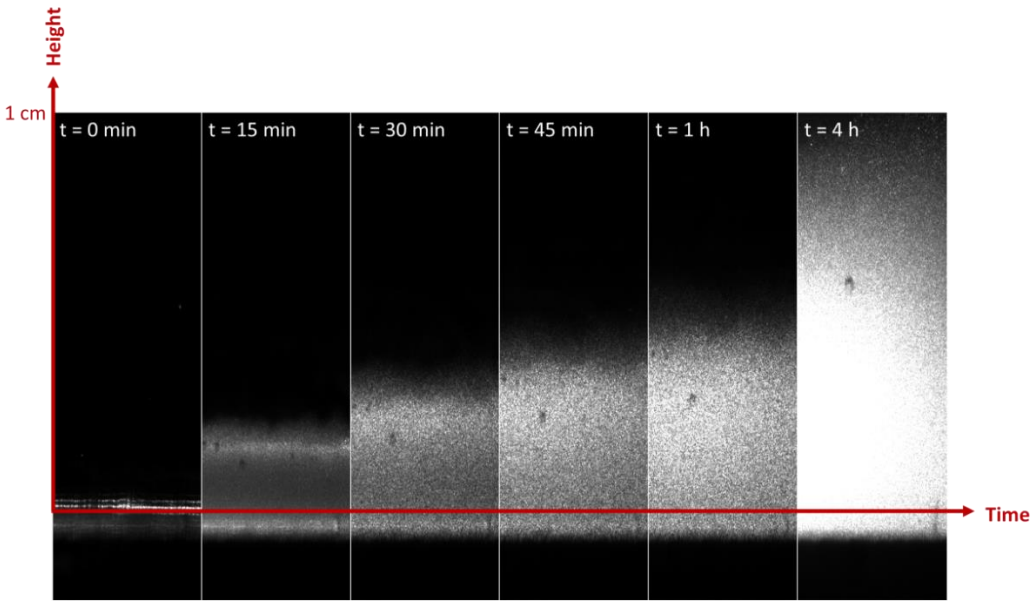

Figure 5-6: Swelling of a 50 µm GP layer in deionized water. Gel height increases up to 1 cm in 4 hours.

Of course, for a given sample, the speckle measured intensity varies linearly with the exposure time. We call intensity the absolute intensity $\mathrm{I} = \frac{\text{Measured intensity}}{\text{Exposure time}}$. I is directly related to polymer concentration in the gel. A calibration was made with polymer solutions of given concentrations filling the tank. The calibration curve is presented on Figure 5-7 where the concentration is plotted as a function of the measured absolute intensity. We were able to calibrate the concentration up to C_{max} = 0.015 g/g. For more concentrated solutions, we believe intensity to become non-linear, although it is difficult to quantify this effect.

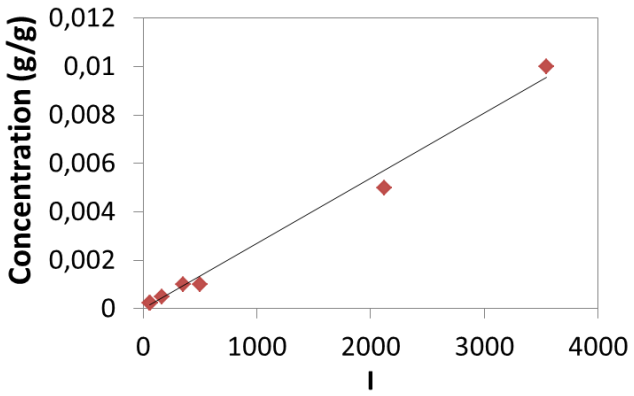

Figure 5-7: Calibration curve for GP swelling in the 1D swelling experiment. $\Phi = 2.7 \cdot 10^{-6} I$.

The range of intensity that could be measured was increased by using three different exposure times. During the course of a 1D swelling experiment, three pictures are therefore taken in a row with three different exposure times for every measurement. The exposure times were chosen so as to maximize the accessible range of concentration. Typical images are shown in Figure 5-8. Intensity is averaged over the all pixel line for each height value z. In cases where intensity saturates or is too low, data are discarded. The three intensity profiles obtained for the three exposure times are converted into a single concentration profile C(z) thanks to the calibration curve presented on Figure 5-7. The maximal polymer mass fraction is 0.015 g/g owing to the impossible calibration of concentration above that value.

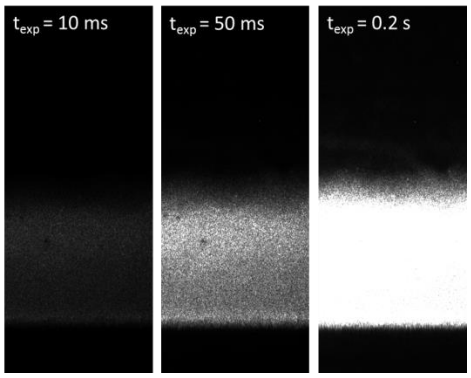

Figure 5-8: GP gel after 45 min of swelling in deionized water at three different exposure times

The acquisition frequency was chosen according the experiment duration. For instance, f=0.04 Hz for a 20000 s experiment.

Typical concentration profile curves at different times for the swelling of a GP layer in deionized water are presented on Figure 5-9.

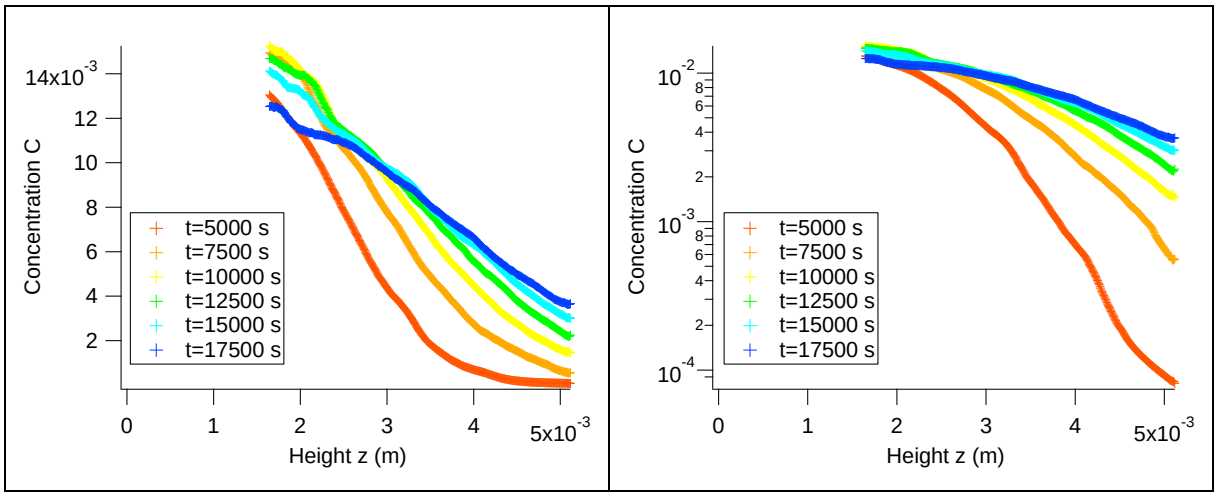

Figure 5-9: Swelling of a 50 µm GP layer in deionized water. Measured concentration profile C(z) versus distance to the polymer layer. Each curve corresponds to a different time t. Small heights, which corresponds to concentrations larger than 0.015 g/g, are cut. Left: linear scale. Right: semi-logarithmic scale. The concentration measurements are accurate over more than two decades.

Polymer concentration increases with time at large heights due to gel swelling. In parallel, the finite amount of polymer in the layer is responsible for the decrease in concentration at small heights at longer times.

5.2.2 Swelling of a polymer layer

5.2.2.1 Diffusive swelling behavior

The lateral dimensions of the layer were chosen to be much larger than the thickness and hence the edge effects were neglected. The gel was assumed to swell only in the vertical direction z.
From the small scale experiments presented in paragraph 5.1, the swelling behavior is expected to be a diffusive behavior. Consequently, concentration profiles were fitted with the diffusion equation for a planar source, infinite in the xy plan, of initial thickness h_0 and initial concentration C_0, which diffuses in the z direction into a semi-infinite reservoir (see Figure 5-10)[55]:

$$C(z,t) = C_0\left[\mathrm{erf}\left(\frac{h_0 - z}{2\sqrt{Dt}}\right) + \mathrm{erf}\left(\frac{h_0 + z}{2\sqrt{Dt}}\right)\right] \qquad \textit{(Eq 5-1)}$$

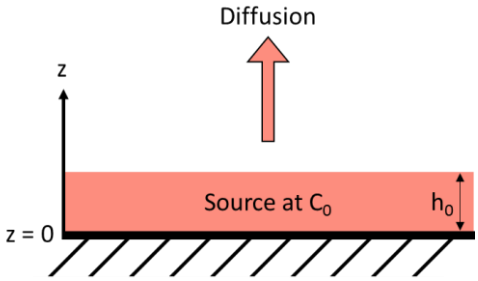

Figure 5-10: Schematic representation of the geometry considered in (Eq 5-1)

h_0 is the initial thickness of the dry polymer layer measured with a mechanical sensor and C_0 and D are the fitting parameters. They were determined from the C(z) variations at six different times smaller than five hours.

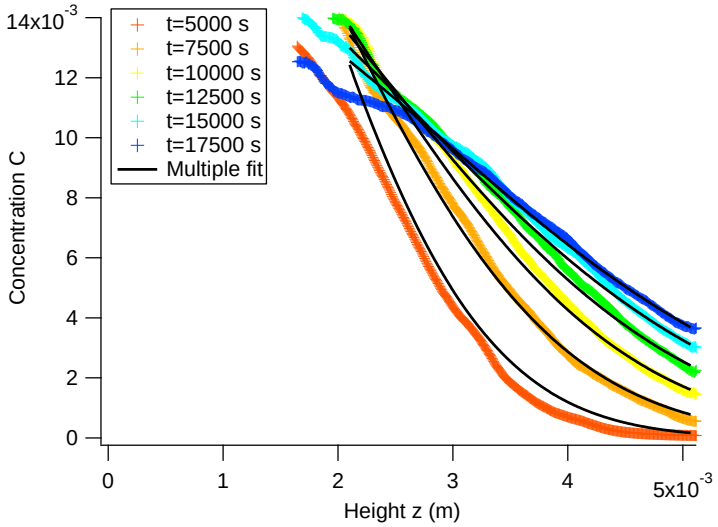

Figure 5-11: Swelling of a GP layer (h_0=50 µm) in deionized water – Data fitted with (Eq 5-1): D=2.5·10^{-10} ±7·10^{-13} m²/s and C_0=0.6 ± 0.001

A value for the diffusion coefficient was thus obtained for the first five hours of swelling:

$$D = 2.5 \cdot 10^{-10} m^2/s$$

However, at later times, this value fails to fit the C(z) curves. There is no analytical solution for the diffusion equation with a concentration-dependent diffusion coefficient in the case of a thin polymer layer. The equation can only be solved for an infinite polymer reservoir[55]. Nonetheless, several empirical laws for the diffusion coefficient as a function of the polymer concentration have been proposed[47,54], and used in numerical simulations. The results are not convincing.

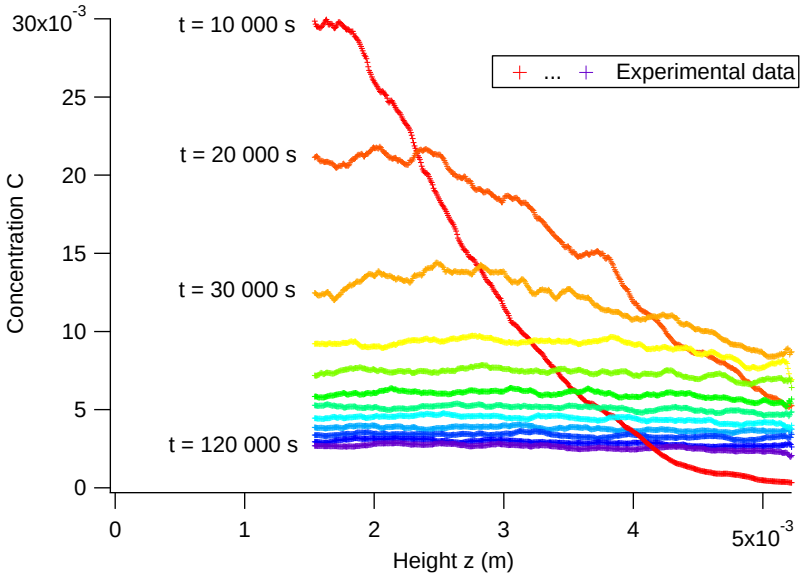

Figure 5-12: Swelling of a GP layer (h_0=70 µm) in deionized water – same experimental conditions as Figure 5-11.

In our case, the concentration in the gel is uniform for t > 40000 s (see Figure 5-12). Each concentration versus height curve could be fitted separately according to (Eq 5-1) to obtain a diffusion coefficient D corresponding to a given concentration C. However, the values obtained by this method are one order of magnitude larger than the value of D obtained at short times (see Figure 5-11) even though the corresponding concentrations are in the same range.
It is thus not possible to obtain a satisfactory empirical law for the diffusion coefficient as a function of polymer concentration with our method. However, qualitatively, it is likely that D should be found to decrease with concentration.

5.2.2.2 Salt influence

GP being a polyelectrolyte, the presence of salt in the solvent is expected to have a strong influence on the swelling behavior.
Several 1D swelling experiments were realized with 10^{-3} mol/L, $2 \cdot 10^{-2}$ mol/L and 0.5 mol/L NaCl solutions as solvents. For all those experiments, dry GP layers of similar thicknesses (between 50 µm and 70 µm) were used. The largest chosen NaCl concentration was 0.5 mol/L because it is approximately the salt concentration in sea water and sea water is often used as solvent on the field for offshore drilling operations.

Concentration profiles C(z,t) were obtained for all those solutions (see Figure 5-13). A multiple fit was performed with (Eq 5-1) for each profile.

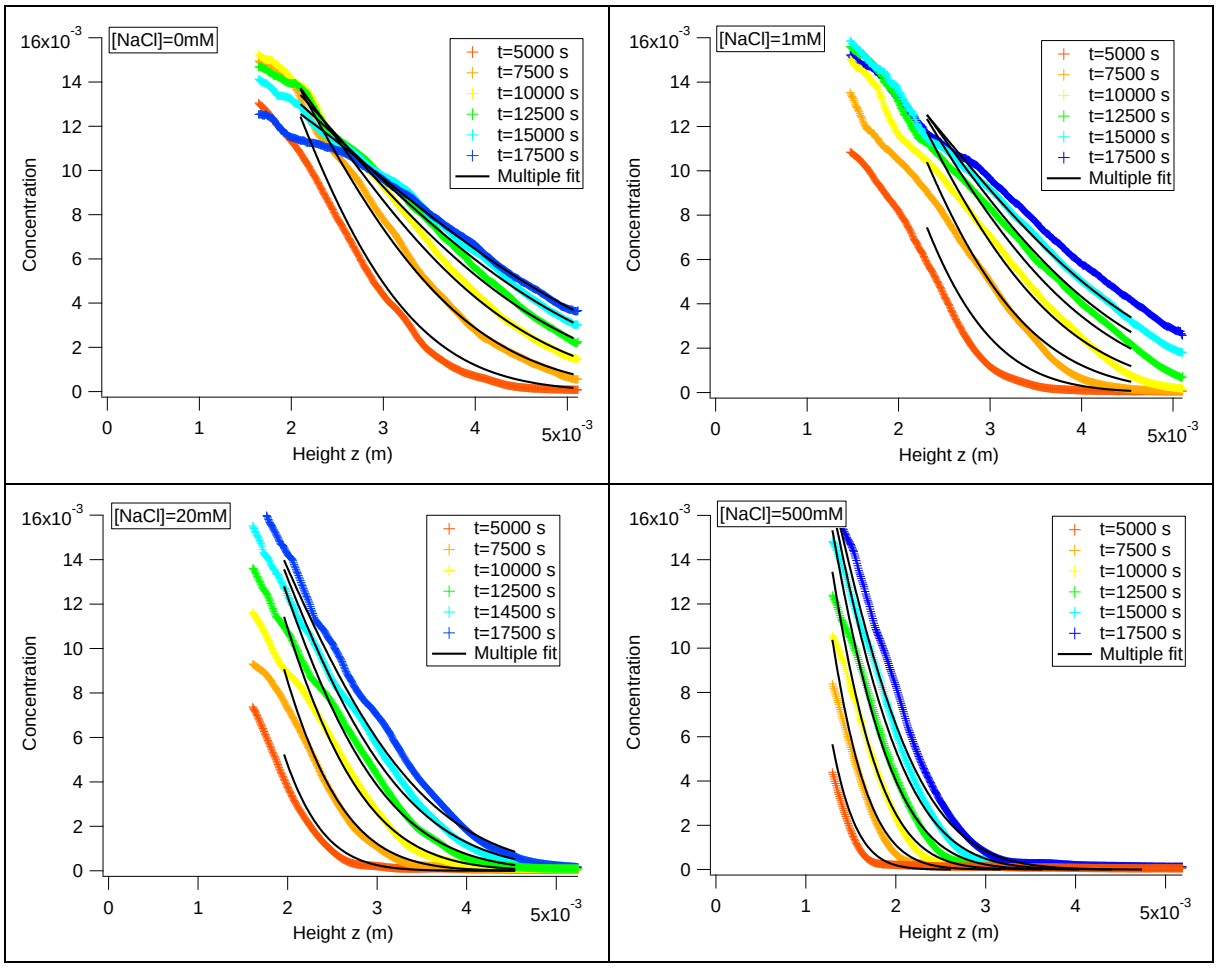

Figure 5-13: Concentration profiles for 1D swelling experiments in NaCl solutions

As shown in Figure 5-13, salt addition slows down the gel swelling. Indeed, additional ions screen the effect of polymer charges in the osmotic pressure term which is a driving term for swelling. That effect will be detailed in the following.

At early times ($t \leq 5$ h), a single large polymer concentration diffusion coefficient D could be measured for every salt concentration. These diffusion coefficients are plotted on Figure 5-14 as a function of ionic strength I, which is equal to salt concentration for monovalent ions. For deionized water, the ions responsible for the ionic strength of the solvent comes from the free salt present in the polymer powder which are rapidly released in the water at the beginning of the experiment. It correspond to a ionic strength of 10^{-6} mol/L.

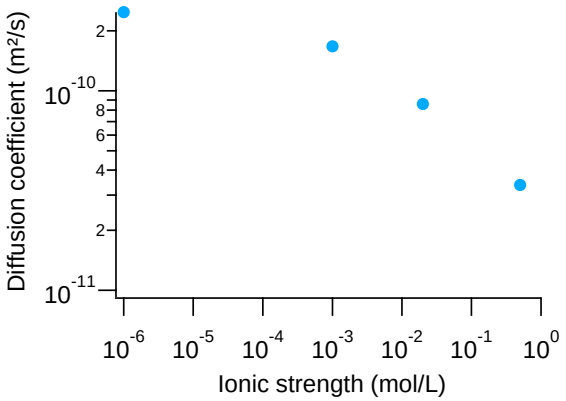

Figure 5-14: Diffusion coefficient versus ionic strength for the swelling of a GP layer in a NaCl solution

Salt addition has a huge effect in terms of swelling kinetics, decreasing the diffusion coefficient by one order of magnitude.
Numerical agreement with the theory of polymer swelling will be discussed later in paragraph 5.2.3.

Another way to present the results of a 1D swelling experiment is to choose a concentration C_{cut} and to plot the height z at which the gel is at this concentration as a function of time. This is like plotting an horizontal cut of the concentration profile C(z,t). Such a plot is presented on Figure 5-15 for GP layers in salted solutions.

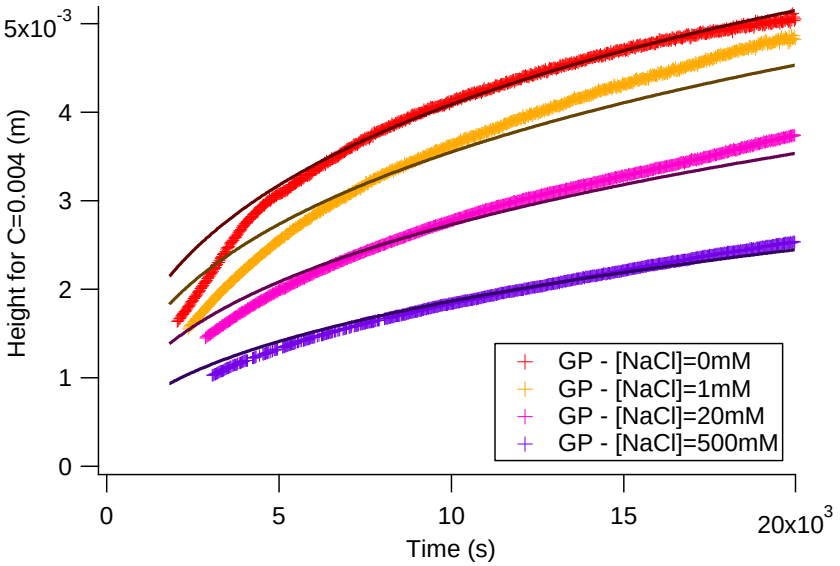

Figure 5-15: Swelling of GP layers in deionized water and NaCl solutions - Height versus time for $C_{cut}=4\cdot10^{-3}$. Experimental data are represented with markers. The lines are theoretical curves obtained from (Eq 5-1) with the multiple fit parameters of the corresponding experiment.

Figure 5-15 is a convenient way to compare different experiments. With this representation, it is very clear that salt addition slows down the swelling because for a given time, the height reached by the gel at a given concentration decreases with the ionic strength of the solvent.
The discrepancies between experimental results and theoretical curves can be explained by the concentration dependency of the diffusion coefficient. We will demonstrate later that, theoretically, it

decreases with concentration, which means that it increases with time during the experiment. This is why the theoretical prediction at constant diffusion coefficient is faster than reality at the beginning of the experiment (the theoretical gel height is larger than the experimental one) and slower at the end (it is smaller). This was already the case with some of the concentration profiles presented on Figure 5-13.

GP is both a polyelectrolyte and a polymer of very large molar mass. Salt allows to tune the charge effects. In order to isolate the effect of the molar mass, we turned to a neutral polymer of varied molar mass, Polyethylene oxide (PEO).

5.2.2.3 Comparison with a neutral polymer – Influence of the molar mass

Polyethylene oxide is a neutral polymer. 1D swelling experiments were performed on PEO layers using the same protocol as for GP layers. PEO with all the molar masses presented on paragraph 3.1.3 were used. Layer thicknesses were comprised between 30 µm and 100 µm. Deionized water was employed as a solvent for all the experiments. Intensity versus concentration calibration curves were obtained for every molar mass.

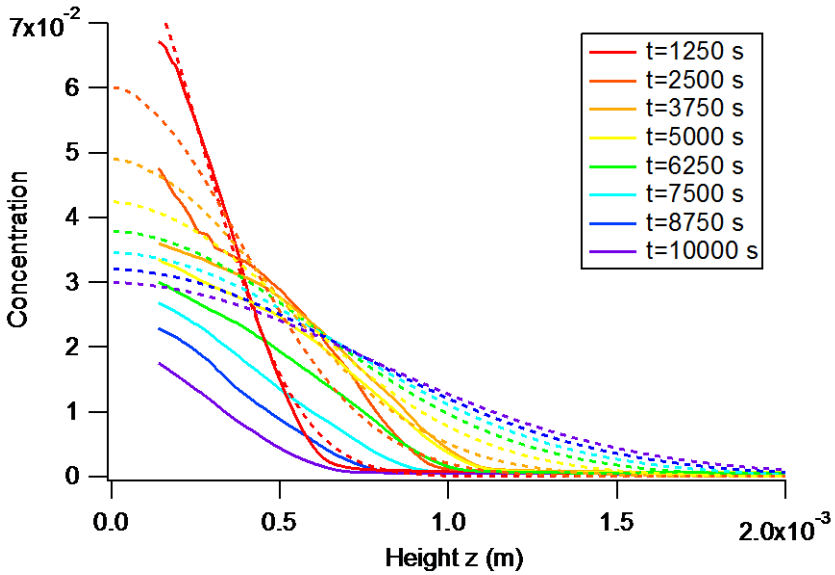

Figure 5-16: Swelling of a PEO $1{\cdot}10^6$ g/mol 50µm layer in deionized water. The full lines are the experimental data. The dashed lines are the theoretical data for a diffusive swelling described by (Eq 5-1) with h_0=50µm and C_0 and D obtained by fitting the experimental curve at t=1250 s only with (Eq 5-1).

For the GP concentration profile curves, the area under the curves, corresponding to the amount of polymer in the gel, remains constant during the first hours of the 1D swelling experiments. This is consistent with a diffusive behavior. For PEO it is not the case. It clearly appears on Figure 5-16 that PEO behavior cannot be described with (Eq 5-1) because after a first period of swelling similar to GP behavior corresponding with the first thee curves on Figure 5-16, the area under the C(z) curve decreases with time, even though the initial amount of polymer in the layer is approximately the same.

1D swelling experiments were realized with several molar masses PEO and the behavior is always the same. Results are summarized on Figure 5-17. The decrease of the gel height is also visible on those curves. The height at which the gel is at the concentration C_{cut} increases at the beginning of the experiment like for GP swelling but at a certain critical time t^*, it begins to decrease. In other words, the polymer is transferred from the gel into the solution through a process that is faster than diffusion. The critical time t^* depends on the PEO molar mass. However, the behavior at times shorter than this critical time seems to be independent of the molar mass because the slopes of the curves of Figure 5-17 are the same.

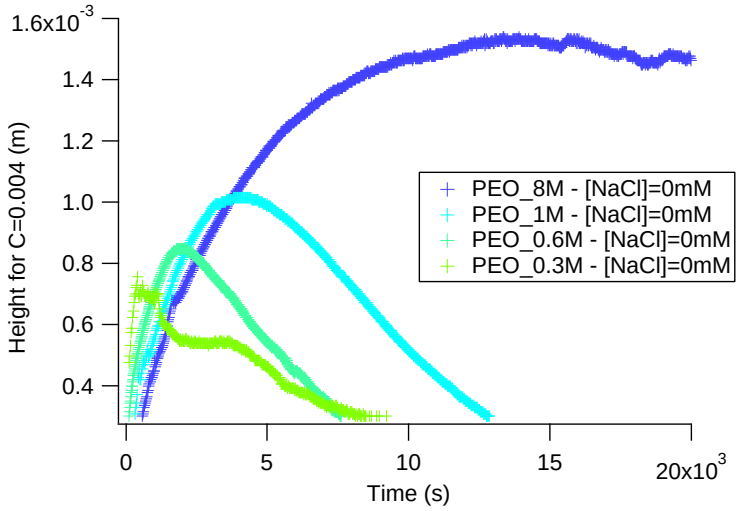

Figure 5-17: Influence of the molar mass on the swelling of PEO layers in deionized water - Height versus time for C_{cut}=4·10-3.

The critical time t^* increases with the PEO molar mass. It is independent of C_{cut} in the range of C_{cut} measured in the 1D swelling experiments (see Figure 5-18).

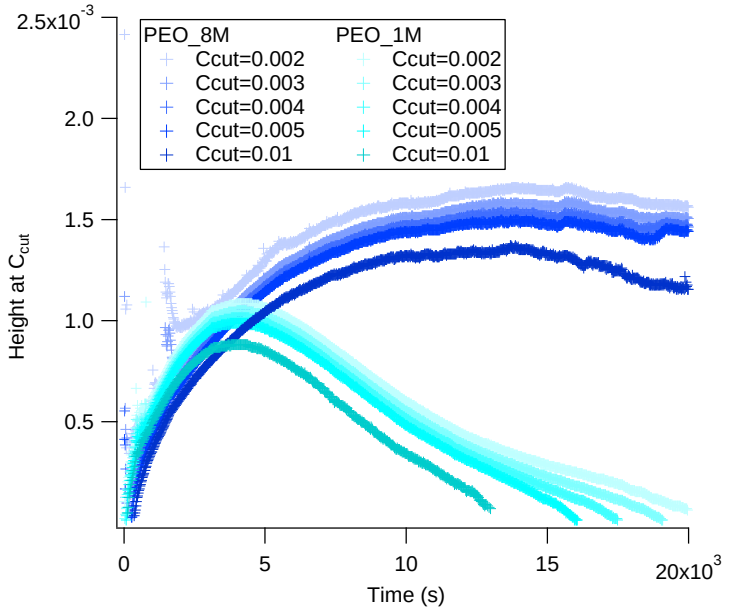

Figure 5-18: Swelling of PEO layers in deionized water - Height versus time for different C_{cut}.

The values of the critical times t^* for the different PEO molar masses are gathered in the following table.

Polymer name	Critical time t^*
PEO_0.3M	800 s
PEO_0.6M	2000 s
PEO_1M	4000 s
PEO_8M	15000 s

Reptation time in a PEO_8M solution at 2%wt is around 10 s, which is much smaller than the critical time. Moreover, we have shown that the critical time does not depend on the concentration whereas the reptation time does.

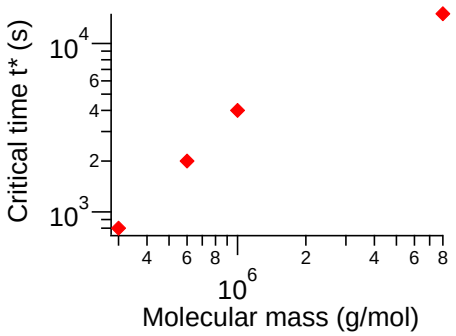

Figure 5-19: Critical time versus molar mass for the swelling of PEO layers.

Alternatively, we tested the dependence of t* with the overlap concentration of each polymer molar mass. Experimentally, data can be fit to

$$t^* \sim \frac{1}{C^*}$$

(see Figure 5-20).

This scaling suggests that the gel dissolution is due to the cooperative swelling of the gel up to the overlap concentration.

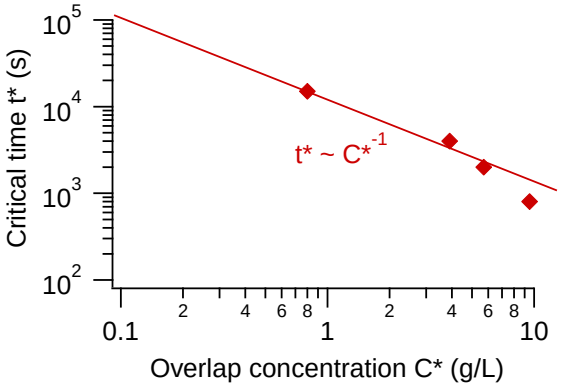

Figure 5-20: Critical time versus overlap concentration for the swelling PEO layers.

Extrapolation for GP layers based on the measured GP overlap concentration predicts a critical time t* around 10^5 s (see Figure 5-20). This provides us with an explanation for our measurements on GP: the critical time cannot be observed for GP because at this time, the gel/solvent interface is out of the camera range (the concentration is uniform in the camera range as seen in Figure 5-12).

5.2.2.4 Overview of the swelling without convection experimental results

As demonstrated in the previous paragraph, reptation is not involved in the swelling experiments with PEO. It is also the case for GP behavior. Indeed, the same diffusion kinetics was observed for the grains and pancakes dissolution presented on paragraph 5.1 where the experiment duration is shorter than the reptation time value at any observed concentration and for the 1D swelling experiments where it is longer (see Figure 5-21).

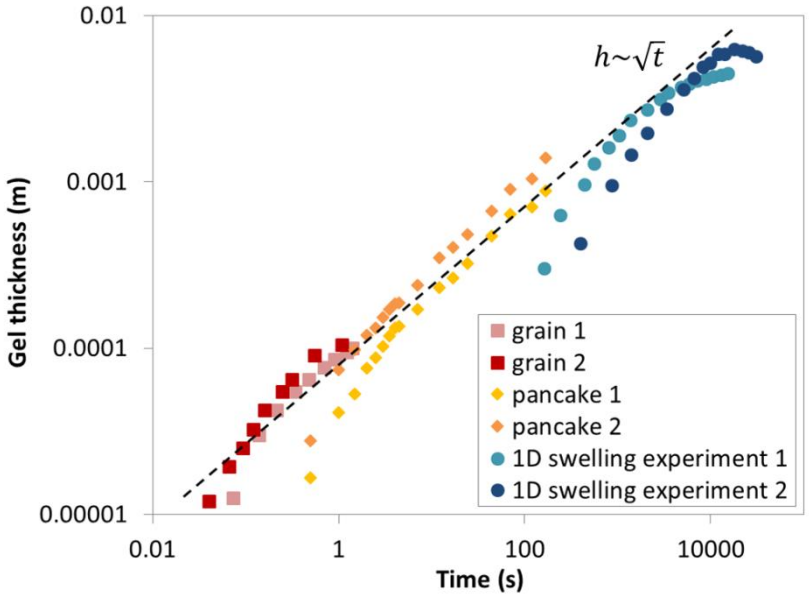

Figure 5-21: Gel thickness versus time: Comparison between small scale dissolution experiments and 1D swelling experiments. The gel thickness for the water tank experiment was measured on the naked eye without defining a precise concentration criterion to be consistent with the gel thickness measurements for the other experiments.

The differences in the diffusion coefficients values measured in the small scale experiments and calculated by fitting the data of 1D swelling experiment come from the arbitrary definition of the gel/liquid frontier in the grain and pancake dissolution experiments. When the same method "on the naked eye" is used for the definition of the gel thickness in the 1D swelling experiment, all the data "gel thickness versus time" collapse on a single mastercurve. The scaling law is of course $h \sim t^{1/2}$. No difference is observed between short experiments, where no reptation is possible and long experiments, where reptation could happen.

In the following paragraph, we will try to understand why, in contrast with predictions by Brochard and De Gennes[42], no influence of the reptation time is observed.

5.2.3 Why does reptation time play no role in the swelling process?

In this paragraph, a theoretical calculation of polymer swelling kinetics is presented, first in the case of a neutral polymer and then in the case of a polyelectrolyte. Numerical applications are done for GP characteristics. The theoretical findings are compared to the experimental ones. The aim is to understand and quantify the mechanisms at stake during swelling and dissolution of the polymer gel.

5.2.3.1 Definitions - Preliminary results

A semi diluted polymer solution in a good solvent with real chains described by Kuhn model is considered. Edwards tube model is used to describe entanglements in the solution (see paragraph 2.1).

N is the chain monomer number.
b is the length of a Kuhn monomer, called monomer length.
v_m is the monomer volume.
φ is the polymer volume fraction in the solution.
g(φ) is the number of monomers by correlation blob and $\xi(\varphi)$ the correlation blob size.

For a real chain in good solvent

$$\xi = l g^{3/5}$$

with $l = b\left(\frac{v_m}{b^3}\right)^{2\nu-1}$.

For a real chain, ν=3/5 so $l = b\left(\frac{v_m}{b^3}\right)^{1/5} = b^{2/5} {v_m}^{1/5}$.

The volume fraction is

$$\varphi = \frac{v_m g}{\xi^3}$$

So

$$\xi = g b \varphi^{1/2}$$

5.2.3.2 Chain contraction inside its tube

In this paragraph, we consider the case of a swelling gel. First, the chains network extends, leading to chain stretching between the entanglement points which corresponds to an increase of the length of the chains Edwards tubes. Then, the chains can relax inside their tube i.e. contract to return to their equilibrium length. This contraction happens to minimize the entropy with characteristic time τ_{cont}. As the distance between the entanglements points has increase, this contraction can lead to chains disentanglement. In this paragraph we will calculate the characteristic time of the chain contraction inside its tube and compare it with the reptation time. We will demonstrate that it is too small (a few seconds) to account for experimental observations.

In equilibrium, the curvilinear length of a chain is L_{eq}.

$$L_{eq} = \left(\frac{N}{g}\right)\xi = N b \varphi^{1/2} \qquad \textit{(Eq 5-2)}$$

During swelling, a chain is first stretched inside its tube with a curvilinear length L. L is both the chain length and the Edwards tube length for the chain.
We consider a small and fast variation of the volume fraction φ ➔ φ + δφ. It corresponds to a small rapid isotropic variation of the volume V ➔ V - δV. During this variation, the chains length follows the macroscopic variation, and thus L^3/V remains constant, which is equivalent to L^3 φ remains constant. This writes

$$L_{eq}{}^3\varphi = \left(L_{eq} + \delta L\right)^3(\varphi + \delta\varphi)$$

And leads to the length variation

$$\delta L = -L_{eq}\frac{\delta\varphi}{3\varphi}$$

During this variation, the equilibrium length varies differently.
Using (Eq 5-2), we get

$$\delta L_{eq} = L_{eq}\frac{\delta\varphi}{2\varphi}$$

So after an instantaneous variation we have

$$\delta\left(L - L_{eq}\right) = -L_{eq}\frac{5\delta\varphi}{6\varphi} \qquad \textit{(Eq 5-3)}$$

Using (Eq 5-3) for an infinitesimal variation of dφ during dt we have:

$$\frac{\partial\left(L - L_{eq}\right)}{\partial t} = -\frac{L_{eq}5\partial\varphi}{6\varphi\partial t}$$

After this variation, the chain length relaxes to its equilibrium value by contraction of the chain inside the tube due to stretching entropy S:

$$S = -k\left(\frac{3\left(L - L_{eq}\right)^2}{2Nb^2}\right) \qquad \textit{(Eq 5-4)}$$

S is calculated from probability that a primitive chain has a contour length L[56].

We assume that the chain relax inside its tube with a unique relaxation time.
Chain disentanglement can be the consequence of chain contraction inside the tube. To evaluate this hypothesis we will calculate this relaxation time.
We consider that the contraction of the polymer chain inside the tube occurs with a speed depending on the position inside the tube. By symmetry, the speed is equal to zero at the center of the tube.
sL is the curvilinear abscissa is the tube (0 ≤ s ≤ 1). The chain speed inside the tube v can be written as

$$v(s) = -u\left(s - \frac{1}{2}\right)$$

With

$$u = \frac{\partial\left(L - L_{eq}\right)}{\partial t}$$

The viscous friction force by blob is $\overrightarrow{F_v} = \zeta\,\vec{v}$ where ζ is the friction coefficient of a blob.

Now we will calculate the energy dissipated in the gel by viscous friction when the polymer chains move inside their tubes.
E is the energy density dissipated in the gel by the viscous friction force by chain and by unit of time.

$$E = \int_0^1 \frac{N}{g} \overrightarrow{F_v} . \vec{v}\, ds$$

Using the chain speed expression we get

$$E = \frac{1}{12}\frac{N}{g}\zeta\left(\frac{\partial(L - L_{eq})}{\partial t}\right)^2 \qquad \textit{(Eq 5-5)}$$

On the other hand, the deformation contribution to the free energy density of the gel by chain is, according to (Eq 5-4):

$$F_{str} = kT\frac{3(L - L_{eq})^2}{2Nb^2} = \frac{3NkT(L - L_{eq})^2}{2{L_{eq}}^2}\varphi \qquad \textit{(Eq 5-6)}$$

So we can compare this motive energy by unit of time to the energy dissipated in the gel during the chain motion (Eq 5-5). We have

$$\frac{\partial F_{str}}{\partial t} = E$$

We thus get the dynamics for the chain contraction.

$$\frac{\partial(L - L_{eq})}{\partial t} = \frac{kT36g(L - L_{eq})}{\zeta N^2 b^2}$$

So the characteristic relaxation time is

$$\tau_{cont} = \frac{\zeta N^2 b^2}{kT36g} \qquad \textit{(Eq 5-7)}$$

The resulting equation of motion is

$$\frac{\partial(L - L_{eq})}{\partial t} = -\frac{(L - L_{eq})}{\tau_{cont}} - \frac{L_{eq}5\partial\varphi}{6\varphi\partial t}$$

Now we want to compare the relaxation time to the reptation time.
The reptation time is given by a curvilinear diffusion inside the tube with a diffusion coefficient equal to

$$D = \frac{kT}{\zeta N/g}$$

This diffusion is along the tube of length L so

$$\tau_{rep} = \zeta\frac{NL^2}{gkT} = \zeta\frac{N^3 b^2 \varphi}{gkT}$$

So the relation between the two characteristic times is

$$\tau_{cont} = \frac{1}{36\,N\,\varphi}\tau_{rep} \qquad \text{(Eq 5-8)}$$

The monomer number is $N_{monomer} = \frac{M_{poly}}{M_{mono}} = \frac{5\cdot10^6}{10^3} = 5000$.

We decide that the Kuhn segment is equal to one monomer so

$$N = N_{monomer} = 5 \cdot 10^3$$

So we obtain the following expression for the contraction time of a GP chain:

$$\tau_{cont} = \frac{\tau_{rep}}{1.8 \cdot 10^5\,\varphi}$$

The GP overlap concentration is c*=0.15 g/L so the overlap volume fraction is $\varphi^* = 10^{-4}$.

By definition of a gel, we always have $\varphi > \varphi^*$ for the GP gel so even for very diluted gels,

$$\tau_{cont} \ll \tau_{rep}$$

For instance, for a 1%wt gel, the reptation time is close to 10^3 s and the contraction time to 1 s.

This relaxation time is much smaller than the characteristic time of our experiments. Consequently, this phenomenon is not critical for the understanding of the swelling mechanism and it can be neglected. In most of our experiments, the chain has the time to relax its length in the tube. Thus the stretching of the chain has no influence on the swelling dynamics. In the following paragraph, we will use the classical approach of a balance between elasticity and osmotic pressure to describe the swelling of a polymer gel.

5.2.3.3 Swelling of a neutral polymer network

Swelling is controlled by the income of water inside the polymer gel. This phenomenon is driven by the pressure inside the gel and described by Darcy's law.

$$v_{solvent} - v_{polymer} = -\kappa\nabla\pi \qquad \text{(Eq 5-9)}$$

where κ is the permeability.

To apply Darcy's law we have to calculate the pressure inside the GP gel. There are two contributions to this pressure: the osmotic pressure due to the mixing of polymer with water and the elastic pressure due to chain stretching.

To calculate the osmotic pressure we take the expression given by the de Gennes scaling theory[4]. It is a Van't Hoff Law corrected by a function of the concentration, and it is in better agreement with experiments than the Flory Huggins means field prediction which does not take into account the correlations between monomers along the chain.

$$\pi_{mix} = \frac{kT}{Nb^3}\varphi\left(1 + \left(\frac{\varphi}{\varphi^*}\right)^{1.3}\right)$$

where φ^* is the overlap concentration.

$$\varphi^* = \left(\frac{b^3}{v_m}\right)^{6\nu-3} N^{1-3\nu} = \left(\frac{b^3}{v_m}\right)^{3/5} N^{-4/5}$$

We work at $\varphi \gg \varphi^*$ so

$$\pi_{mix} = \frac{kT{v_m}^{0.78}}{b^{5.34}}\varphi^{2.3} \qquad \text{(Eq 5-10)}$$

To calculate the elastic pressure we need the total stretching energy which is given by the deformation contribution to the free energy density of the gel by chain multiplied by the number of chain N_c.

$$F_{tot} = kT\frac{3\left(L - L_{eq}\right)^2}{2Nb^2}N_c$$

The elastic pressure is

$$\pi_{el} = -\frac{\partial F_{tot}}{\partial V}$$

Using $= \frac{Nv_m}{V}N_c$, (Eq 5-2) and (Eq 5-3) we have

$$\pi_{el} = -\frac{\partial F_{tot}}{\partial V} = -\frac{\partial F_{tot}}{\partial\left(L - L_{eq}\right)}\frac{\partial\left(L - L_{eq}\right)}{\partial\varphi}\frac{\partial\varphi}{\partial V} = -kTN_c\frac{3\left(L - L_{eq}\right)}{Nb^2}\frac{-5L_{eq}}{6\varphi}\frac{-\varphi^2}{Nv_mN_c}$$

So

$$\pi_{el} = -\frac{5}{2}\frac{kT\left(L - L_{eq}\right)}{v_mNb}\varphi^{3/2} \qquad \textit{(Eq 5-11)}$$

The pressure inside the gel is

$$\pi = \pi_{el}+\pi_{mix} = -\frac{5}{2}\frac{kT\left(L - L_{eq}\right)}{v_mNb}\varphi^{3/2} + \frac{kT{v_m}^{0.78}}{b^{5.34}}\varphi^{2.3}$$

The continuity equation is

$$\frac{\partial\varphi}{\partial t} + \frac{\partial j_p}{\partial z} = 0$$

where $j_p = v_p\varphi$ is the polymer flux in the z direction.

As derived by Barrière et Leibler[57], volume conservation writes

$$\varphi v_{polymer} + (1 - \varphi)v_{solvent} = 0$$

Yielding

$$j_p = v_p\varphi = \varphi(1 - \varphi)\kappa\frac{\partial\pi}{\partial z}$$

and

$$\frac{\partial\varphi}{\partial t} = -\frac{\partial j_p}{\partial z} = -\frac{\partial}{\partial z}\left(\varphi(1 - \varphi)\kappa\frac{\partial\pi}{\partial z}\right) = -\frac{\partial}{\partial z}\left(\varphi(1 - \varphi)\kappa\left(\frac{\partial\pi_{el}}{\partial z} + \frac{\partial\pi_{mix}}{\partial z}\right)\right)$$

$$\frac{\partial\varphi}{\partial t} = -\frac{\partial}{\partial z}\left(\varphi(1 - \varphi)\kappa\left(\frac{\partial\pi_{el}}{\partial z} + \frac{\partial\pi_{mix}}{\partial\varphi}\frac{\partial\varphi}{\partial z}\right)\right)$$

Using (Eq 5-10) and (Eq 5-11) we get

$$\frac{\partial\varphi}{\partial t} = \frac{\partial}{\partial z}\left(\left(-\frac{15kT\kappa}{4Nbv_m}\left(L - L_{eq}\right)(1 - \varphi)\varphi^{3/2} + 2.3\frac{kT{v_m}^{0.78}\kappa}{b^{5.34}}(1 - \varphi)\varphi^{2.3}\right)\frac{\partial\varphi}{\partial z}\right.$$

$$\left. - \frac{5kT\kappa}{2Nbv_m}\frac{\partial\left(L - L_{eq}\right)}{\partial z}(1 - \varphi)\varphi^{5/2}\right)$$

The first part of this equation correspond to a diffusive behavior with an effective diffusion coefficient D_0^{eff}.

$$\frac{\partial \varphi}{\partial t} = D_0^{eff} \frac{\partial^2 \varphi}{\partial z^2} - \frac{\partial}{\partial z}\left(\frac{5kT\kappa}{2Nbv_m} \frac{\partial (L - L_{eq})}{\partial z} (1-\varphi)\varphi^{5/2} \right)$$

With

$$D_0^{eff} = -\frac{15kT\kappa}{4Nbv_m}(L - L_{eq})(1-\varphi)\varphi^{3/2} + 2.3\frac{kT{v_m}^{0.78}\kappa}{b^{5.34}}(1-\varphi)\varphi^{2.3}$$

The first term of the expression of D_0^{eff} corresponds to a slowing down due to the tube stretching. In practice, we have shown in what precedes that L relaxes to its equilibrium value L_{eq} very quickly compared to the duration of the experiment. Thus this term is negligible and will not be taken into account.

Lastly we must express the permeability κ.

There is only few studies in the literature about the permeability of a polymer swollen by a solvent κ. In the following we will use the expression given by Barrière and Leibler[57]:

$$\kappa = \frac{\xi^2 (1-\varphi)^3}{\eta_S}$$

We have $\xi = \frac{{v_m}^{1/2}}{\varphi^{3/4} b^{1/2}}$ so

$$\kappa = \frac{v_m (1-\varphi)^3}{b\eta_S \varphi^{3/2}} \qquad \textit{(Eq 5-12)}$$

So we have

$$D_0^{eff} = 2.3\frac{kT{v_m}^{1.78}}{b^{6.34}\eta_S}\varphi^{0.8}(1-\varphi)^4 \qquad \textit{(Eq 5-13)}$$

This calculation was made for a neutral polymer. In the case of a polyelectrolyte like GP we have to take into account the presence of charges.

5.2.3.4 Swelling of a polyelectrolyte network

For a polyelectrolyte network, the osmotic pressure is due to the mixing entropy of the counter-ions liberated by the chains. For GP there is one counter-ion liberated by monomer. The distance between charges is then around the monomer length, i.e. larger than the Bjerrum length which is equal to 0.7 nm in water so there is no condensation of the counter-ions.

The number of counter-ions by volume unit is equal to 84% of the number of monomers by volume unit which is $\frac{\varphi}{v_m}$. To simplify we will consider them as equal.

According to Cabane and Hénon[58], the osmotic pressure is then equal to that of a perfect gas of counter-ions:

$$\pi_{mix} = kT\frac{\varphi}{v_m}$$

So

$$\frac{\partial \pi_{mix}}{\partial \varphi} = \frac{kT}{v_m}$$

The effective diffusion coefficient for a polyelectrolyte is

$$D_p^{eff} = \frac{kT\kappa}{v_m}(1-\varphi)\varphi = kT\frac{(1-\varphi)^4}{b\eta_S\varphi^{1/2}} \qquad \textit{(Eq 5-14)}$$

5.2.3.5 Swelling of a polyelectrolyte network in a salted solvent

The charges can be screened by the presence of salt. In that case, the osmotic pressure due to the presence of charges is modified.
For a polyelectrolyte with one counter-ion by monomer swelling in a solution of monovalent salt with a molecular concentration c_s, the osmotic pressure is controlled by the presence of additional ions[58].

$$\pi_{mix} = kT\frac{\varphi}{v_m}\left(\sqrt{1+\frac{4}{x^2}}-\frac{2}{x}\right)$$

with $x = \frac{\varphi}{c_s v_m}$

For the asymptotic regimes:
For $c_s \ll \frac{\varphi}{v_m}$ (x>>1)

$$\pi_{mix} = kT\frac{\varphi}{v_m}$$

And for $c_s \gg \frac{\varphi}{v_m}$ (x<<1)

$$\pi_{mix} = kT\frac{\varphi^2}{4c_s v_m^2}$$

We write

$$\pi_{mix} = kTc_s\left(\sqrt{x^2+4}-2\right)$$

So

$$\frac{\partial\pi_{mix}}{\partial\varphi} = \frac{kT}{v_m}\frac{x}{\sqrt{x^2+4}}$$

So we obtain for the effective diffusion coefficient:

$$D_s^{eff} = kT\kappa c_s(1-\varphi)\frac{x^2}{\sqrt{x^2+4}}$$

$$D_s^{eff} = \frac{kT}{b\eta_S}\left(\frac{(1-\varphi)^4\varphi^{1/2}}{\sqrt{\varphi^2+4v_m^2c_s^2}}\right) \qquad \textit{(Eq 5-15)}$$

In this equation, the concentration is in number of counter-ions per unit volume.

5.2.3.6 Numerical calculation of the diffusion coefficients

In this paragraph we used the previous equations to estimate a numerical value of the diffusion coefficients by taking the GP in water characteristics.

GP monomer length is $l_m = 3 \cdot 10^{-9}\ m$.
We have decided that the Kuhn segment is equal to one monomer so

$$N = N_{monomer} = 5 \cdot 10^3$$
$$b = l_m = 3 \cdot 10^{-9} m$$

GP monomer dry volume is $v_m = \frac{M_{mono}}{d\mathcal{N}_\mathcal{A}} = \frac{10^3}{1.5 \cdot 10^6 \text{x} 6 \cdot 10^{23}} = 1.1 \cdot 10^{-27}\ m^3$.
GP density is d = 1.5.

First in the case of a neutral polymer, according to (Eq 5-13) we have

$$D_0^{eff} = 4.8 \cdot 10^{-9} \varphi^{0.8} (1-\varphi)^4\ m^2/s$$

For instance, for a 1%wt gel, $D_0^{eff} = 8 \cdot 10^{-11}\ m^2/s$

Then for a polyelectrolyte, according to (Eq 5-14) we have

$$D_p^{eff} = 1.3 \cdot 10^{-9} \varphi^{-1/2} (1-\varphi)^4\ m^2/s$$

For instance, for a 1%wt gel, $D_p^{eff} = 1.6 \cdot 10^{-8}\ m^2/s$

Taking into account the effect of salt, according to (Eq 5-15) we obtain

$$D_s^{eff} = 1.3 \cdot 10^{-9} \left(\frac{1}{\sqrt{\varphi^2 + 1.7 \cdot 10^{-6} c_s^2}} \right) (1-\varphi)^4 \varphi^{1/2}\ m^2/s$$

Where c_s is in mol/m^3.
We calculate the values for the salt concentrations used in the 1D swelling experiments described in paragraph 5.2.2.2 for 1%wt GP gels.
For $c_s = 500\ mol/m^3$, $D_s^{eff} = 1.6 \cdot 10^{-10}\ m^2/s$.
For $c_s = 20\ mol/m^3$, $D_s^{eff} = 3.8 \cdot 10^{-9}\ m^2/s$.
For $c_s = 1\ mol/m^3$, $D_s^{eff} = 1.5 \cdot 10^{-8}\ m^2/s$.
For $c_s = 0\ mol/m^3$, we recover the same result as for a polyelectrolyte without salt (Eq 5-14).

All the diffusion coefficient laws are plotted on Figure 5-22 as a function of the polymer volume fraction φ.

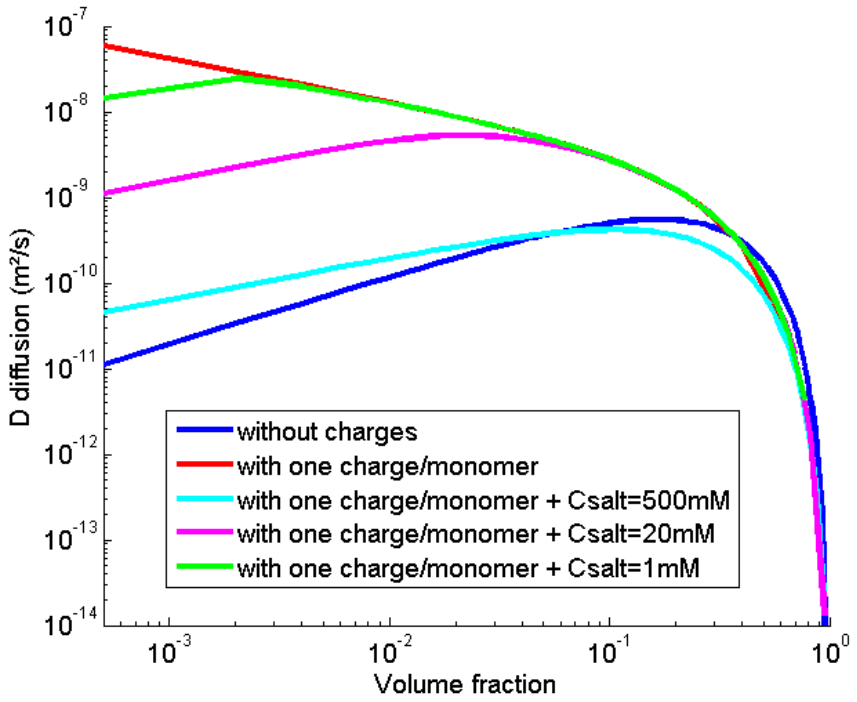

Figure 5-22: Theoretical swelling behavior of a neutral polymer and a polyelectrolyte with or without salts

In the 1D swelling experiments, the polymer volume fraction range corresponds to small volume fractions ($\varphi \ll 1$) so the term in $(1-\varphi)^4$ in the expression of the diffusion coefficient can be considered equal to 1. In this case, for a neutral polymer, the diffusion coefficient increases with concentration with an exponent ½ whereas for a polyelectrolyte, it decreases with the same exponent. An increase in the solvent ionic strength induces a decrease in the diffusion coefficient. For a large enough amount of added salt, the diffusion coefficient for a polyelectrolyte becomes similar to the diffusion coefficient of a neutral polymer because salt presence screens the osmotic pressure term due to counter-ions presence.

5.2.3.7 Comparison with the experiments

We have found experimentally (see paragraph 5.2.2.2) that for a polyelectrolyte, the diffusion coefficient decreases with ionic strength.
A comparison between the theory and the experiments is presented on Figure 5-23.

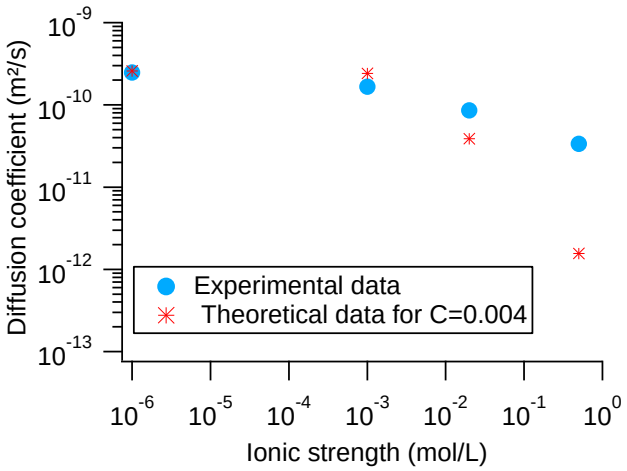

Figure 5-23: Comparison between experiment and theory (for C=0.004, i.e. φ=0.0027) - Diffusion coefficient versus ionic strength – The prefactor in the diffusion coefficient theoretical expressions is an approximation .It is modified such as to plot the theoretical data be on the same range as the experimental one.

The tendency is correct but the exponent is different between the theoretical prediction and the experimental results. This is probably due to the fact that there is in reality less than one counter-ion per monomer because some of the carboxylic acid functions are in the acid form.

5.2.4 Conclusion

It has been shown in paragraph 5.1 that the water penetration in the glassy region of the polymer layer is a fast phenomenon. Indeed, even if the diffusion coefficient of water in a glassy polymer is usually smaller than in a gel, the presence of a nanoscopic porosity inside the grains could explain the fast penetration of water in the glassy polymer. Water penetrates inside the pores, they are rapidly clogged by the formation of a gel but water still diffuses inside this gel to penetrate inside the grains.
The limiting step in the dissolution process is then the swelling and dissolution of the gel phase. This swelling follows a diffusive kinetics which is the same at all investigated timescales and lengthscales. It has been quantitatively studied with a homemade experimental set-up where the polymer concentration inside the gel is monitored by dynamic light scattering.

For GP a value of the diffusion coefficient was estimated ($D = 2.5 \cdot 10^{-10} m^2/s$). But the approach with a single D value fails to fully describe the behavior at all times. No quantitative measurements could be obtained, but it is likely that D depends on the polymer concentration, with D decreasing with the concentration such as predicted by the theoretical calculation.

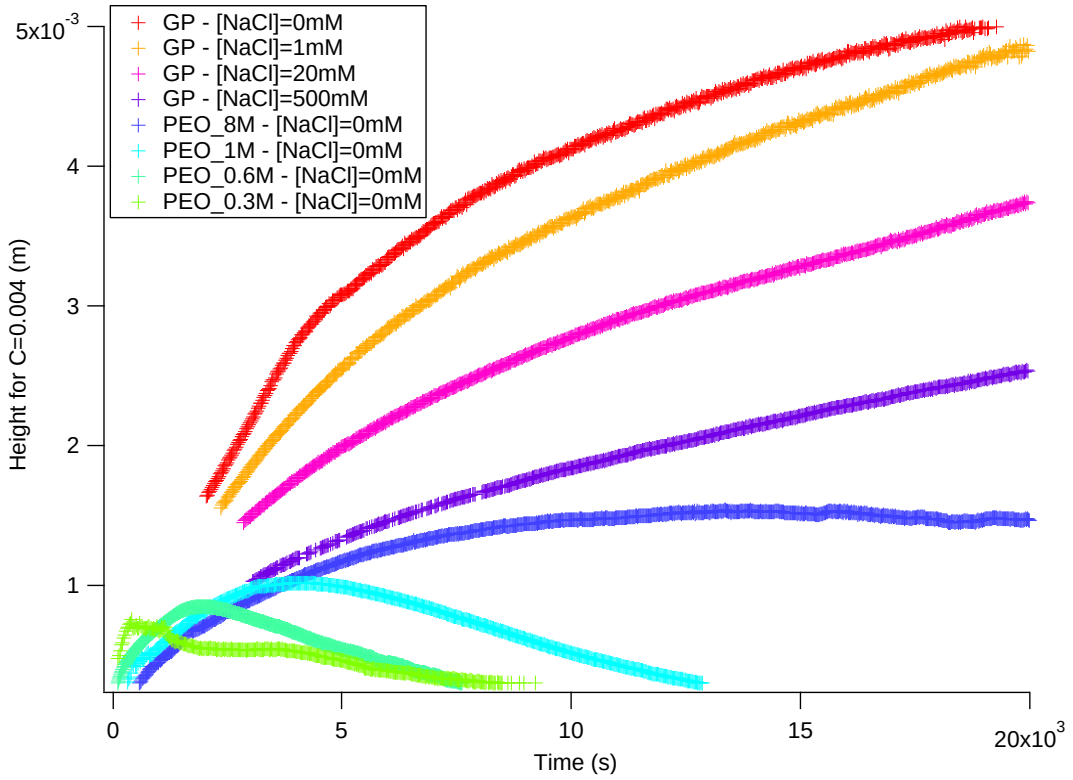

Figure 5-24: Swelling of a polymer layer in a solvent - Height at C_{cut}=0.004 versus time – Summary for GP and PEO of different molar masses in deionized water or NaCl solutions

The diffusion coefficient also depends on solvent ionic strength. It decreases with ionic strength as predicted for a polyelectrolyte in paragraph 5.2.3.5. For a very high ionic strength, GP behavior becomes similar to those of a neutral polymer like PEO, at least at the beginning of the experiment (see Figure 5-24).

However, PEO swelling is not a diffusive process only. Indeed, there is a drop in the gel height at C_{cut} versus time curves which is not predicted by the diffusion equation. The critical time at which this drop happens depends on the molar mass but it seems that it is not related with the reptation time because the exponent and the order of magnitude are very different but with the inverse overlap concentration. This brings up a hypothetic mechanism for the dissolution: dissolution is only due to the cooperative diffusion of water in the gel until the overlap concentration is reached.

For GP swelling this drop is not observed. Extrapolation for GP layers based on the measured GP overlap concentration predicts a critical time t* around 10^5 s which is larger than the measurement duration. However, even after several days of swelling the GP gel height does not decrease. The concentration becomes uniform and decreases slowly. After 5 days we observed a fragmentation in the gel and pieces of gel are removed from the layer and leave by convection. Those phenomena are not yet well understood.

6 Swelling with convection

In real dissolution conditions on the field, water is stirred when powder is added to it. This additional convection plays an important part in the increase of the dissolution rate. In the previous chapter, swelling of the gel phase was established to be the limiting step in GP dissolution mechanism. In this chapter, the influence of convection on this step will be studied. First, the dissolution kinetics will be macroscopically studied using a rheological set-up. Then, the erosion of the gel phase will be monitored using a microfluidic channel.

6.1 Macroscopic experiment

6.1.1 Set-up and calibration

A home-made geometry presented in Figure 6-1 was designed to monitor powder dissolution with time by measuring viscosity. This set-up allows for controlled convection during mixing by adjusting the rotation speed.

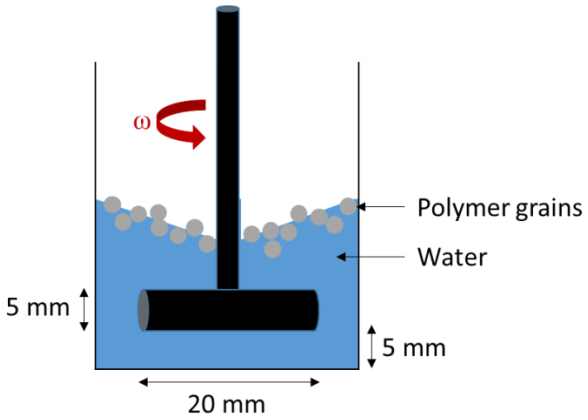

Figure 6-1: Rheology geometry for macroscopic dissolution experiments.

Solvent and polymer powder are placed in the vial and a rheometer is used to impose a rotation speed to the bar fixed at the bottom of the rotation axis. The resulting torque is measured by the rheometer. It is related to the sample viscosity and hence to the GP concentration in the sample but the “bar and vial” geometry is too different from a model cone and plate geometry for a direct calculation of the viscosity from the measured torque. The geometry was hence calibrated to obtain the GP concentration as a function of the measured torque. Calibration measurements were done using silicone oils of different viscosities and GP solutions of different concentrations prealably mixed. Torque was measured as a function of rotation speed for several GP solutions at different concentrations. Plotting all the data on the same abacus, calibration curves relating GP concentration to the measured torque for different rotation speeds were obtained. They are presented in Figure 6-2. GP dissolution can thus be observed by monitoring the increase of concentration in the vial when deionized water is placed in it and GP powder is added at the beginning of the experiment.

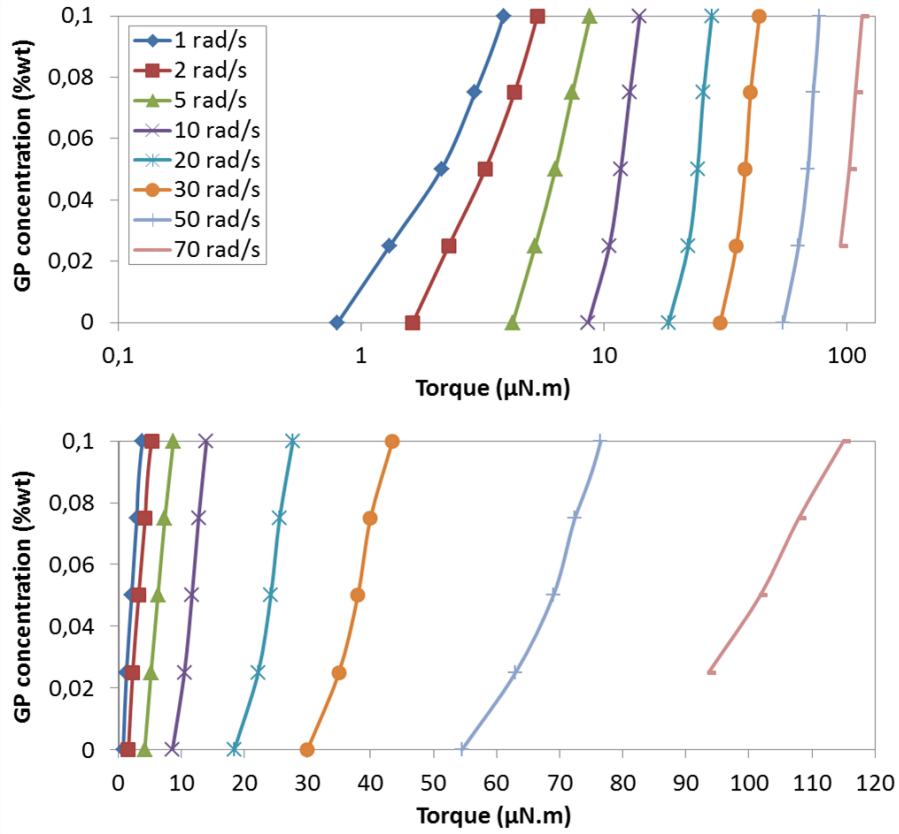

Figure 6-2: Calibration curves: GP concentration versus torque for different rotation speeds. Top: semi-logarithmic axis. Bottom: linear axis.

Adding all the powder at the same time made it difficult to avoid lumps formation. Nevertheless, a good reproducibility was ensured by using the same mixing protocol for all the experiments. The vial is filled with 6 mL of pure deionized water and the bar is immersed in the solution. The gap between the bar and the bottom of the vial is 5 mm large.

A volume of 6 mL corresponds to a homogeneous repartition of the liquid around the bar, allowing the best possible mixing for the powder. Indeed, for a larger volume (> 8 mL), the lumps will float on the water surface without being sheared, and, for a smaller volume (< 4 mL), the measurement will be impossible because the bar will not be totally immersed. The influence of sample volume variations on the torque measurements was investigated by varying the volume of two silicone oils in the appropriate range of viscosity between 5.5 mL and 6.5 mL. It was found to be negligible compared to measurement accuracy.

A cup of polymer powder is placed on a weighting scale and a small amount is sampled with a spatula. The sampled powder weight is determined by difference. The precision scale used for powder sampling allows an accuracy of 0.1 mg but the sampling itself for such a small amount of powder is subject to variations. For all experiments, final polymer concentration was chosen to be theoretically equal to 0.1%wt because it is the working concentration recommended by Schlumberger for GP on the field. It corresponds to an initial powder sample of 6 mg. Practically, the sampled amount of powder varied between 6 mg and 7.5 mg, meaning that the final concentration varied between 0.1%wt and 0.125%wt.

The bar is put in rotation at 50 rad/s which creates a vortex at the center of the vial. After 30 s, the sampled powder is introduced in the vial right above this vortex. 5 seconds after powder introduction, rotation speed is modified to its defined value for the experiment and measurement begins. This step at 50 rad/s is done to ensure an optimized dispersion of the powder in the water and to minimize lumps formation. However, a few lumps of hundreds micrometers size are sometimes observed. Indeed, the way of introducing the powder in the water determines the possible formation of lumps and their size, leading to the largest source of inaccuracy.

With this protocol, dissolution curves where the concentration of polymer in solution is plotted over time were obtained. Figure 6-3 presents the dissolution curve obtained when 6 mg of GP was put in 6 mL of water at a rotation speed of 50 rad/s. Polymer concentration in the solution increases with time until it reaches a plateau at the final concentration, meaning that all the polymer powder is dissolved. A dissolution time $t_{1/2}$ was used to characterize the dissolution kinetics and to compare different experiments. It is defined as the time required to reach 50% of the final concentration.

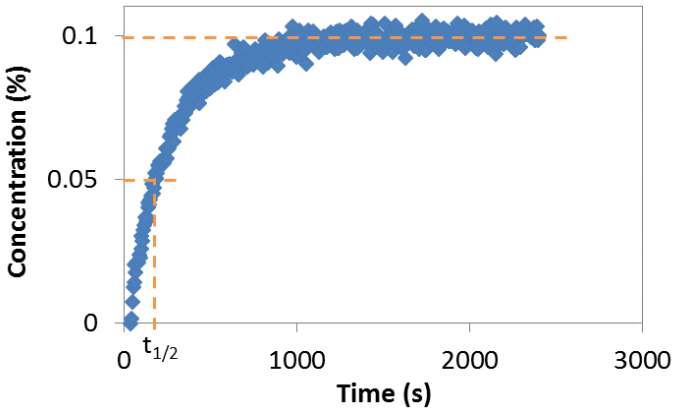

Figure 6-3: Dissolution curve of GP mixed in deionized water at 50 rad/s for a final concentration of 0.1%wt. $t_{1/2}$ = 150 s

Measurements of GP powder dissolution were realized for final concentrations ranging from 0.075%wt to 0.125%wt. Concentration influence on the dissolution time was found to be negligible with respect to the accuracy of the dissolution time at a given concentration due to variability in the powder introduction. Thus, the powder sampling variations between 6 mg and 7.5 mg have no influence on the dissolution time measurement accuracy.
For concentrations larger than 0.25%wt, variability due to lumps formation increases drastically and the definition of a dissolution time loses its meaning.

The influence of mixing velocity, grain size, ionic strength of the solvent and temperature on the dissolution kinetics was studied with this set-up.

6.1.2 Mixing velocity influence

The influence of mixing velocity was investigated using the protocol described in paragraph 6.1.1. All the experiments were realized with GP powder at 200 mesh (d < 74 µm) for a final concentration of 0.1%wt ± 0.02%wt and a rotation speed varying from 1 rad/s to 70 rad/s. Several experiments were

done at the same rotation speed in order to evaluate the measurements reproducibility. For each experiment, the dissolution time $t_{1/2}$ was measured. Results are presented in Figure 6-4 where the dissolution time $t_{1/2}$ is plotted as a function of rotation speed.

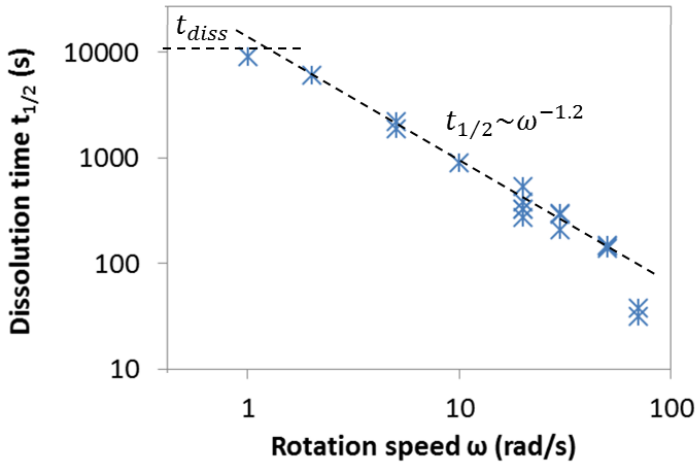

Figure 6-4: Influence of the mixing velocity on the GP dissolution kinetics: variations of the dissolution time $t_{1/2}$ as a function of rotation speed for a final concentration of 0.1%wt ± 0.02%wt

GP dissolution time strongly depends on mixing velocity and decreases by almost three decades when the rotation speed increases from 1 rad/s to 70 rad/s. Indeed the shear induced by mixing erodes the gel layer around the grains, accelerating the dissolution process. GP dissolution time values are very large in all the explored velocity range compared to the dissolution time of 1 min expected for GP powder on the field.

At intermediate velocities (between 2 rad/s and 50 rad/s), the dissolution time can be fit to a power law of the rotation speed with an exponent -1.2.

At very small rotation speeds, the dissolution time is expected to reach a plateau corresponding to the zero-shear dissolution time. This plateau value should be around 10000 s (almost 3 h!). The problem is similar to the one studied in the previous chapter where dissolution was studied without convection. The dissolution is controlled by the time t_{diss} needed by the water to diffuse across the GP grains radius.

$$t_{diss} = \frac{L^2}{D}$$

More precisely, t_{diss} is the time needed by a grain to swell until the polymer concentration decreases to the overlap concentration. L is thus defined as $V_{final} = \frac{4}{3}\pi L^3$ with $V_{initial}/V_{final} = C^* = 10^{-4}$.

So $R_{grain}/L = C^{*1/3}$. R_{grain} is taken as the maximal grain radius in the powder which is close to 50 µm so $L \cong 5 \cdot 10^{-5} \cdot 10^{4/3} \cong 1\ mm$.

With $D = 10^{-10}\ m^2/s$ we find

$$t_{diss} = 10^4\ s$$

This dissolution time is the same as the dissolution time $t_{1/2}$ measured in the macroscopic dissolution experiment when the rotation speed is small. Both results are thus consistent.

6.1.3 Grain size influence

Grain size influence was investigated using the protocol described in paragraph 6.1.1. GP powder at 80 mesh (d < 200 µm) was used. Dissolution experiments were conducted at a rotation speed varying from 1 rad/s to 70 rad/s as for classical GP powder at 200 mesh. Results are presented on Figure 6-5.

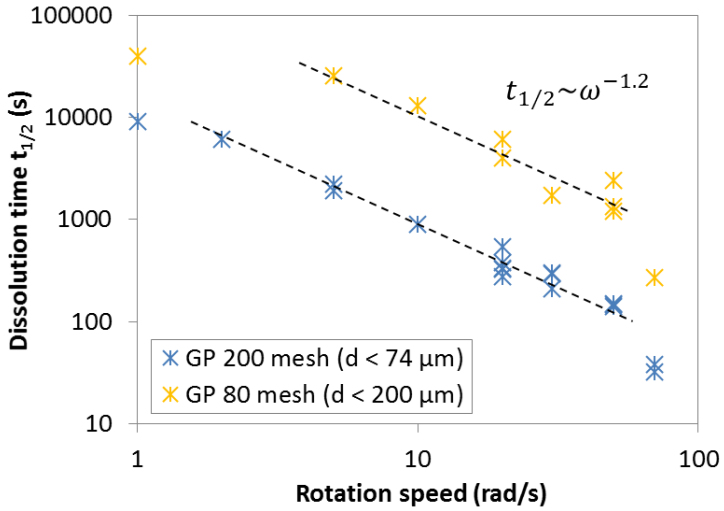

Figure 6-5: Dissolution time comparison between two different grades of GP powder as a function of the rotation speed

The shape of the curve is the same for both granulometries, with a one decade shift towards the large values of time for the larger grains. Remarkably, the same power law dependence of the dissolution time with rotation speed is found for both grain size distributions, with the dissolution time $t_{1/2}$ varying as $\omega^{-1.2}$.

Moreover, we verify that the larger the maximum grain size R_{grain}, the larger the dissolution time at vanishing rotation speeds.

However, with those results, it is impossible to quantitatively conclude about the grain size influence because 80 mesh and 200 mesh are not narrow fractions and every grain sizes under a certain cut length are represented in the sample.

Three narrow powder fractions were prepared by sieving an 80 mesh GP powder with a pile of decreasing mesh size sieves:

- Fine fraction: 32 µm – 40 µm
- Intermediate fraction: 63 µm – 90 µm
- Large fraction: 150 µm – 180 µm.

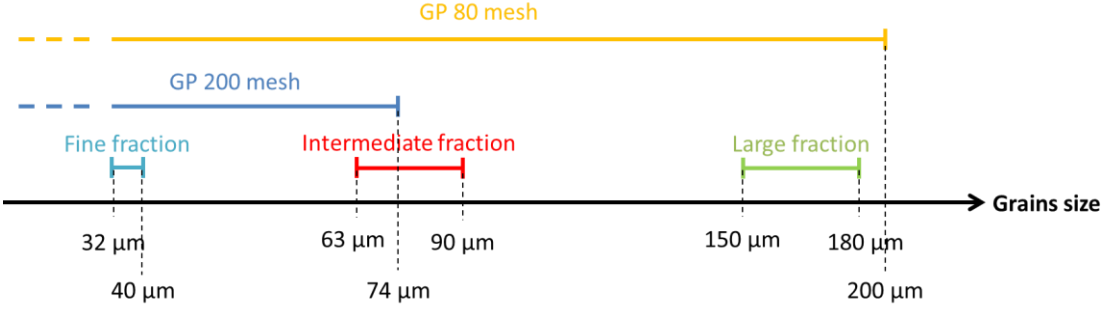

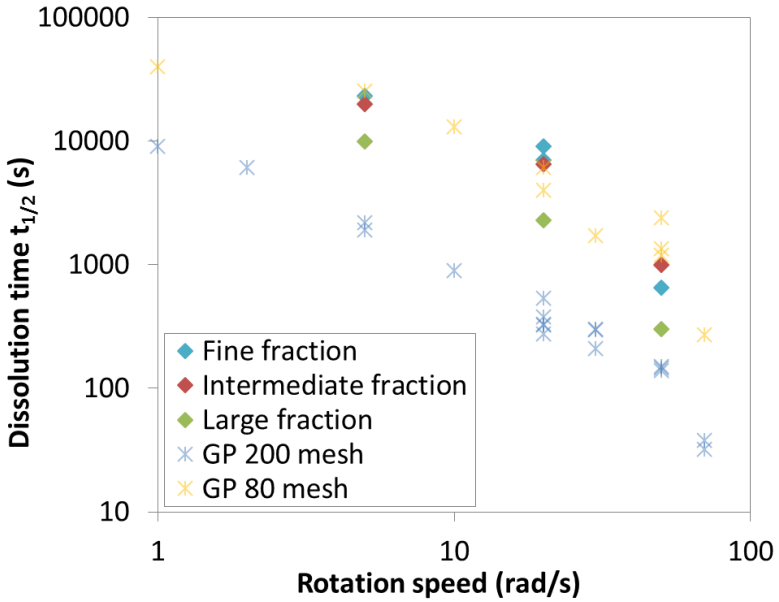

Figure 6-6: GP grains sieved fractions dissolution

All the dissolution times measured on sieved fractions are larger than the dissolution time of GP 200 mesh, even the dissolution time of the fine fraction. A possible explanation is that grains of the fine fraction stick together and form lumps more easily than larger grains, increasing the effective grain diameter and hence the dissolution time.
The increase of the dissolution rate with the grain size observed for non-sieved fractions (200 mesh and 80 mesh comparison in Figure 6-5) is in good agreement with the literature. Parker et al also observed that, for an unfractionated powder sample, lump formation is governed by the fraction of small grains in the sample (see Figure 2-14). This is in good agreement with the fact that the dissolution time of the large fraction is smaller than the dissolution time of the fine fraction, which governs the dissolution of the non-sieved 200 mesh sample.

The fastest dissolution is obtained with a polydisperse sample of small and very small grains. The dissolution rate is thus clearly not only controlled by the size of the grain but also by the dry powder ability to “flow” which governs the size of the lumps.

6.1.4 Ionic strength influence

The influence of ionic strength of the solvent was investigated using the protocol described in paragraph 6.1.1. Dissolution experiments were performed at a mixing velocity of 50 rad/s, using 200 mesh GP powder and NaCl solutions instead of deionized water as solvent. The same NaCl concentrations as the ones used for the swelling of a polymer layer study presented in paragraph 5.2.2.2 were chosen. The measured dissolution times are plotted versus ionic strength on Figure 6-7. For deionized water, the ions responsible for the ionic strength of the solvent comes from the free salt present in the polymer powder which are rapidly released in the water at the beginning of the experiment. For a 0.1%wt GP solution, the concentration of free salts is close to 10^{-4} mol/L.

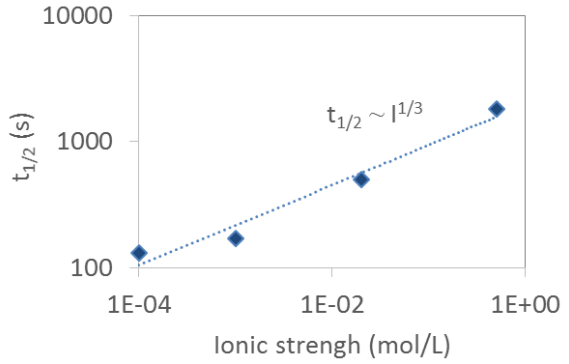

Figure 6-7: Solvent Ionic strength influence on the dissolution time for 200 mesh GP powder at 50 rad/s

As it was already observed for the swelling of GP layer without convection, increasing the solvent ionic strength slows down the dissolution. Dissolution time is multiplied by more than ten between pure water and an equivalent of sea water.

A simple comparison of the data with and without convection consists in plotting the dissolution time $t_{1/2}$ as a function of the diffusion coefficient D measured for a GP layer in the 1D swelling experiment with NaCl solutions used as solvents (see Figure 5-14). The result is plotted in Figure 6-8.

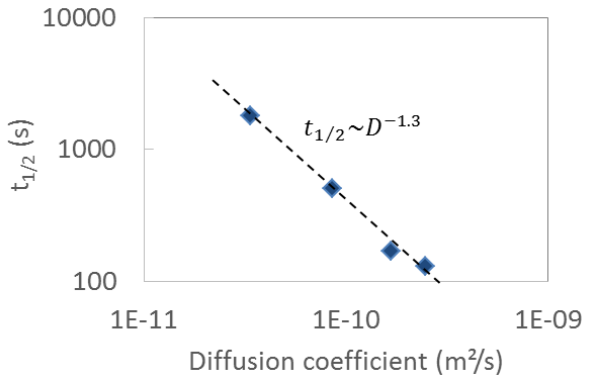

Figure 6-8: Dissolution time versus Diffusion coefficient for GP samples

The dissolution time $t_{1/2}$ varies with the polymer diffusion coefficient in NaCl solutions as

$$t_{1/2} \sim D^{-1.3}$$

This exponent will be commented in the following.

6.1.5 Temperature influence

The influence of temperature was also investigated in the range of 10°C to 40°C which is the range of temperature that can be encountered on the field. No noticeable effect was found. It is consistent with the fact that neither the swelling kinetics, nor the rheological properties of GP strongly depends on the temperature.

6.1.6 Conclusion

The measurement of a macroscopic dissolution time was performed. It was shown to be dependent on grains size distribution, ionic strength of the solvent and mixing velocity.

Polydispersity of the powder influences its tendency to form lumps which are responsible for an increase in the dissolution time. Surprisingly, the fastest dissolution rate is obtained for polydisperse samples composed of small and intermediate size grains. For a given polydispersity, the dissolution time at different ionic strengths varies with the diffusion coefficient D obtained for the swelling of a GP gel without convection with a power law $t_{1/2} \sim D^{-1.3}$.

We have also established that the dissolution time decreases with the mixing velocity following a power law:

$$t_{1/2} \sim \omega^{-1.2}$$

for $1\ rad/s < \omega \leq 50\ rad/s$.

However, it is difficult to calculate the shear rate/stress corresponding to the velocity with this geometry. A more controlled experimental set-up using a microfluidic channel was designed. The set-up and results are presented in the next paragraph.

6.2 Microfluidic experiment

The aim of this experiment was to observe the swelling and erosion of a gel layer at a microscopic scale. A microfluidic channel with one polymer wall and three inert silicone (PDMS) walls was designed to study the polymer behavior at various solvent velocities in the channel. Experimental set-up and results are presented in the following paragraphs.

6.2.1 Experimental set-up

GP layers deposited on glass slides prepared as described in paragraph 3.3 were used for the polymer wall. They are about 1.5 cm long, 5 mm large and 50 µm thick. It is exactly the same kind of layers as those used for the swelling followed by light scattering experiment. The layer edges were carefully cut with a scalpel to obtain straight edges and cleaned to avoid any residual polymer pieces around them.

PDMS lids were prepared by curing a mixture of PDMS and curing agent against a mold. The mold consists in a plastic dish at the bottom of which a piece of stainless steel shim stock is glued. Dimensions of the shim stock are adjusted so as to fit to the polymer layer prepared on a glass slide, with a width 1 mm larger than the polymer layer. After curing, the PDMS is peeled off the mold and a lid with a cavity is obtained. Two holes of 500 µm diameter are punched at the cavity edge to deliver solvent in the channel. PDMS lid is then stuck to the glass slide by plasma bonding to obtain a microfluidic chip. The PDMS lid was carefully placed to form a 1 mm wide channel along the polymer layer.

The microfluidic chip is presented on Figure 6-9.

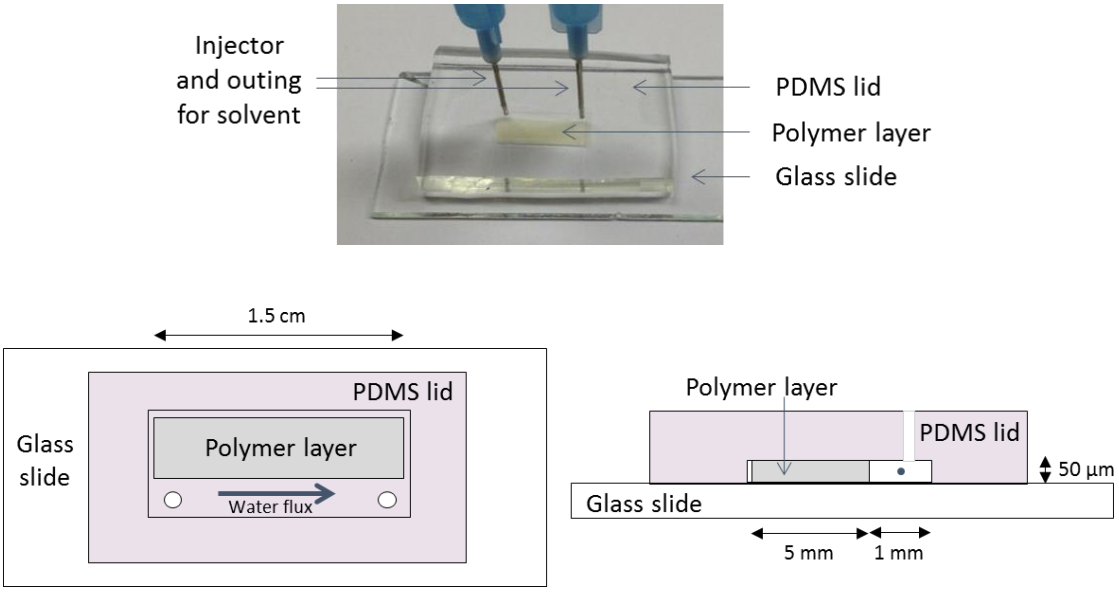

Figure 6-9: Microfluidic experimental set-up. Top: photography of a chip. Left: top view. Right: side view.

A syringe pump with a 50 mL syringe was used to set the solvent flow inside the channel between 200 µL/min and 9000 µL/min. Solvent used in this experiment was deionized water with micrometric hollow glass beads (sphericels) used as tracers to measure the velocity inside the channel.

The microfluidic chip was observed in reflection with an inverted microscope. Pictures of the experiment were acquired with a Sentech camera through the glass slide at a frequency of 1 Hz. Shutter time was set to detect glass beads trail. The length of the trail divided by the shutter time gave a measurement of the average velocity of the solvent.

Monitoring the gel swelling and erosion was done by monitoring several impurities in the polymer matrix during the experiment. An example in given on Figure 6-10 where the impurity is circled in red.

The swelling gel/liquid interface is set by the erosion. It is very visible thanks to the glass beads trails in the liquid zone. In Figure 6-10, gel swelling is not totally balanced by erosion and the gel grows in the channel during the experiment.

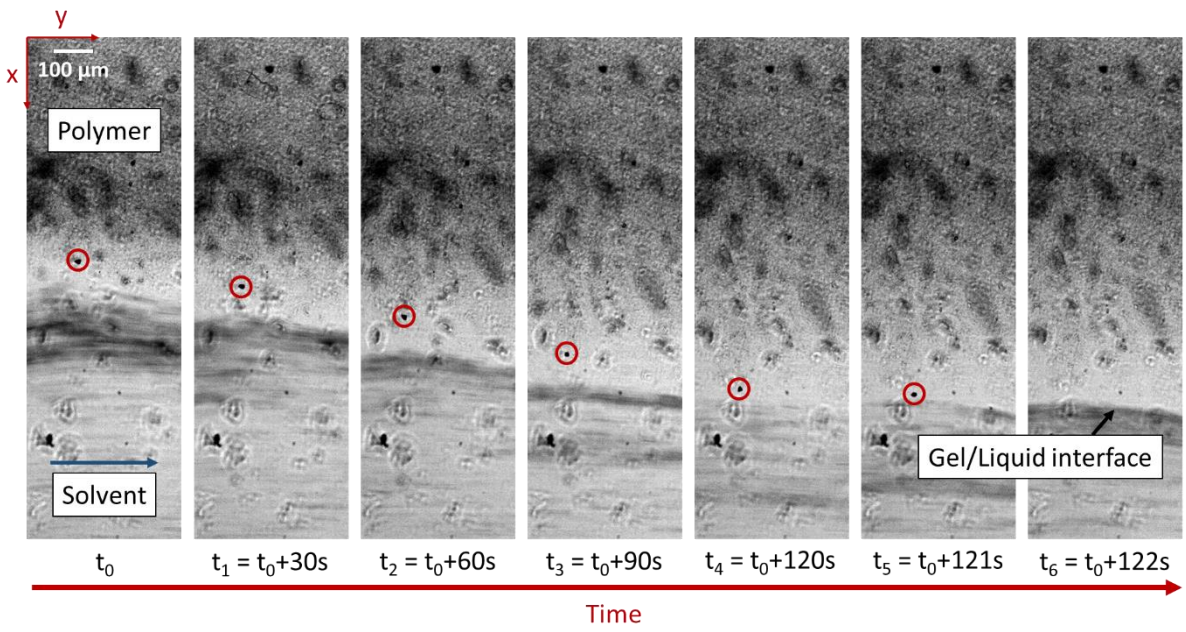

Figure 6-10: Series of images at increasing times of the gel/water interface. The gel grows and its interface is displaced into the water channel.

Several experiments were conducted at different water velocities.

6.2.2 Erosion of the gel layer

A schematic representation of the channel geometry is presented on Figure 6-11. Polymer swells in the x direction and is eroded in the y direction.

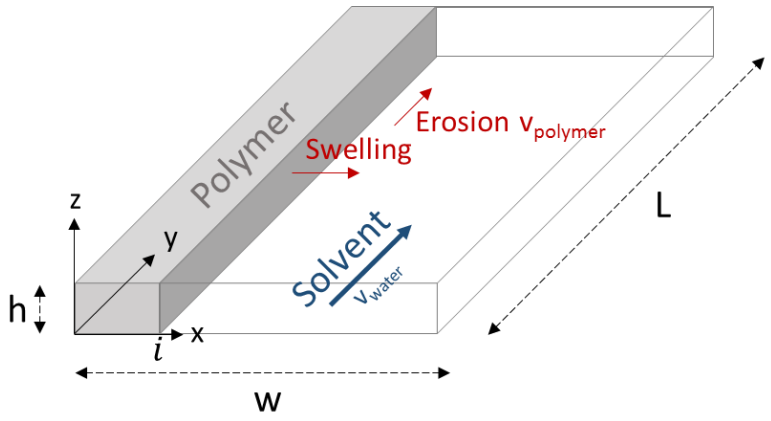

Figure 6-11: 3D representation of the channel

In order to quantify the erosion of the swollen polymer, we want to estimate the shear rate at the solvent/polymer interface.
The tangential stress is continuous at the interface:

$$\sigma_{i^-} = \sigma_{i^+}$$

With $\sigma_{i^-} = \eta_{gel}\dot{\gamma}_{i^-}$ and $\sigma_{i^+} = \eta_{water}\dot{\gamma}_{i^+}$.

The shear rate in the polymer at the interface is

$$\dot{\gamma}_{i^-} = \left(\frac{dv_y}{dx}\right)_{i^-} \sim \frac{v_{polymer}}{h}$$

with the smallest channel dimension h being taken for the shear gradient scale.

And similarly the shear rate in the water at the interface is

$$\dot{\gamma}_{i^+} = \left(\frac{dv_y}{dx}\right)_{i^+} \sim \frac{v_{water}}{h}$$

Where v_{water} is the average solvent velocity in the channel.
So

$$\sigma_{i^-} = \sigma_{i^+} = \eta_{water}\frac{v_{water}}{h}$$

These relations will be used in the following to estimate an erosion criterion.

The polymer velocity along the y axis $v_{polymer}$ is taken equal to the last velocity measured before the particle is driven away by the water flux. For instance for the experiment presented on Figure 6-10, $v_{polymer}$ is measured between t_4 and t_5. This is a rough estimation of the polymer velocity at the erosion interface because it is impossible to know when exactly between t_5 and t_6 the red circled particle has been taken away from the polymer layer. The acquisition frequency introduces an error on the velocity measurement. The polymer velocity at the erosion interface is thus systematically underestimated. However, as the acquisition frequency is the same for all the experiments, this error is also the same for all the experiments. It is evaluated to a few micrometers per second. It is a large value but we will see on the following paragraph that it has no influence on the erosion concentration measurements.

Polymer velocity v_y is plotted as a function of the position X for three tracers in the polymer at three different times during an experiment where $v_{solvent}$ is constant (see Figure 6-12). The polymer erosion velocity $v_{polymer}$ is very close for all tracers: $v_{polymer}$ = 9.5 µm/s ± 1 µm/s.

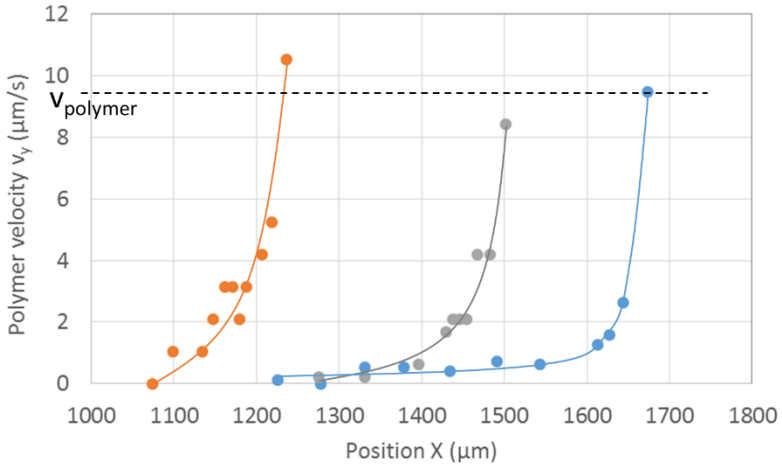

Figure 6-12: Polymer velocity in the Y direction due to erosion versus position along the X axis for 3 impurities used as tracers. $V_{solvent}$ = 0.2 m/s.Full lines are guides for the eye.

Within the experimental conditions of Figure 6-12, we obtain

$$\dot{\gamma}_{i^-} = \frac{v_{polymer}}{h} = 0.19\ s^{-1}$$

$$\sigma_{i^-} = \eta_{water}\frac{v_{water}}{h} = 4\ Pa$$

According to Figure 6-13 in which rheological measurements of $\sigma(\dot{\gamma})$ are displayed for polymer solutions of different concentrations for $\dot{\gamma}_{i^-} = 0.19\ s^{-1}$, a shear stress of 4 Pa corresponds to a concentration of 0.5%wt in the GP layer. This allows us to define the erosion concentration c_{er}.

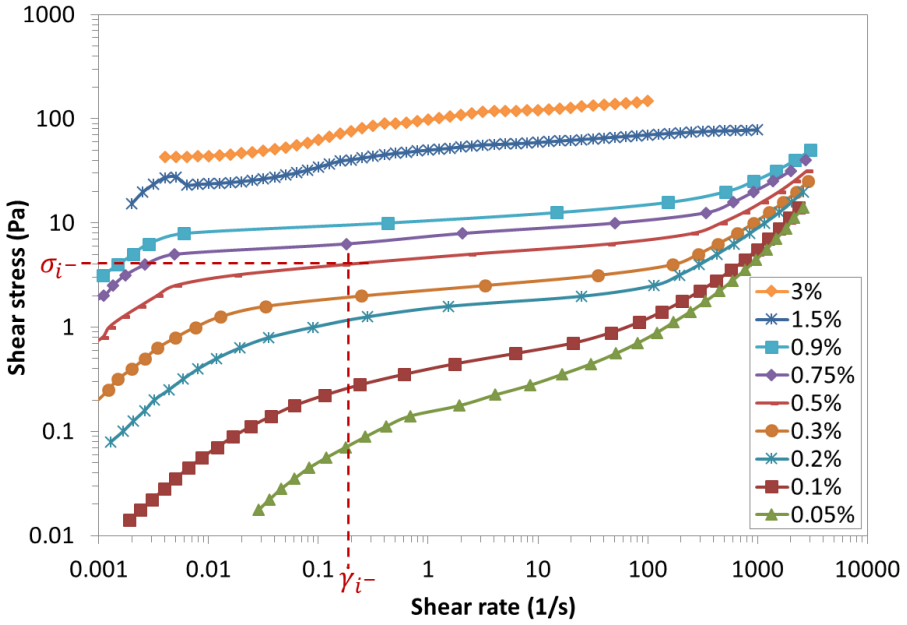

Figure 6-13: Shear stress versus shear rate for GP solutions at different concentrations. Measurements were realized as presented on paragraph 3.2.5

Several experiments were conducted at different water velocities ranging from 0.06 m/s to 3 m/s. Results are summarized in the following table where c_{er} is estimated from values of $\dot{\gamma}_{i^+}$ and σ_{i^-} at various water flow rates.

v_{water} (m/s)	$\dot{\gamma}_{i^+}$ (s^{-1})	$v_{polymer}$ (m/s)	$\dot{\gamma}_{i^-}$ (s^{-1})	σ_{i^-} (Pa)	c_{er} (g/g)
0.06	1200	1.40E-05	0.28	1.2	0.002
0.08	1600	6.00E-06	0.12	1.6	0.003
0.2	4000	9.50E-06	0.19	4	0.005
0.8	16000	7.00E-06	0.14	16	0.010
3	60000	1.50E-05	0.3	60	0.025

We find that in the gel, the shear rate at which erosion occurs $\dot{\gamma}_{i^-}$ is roughly independent of the water velocity. The variations in $\dot{\gamma}_{i^-}$ values are attributed to the error set by the acquisition frequency.

Moreover, the shear rate at which erosion occurs $\dot{\gamma}_{i^-}$ is in the shear rate range where the shear stress at a given concentration is constant (see Figure 6-13). An error in the evaluation of $\dot{\gamma}_{i^-}$ has thus no impact on the determination of the concentration at which erosion occurs.
The error on c_{er} is mainly due to an error on the measurement of σ_{i^-}, i.e. on the water velocity. It is evaluated at 10%.

The concentration at which erosion occurs depends on the water velocity, and more precisely on the shear of the GP gel, which is related to water velocity. c_{er} is plotted in Figure 6-14 as a function $\dot{\gamma}_{i^+}$, the shear rate in water at the interface.

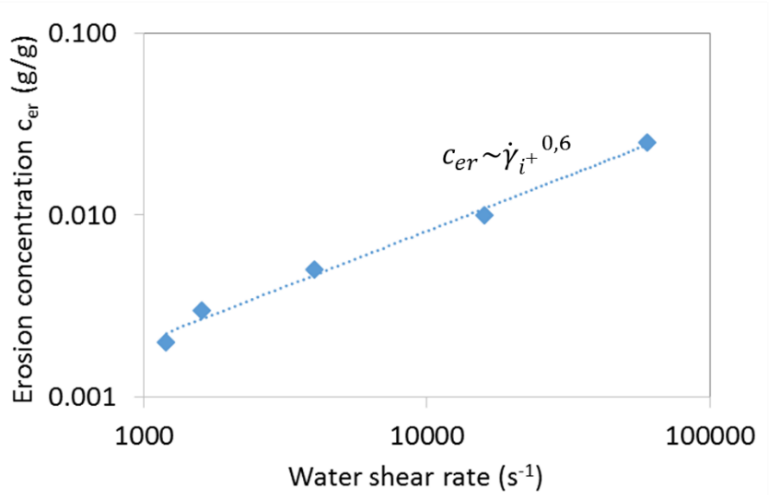

Figure 6-14: Erosion concentration versus shear rate in the water at the gel/liquid interface

Erosion concentration increases with shear rate, following a power law

$$c_{er} \sim \dot{\gamma}_{i^+}^{0.6}$$

Note that for the highest water velocity (3 m/s), gel swelling is totally balanced by erosion: the gel/liquid interface position does not vary during the experiment.

The position of the gel/liquid interface is set by the competition between gel swelling and erosion. Erosion is controlled by the concentration in the gel layer. The concentration at which erosion occurs c_{er} depends on the shear imposed on the gel by the water flow. The dependency follows a power law with an exponent 0.6.

6.2.3 Discussion

Two mechanisms are at stake in the dissolution of a polymer layer with convection, the swelling of a gel layer and the erosion of this gel layer. The dissolution time of GP powder is set by a competition of these two phenomena.
We have established in Chapter 5 that in the case of dissolution without convection experiments, the dissolution time was only controlled by swelling of the gel layer. This swelling is controlled by the mutual diffusion coefficient of water in polymer.

In the case of dissolution in presence of convection, the dissolution time varies with water velocity. This is due to the erosion of the gel layer, which accelerates the dissolution process. In the following paragraph, we will try to quantify this process by presenting some scaling law calculations.

6.2.3.1 Velocity dependence in the intermediate regime

In the regime 2 rad/s < ω < 50 rad/s, we have seen in paragraph 6.1.2 that the dissolution time varies as the rotation speed to the exponent -1.2.

$$t_{1/2} \sim \omega^{-1.2}$$

To explain this behavior, we will begin by considering a 1D situation where a polymer solution of concentration $c_{x=0}$ is placed at x=0.
The polymer swells with a diffusion coefficient D and is eroded with a characteristic time τ(C). A schematic representation of the concentration as a function of the distance x from the polymer source is presented on Figure 6-15.
c_{er} is the concentration at which erosion occurs and ξ is the length at which $c = c_{er}$.

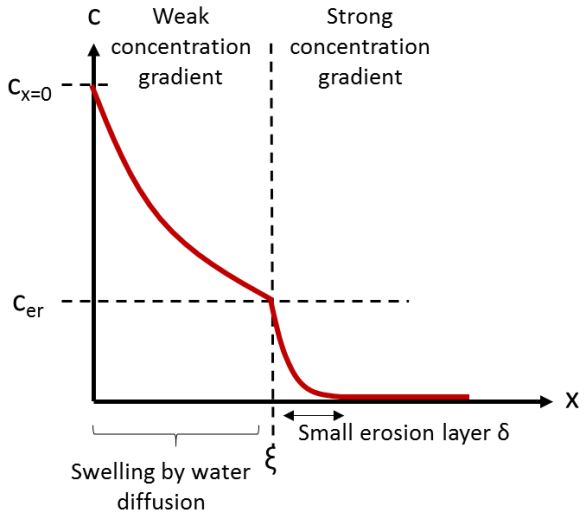

Figure 6-15: Schematic representation of the dissolution of a polymer layer. Swelling/erosion competition.

The general behavior equation in this configuration is:

$$\frac{\partial c}{\partial t} = D\frac{\partial^2 c}{\partial x^2} - \frac{c}{\tau(c)}$$

To simplify, we look for a solution in a stationary regime and we suppose that there is no erosion for $c > c_{er}$, which corresponds to $\tau(C) = \infty$. We further assume that $\tau(C) = \tau$ is constant for $c \leq c_{er}$.

For $x > \xi$, the solution is

$$c(x) = c_{er} e^{-\frac{x-\xi}{\sqrt{D\tau}}} \qquad \textit{(Eq 6-1)}$$

With $c \to 0$ for $x \to \infty$.

The flux j_{er} at $x = \xi$ is given by $j_{er} = -D\left(\frac{\partial c}{\partial x}\right)_{\xi}$, yielding

$$j_{er} = c_{er}\sqrt{\frac{D}{\tau}}$$

The physics does not depend on what happens for $x < \xi$ as long as the concentration gradient in this zone is small.

Q is the quantity of polymer by surface unit.

$$\frac{\partial Q}{\partial t} = -j_{er}$$

For a polymer grain (diameter L, initial concentration c_0), the initial polymer content in the grain by surface unit is Lc_0. The dissolution time of the grain is t_{diss}. So

$$\frac{\partial Q}{\partial t} \sim \frac{Lc_0}{t_{diss}}$$

So t_{diss} can be estimated as

$$t_{diss} = \frac{Lc_0}{j_{er}} = \frac{Lc_0}{c_{er}}\sqrt{\frac{\tau}{D}}$$

The exact calculation of the erosion time τ is difficult and we will only give a naïve estimation. τ is related to the time during which the solvent is in contact with the gel/liquid interface: $\tau \sim L/U$, where L is the lateral size of the eroded zone and U is the water velocity at some distance δ from the interface (see Figure 6-16).

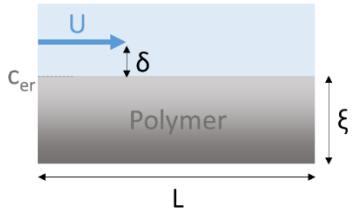

Figure 6-16: Schematic representation of the polymer/solvent interface

The velocity is in fact equal to $U = \dot{\gamma}\delta$.

δ is given in (Eq 6-1) by $\delta = \sqrt{D\tau}$.

So we have

$$\tau \sim L^{2/3}D^{-1/3}\dot{\gamma}^{-2/3}$$

So

$$t_{diss} \sim \frac{c_0}{c_{er}}L^{4/3}D^{-2/3}\dot{\gamma}^{-1/3}$$

The dissolution time increases with the grain size L.

In the previous paragraph we observed that $c_{er} \sim \dot{\gamma}^{0.6}$ (see Figure 6-14)

So

$$t_{diss} \sim \dot{\gamma}^{-0.9} \qquad \textit{(Eq 6-2)}$$

The dissolution time $t_{1/2}$ measured in the dissolution followed by rheology experiments presented in paragraph 6.1.2 was found to follow the law $t_{1/2} \sim \omega^{-1.2}$.
This is in relatively good agreement with (Eq 6-2).

From this, we conclude that in the intermediate regime, the dissolution time is controlled by erosion of the gel layer.

6.2.3.2 Velocity regimes

Several regimes are observed on the dissolution time versus rotation speed curves established by monitoring the dissolution time macroscopically with a rheometer.
They are summarized in Figure 6-17.

At small rotation speed, i.e. $\omega < 2\ rad/s$, the dissolution time is independent of the solvent velocity. Dissolution is governed by the swelling of the polymer gel up to the overlap concentration.
At intermediate rotation speed, i.e. $2\ rad/s < \omega < 50\ rad/s$, the dissolution time varies as the rotation speed to the power -1.2.
Dissolution is controlled by erosion of the gel layer.
At large rotation speed, the exponent of the dissolution time versus rotation speed power law seems to increase. A possible explanation is that it is due to the formation of a vortex in the liquid that modifies the flow. Moreover, larger velocities could not be investigated because of experimental limitations. At $\omega > 70\ rad/s$, the center of the mixing bar is outside the solvent, above the vortex extremity and concentration could no longer be measured.

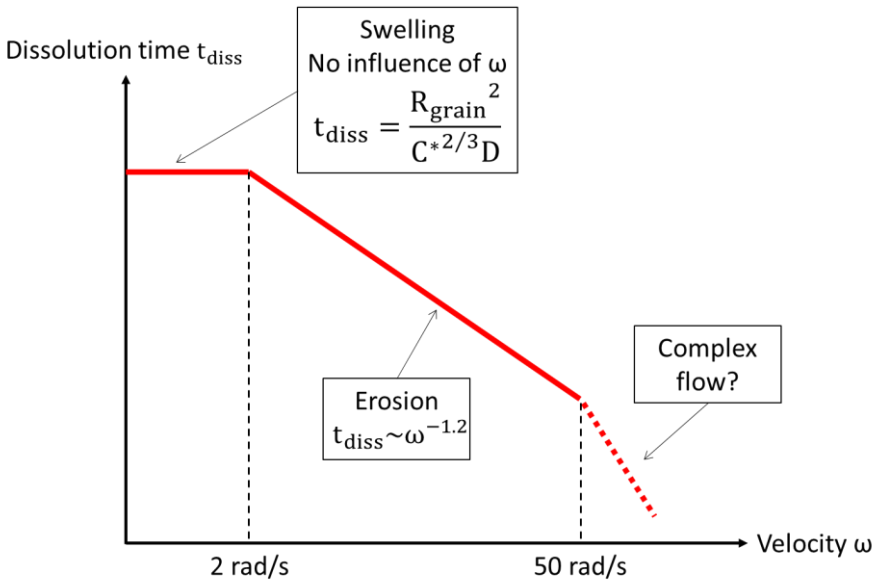

Figure 6-17: Different regimes in the dissolution time dependency with solvent velocity

6.3 Conclusion

Dissolution of GP powder is accelerated when a stirring is imposed to the GP/water mix. At intermediate stirring velocities ω, powder dissolution is controlled by the erosion of the gel phase. Erosion occurs at a given concentration c_{er} which varies with ω to the power of -0.6. As a consequence, the dissolution time varies as ω to the power of -1.2. A simple estimation gives a theoretical exponent of -0.9 which has still to be worked out.

The dissolution time also depends on the grain size, and more precisely on the grain size distribution. The dissolution time increases with the grain size but surprisingly the fastest dissolution rate is not obtained for small grains sieved fraction but for polydisperse samples composed of small and intermediate size grains. It appears that the presence of larger grains tends to prevent lump formation and thus decrease the dissolution time. This is likely due to the high flowability of polydisperse powders which leads to the formation of smaller lumps.

Finally, ionic strength of the solvent also influences the dissolution time ($t_{1/2} \sim I^{1/3}$). The dissolution time can be plotted as a function of the diffusion coefficient of the gel at the corresponding ionic strength. The following law is observed: $t_{1/2} \sim D^{-1.3}$. The exponent of this power law is not understood yet.

7 Conclusion

In this study, we have investigated the mechanisms at stake during the dissolution of GP, a high molar mass, hydrosoluble and charged polysaccharide used to control the rheology of oilfield fluids. Maltodextrins and polyethylene oxides of different molar masses have also been studied to decouple the molar mass effects and the charge effects on the dissolution kinetics.

Wetting by water droplets of layers of giant polyelectrolyte evidenced a hydrophobic behavior with high contact angles at early stage of contact between droplet and substrate. The contact angle was found to depend both on the hydration of the polymer and on the roughness of the surface, varying with the polymer layer thickness and the contact line velocity. Hydration sets the substrate interfacial energy, which drives the spreading, but also the dissipation in the substrate at the contact line, which slows down the spreading. Droplet spreading is stopped by pinning of the contact line due to surface roughness and more importantly to the formation of a viscoelastic gel. This gel is observed for a polymer in solvent concentration that is as low as the polymer molar mass is high and the overlap concentration is low.
Altogether, no capillary imbibition inside the powder beds is possible due to the pinning of the contact lines. Moreover, the onset of the gel phase clogs the pores between polymer grains, preventing further capillary imbibition of the powder. As a result, grains stay stuck together, forming aggregates that are very long lasting. This is why dispersing properly the GP grains in water is critical to minimize lumps formation and ensure a fast dissolution.

Once water is in contact with a polymer grain, three phases arise. First, the water penetrates in the glassy polymer. Then once the glass transition is undergone, water penetrates in a gel phase. Lastly, the overlap concentration is reached, or the gel is diluted enough to be eroded by the water flux. We show that dissolution of the gel phase is the limiting step in the grain dissolution process. Indeed, water diffusion in a glassy polymer is expected to be much slower than in a polymer gel but the nanoscopic porosity inside the polymer grains creates channels. They are rapidly filled by gel swelling but this allows water to diffuse inside the glassy core through the gel channels at the same rate as in the gel. Glassy polymer to gel transition is thus not limiting in the global dissolution process.

Secondly, we concentrated our efforts towards understanding the mechanisms controlling the dissolution of the gel, namely the transfer of polymer chains from the gel phase into the polymer solution.
Contrary to what is claimed in literature, reptation of the polymer chains was found to play no role in the gel swelling or dissolution. Indeed, we suggest that the topological limitation to gel swelling is likely to result from chains contraction in their tubes. This phenomenon is extremely fast, even for GP, and thus it is not a limiting step. Gel swelling is shown to be a cooperative phenomenon due to osmotic pressure inside the gel, described by a cooperative diffusion coefficient D. Qualitatively, D is found to vary with the polymer concentration, although no quantitative measurements could be obtained. It is

likely that D decreases with the concentration in the concentration range investigated. A theoretical model is derived to account for the swelling of a polyelectrolyte by water due to osmotic driven mechanism. The swelling is controlled by water penetration inside the polymer gel network.
Lastly, we demonstrate that the swelling of the polymer gel through the diffusive process described above stops when the polymer concentration decreases down to below the overlap concentration c*. Below this concentration, the solution viscosity is so small that any tiny convection is able to disperse the polymer.

However, using a mixing device to force convection allows to disperse the gel at a concentration larger than c*. To evidence that, powder dissolution experiments were performed on a home-made rheology set-up.
At small mixing velocities, powder dissolution is still controlled by the overlap concentration c* and the grain size, as determined in the gel dissolution experiments without convection. The mixing velocity ω has thus no influence on the dissolution time.
At intermediate velocities ω, the dissolution time decreases with ω. We evidence that applying a shear stress to the gel/solution interface allows for the erosion of the gel layer. Entangled polymer chains flow in the solution under the eroding effect of the shear stress. It corresponds to an increase of the concentration at the gel/solution interface. Quantitatively, we find that the polymer concentration at the gel/solution interface c_{er} varies with the shear rate according to $\dot{\gamma}^{0.6}$, yielding a decrease of the powder dissolution time t_{diss} with mixing velocity ω varing as $t_{diss} \sim \omega^{-1.2}$. A simple model is derived to reconcile our measurements of the concentration at the gel interface with the powder dissolution time upon mixing.

To conclude, we have shown that the two limiting factors for GP powder dissolution are, first, the poor wetting properties that require at least a good dispersion of the powder in water and likely a surface treatment of the grains, and, second, the swelling of the semi-dilute gel phase which is extremely sensitive to the ionic strength of the solution and can only be accelerated by stirring.

8 Annex: Rheological behavior of a polymer solution

γ is the shear strain and σ is the shear stress.
A perfectly elastic solid follows Hook's law $\sigma = G\gamma$ where G is the shear modulus of the material.
A simple fluid follows Newton's law $\sigma = \eta\dot{\gamma}$ where η is the viscosity of the material.
Soft matter such as polymer solutions has intermediate behavior between Hookean solids and Newtonian liquids called **viscoelastic behavior**. It can be described simply by the **Maxwell model** which combines a perfectly elastic element of modulus G_M with a perfectly viscous element of viscosity η_M in series. In this model, the two elements strains are summed:

$$\dot{\gamma} = \frac{\dot{\sigma}}{G_M} + \frac{\sigma}{\eta_M}$$

Considering a step strain of magnitude γ_0, the stress relaxation modulus G(t) is define as

$$G(t) = \frac{\sigma(t)}{\gamma_0}$$

In the Maxwell model,

$$G(t) = G_M e^{-t/\tau_M}$$

where $\tau_M = \frac{\eta_M}{G_M}$ is the **relaxation time**.

Considering an oscillatory shear $\gamma(t) = \gamma_0 \sin(\omega t)$, the linear response of a viscoelastic material is

$$\sigma(t) = \sigma_0 \sin(\omega t + \delta) = \gamma_0[G'(\omega)\sin(\omega t) + G''(\omega)\cos(\omega t)]$$

G' is the **storage modulus** and G'' is the **loss modulus**.
In the Maxwell model,

$$G' = G_M \frac{\omega^2 {\tau_M}^2}{1 + \omega^2 {\tau_M}^2}$$
$$G'' = G_M \frac{\omega \tau_M}{1 + \omega^2 {\tau_M}^2}$$

When $G'(\omega) = G''(\omega)$, $\omega = {}^1/_{\tau_M}$.
The complex modulus G* is defined as

$$G^*(\omega) = G'(\omega) + iG''(\omega)$$
$$\sigma^*(t) = G^*(\omega)\,\gamma^*(t)$$

The complex viscosity η* is defined as

$$\sigma^*(t) = \eta^*(\omega)\,\dot{\gamma}^*(t)$$

So

$$\eta^*(\omega) = \frac{G^*(\omega)}{i\omega}$$
$$|\eta^*(\omega)| = \frac{\sqrt{G'^2 + G''^2}}{\omega} = \frac{\eta_M}{(1 + \omega^2 {\tau_M}^2)^{1/2}}$$

$\eta(\dot{\gamma})$ is the polymer solution viscosity measured under continuous shear.

The **Cox and Merz rule** is an empirical law linking the viscosity measured under continuous shear and the complex viscosity of the polymer solution. It works well for many polymers and especially for polymer melts in the linear regime.

$$\eta(\dot{\gamma}) = |\eta^*(\omega)|_{\omega=\dot{\gamma}}$$

So

$$\eta(\dot{\gamma}) = \frac{\eta_M}{(1+\dot{\gamma}^2{\tau_M}^2)^{1/2}}$$

This law corresponds to a shear-thinning behavior with η_M being the Newtonian plateau viscosity and viscosity decrease beginning for $\dot{\gamma} = {}^1/_{\tau_M}$.

Intuitively, the **reptation time** corresponds to the polymer network "life time" which is the relaxation time in Maxwell model. Therefore it can be measured thanks to modulus oscillatory measurements as the reciprocal of the frequency at which the storage modulus and the loss modulus are equal.

$$\boldsymbol{\tau_{rep} = \tau_M}$$

For $t>\tau_{rep}$, G'<G''. The polymer has a liquid-like behavior. For $t<\tau_{rep}$, G'>G''. The polymer has a solid-like behavior.

If Cox and Merz rule is relevant, reptation time can also by measured thanks to viscosity measurements under continuous shear as the inverse of the shear rate at which viscosity begins to decrease.

At high frequencies G' reaches a plateau. For polymers with molar masses far above the critical entanglement mass like GP, the apparition of this plateau is described in literature by Doi-Edwards model for semi-dilute polymer solutions.

According to Doi-Edwards model, the value for the storage modulus at the plateau G'_p is related to the polymer fraction in the solution by a power law:

$$G'_p \sim \varphi^{9/4}$$

The reptation time dependency with the concentration is

$$\tau_c \sim \varphi^{3/2}$$

Bibliography

1. Dominique Guillot & Erik B. Nelson. *Well Cementing*.

2. Edwards, S. F. The theory of polymer solutions at intermediate concentration. *Proc. Phys. Soc.* **88,** 265–280 (1966).

3. De Gennes. *Scaling concept in polymer physics*. (1979).

4. Rubinstein, M. & Colby, R. H. *Polymer physics*. (Oxford University Press, 2003).

5. De Gennes, P. G. Dynamics of Entangled Polymer Solutions. I. The Rouse Model. *Macromolecules* **9,** 587–593 (1976).

6. Graessley, W. Polymer chain dimensions and the dependence of viscoelastic properties on concentration, molecular weight and solvent power. *Polymer* **21,** 258–262 (1980).

7. Colby, R. H. Structure and linear viscoelasticity of flexible polymer solutions: comparison of polyelectrolyte and neutral polymer solutions. *Rheol. Acta* **49,** 425–442 (2010).

8. Manning, G. S. Limiting laws and counterion condensation in polyelectrolyte solutions. *Biophys. Chem.* **9,** 65–70 (1978).

9. Manning, G. S. Limiting Laws and Counterion Condensation in Polyelectrolyte Solutions I. Colligative Properties. *J. Chem. Phys.* **51,** 924 (1969).

10. De Gennes, P. G., Pincus, P., Velasco, R. M. & Brochard, F. Remarks on polyelectrolyte conformation. *J. Phys.* **37,** 1461–1473 (1976).

11. Dobrynin, A. V., Colby, R. H. & Rubinstein, M. Scaling Theory of Polyelectrolyte Solutions. *Macromolecules* **28,** 1859–1871 (1995).

12. Thomas Young. An Essay on the Cohesion of Fluids. *Philosophical Transactions of the Royal Society of London* 95:65–87 (1805).

13. Voinov, O. V. Hydrodynamics of wetting. *Fluid Dyn.* **11,** 714–721 (1977).

14. Cox, R. G. The dynamics of the spreading of liquids on a solid surface. Part 1. Viscous flow. *J. Fluid Mech.* **168,** 169 (1986).

15. Shanahan, M. E. R. & Carre, A. Viscoelastic Dissipation in Wetting and Adhesion Phenomena. *Langmuir* **11,** 1396–1402 (1995).

16. Carré, A. & Shanahan, M. E. R. Viscoelastic Braking of a Running Drop. *Langmuir* **17,** 2982–2985 (2001).

17. Halperin, A. & de Gennes, P. G. Wetting of polymer covered surfaces. *J. Phys.* **47,** 1243–1247 (1986).

18. Holly, F. J. & Refojo, M. F. Wettability of hydrogels I. Poly(2-hydroxyethyl methacrylate). *J. Biomed. Mater. Res.* **9,** 315–326 (1975).

19. Monteux, C., Tay, A., Narita, T., De Wilde, Y. & Lequeux, F. The role of hydration in the wetting of a soluble polymer. *Soft Matter* **5,** 3713 (2009).

20. Tay, A., Bendejacq, D., Monteux, C. & Lequeux, F. How does water wet a hydrosoluble substrate? *Soft Matter* **7,** 6953 (2011).

21. Tay, A., Monteux, C., Bendejacq, D. & Lequeux, F. How a coating is hydrated ahead of the advancing contact line of a volatile solvent droplet. *Eur. Phys. J. E* **33,** 203–210 (2010).

22. Dupas, J. *et al.* DIFFUSION AND EVAPORATION CONTROL THE SPREADING OF VOLATILE DROPLETS ONTO SOLUBLE FILMS. *Interfacial Phenom. Heat Transf.* **1,** 231–243 (2013).

23. Dupas, J. *et al.* Glass Transition Accelerates the Spreading of Polar Solvents on a Soluble Polymer. *Phys. Rev. Lett.* **112,** (2014).

24. Dupas. PhD thesis: Wetting of solubles polymers. (2012).

25. *Contact Angle, Wettability, and Adhesion*. **43,** (AMERICAN CHEMICAL SOCIETY, 1964).

26. Wenzel, R. N. RESISTANCE OF SOLID SURFACES TO WETTING BY WATER. *Ind. Eng. Chem.* **28,** 988–994 (1936).

27. Cassie, A. B. D. & Baxter, S. Wettability of porous surfaces. *Trans. Faraday Soc.* **40,** 546 (1944).

28. Papadopoulos, P. *et al.* Wetting on the Microscale: Shape of a Liquid Drop on a Microstructured Surface at Different Length Scales. *Langmuir* **28,** 8392–8398 (2012).

29. Hogekamp, S. & Schubert, H. Rehydration of Food Powders. *Food Sci. Technol. Int.* **9,** 223–235 (2003).

30. Forny, L., Marabi, A. & Palzer, S. Wetting, disintegration and dissolution of agglomerated water soluble powders. *Powder Technol.* **206,** 72–78 (2011).

31. Kravtchenko, T. P., Renoir, J., Parker, A. & Brigand, G. A novel method for determining the dissolution kinetics of hydrocolloid powders. *Food Hydrocoll.* **13,** 219–225 (1999).

32. Parker, A., Vigouroux, F. & Reed, W. F. Dissolution kinetics of polymer powders. *AIChE J.* **46,** 1290–1299 (2000).

33. Wang, Q., Ellis, P. R. & Ross-Murphy, S. B. Dissolution kinetics of guar gum powders. I. Methods for commercial polydisperse samples. *Carbohydr. Polym.* **49,** 131–137 (2002).

34. Wang, Q., Ellis, P. . & Ross-Murphy, S. . Dissolution kinetics of guar gum powders—II. Effects of concentration and molecular weight. *Carbohydr. Polym.* **53,** 75–83 (2003).

35. Wang, Q., Ellis, P. R. & Ross-Murphy, S. B. Dissolution kinetics of guar gum powders—III. Effect of particle size. *Carbohydr. Polym.* **64,** 239–246 (2006).

36. Mitchell, Hill, Bardon & Matthews. Measurement of Hydration of Polysaccharides. *Food Hydrocoll.* (1994).

37. Devotta, I., Ambeskar, V. D., Mandhare, A. B. & Mashelkar, R. A. The life time of a dissolving polymeric particle. *Chem. Eng. Sci.* **49,** 645–654 (1994).

38. Papanu, J. S. Dissolution of Thin Poly(methyl methacrylate) Films in Ketones, Binary Ketone/Alcohol Mixtures, and Hydroxy Ketones. *J. Electrochem. Soc.* **136,** 3077 (1989).

39. Pekcan, ö., Uĝur, ş & Yılmaz, Y. Real-time monitoring of swelling and dissolution of poly(methyl methacrylate) discs using fluorescence probes. *Polymer* **38,** 2183–2189 (1997).

40. Manjkow, J. Influence of Processing and Molecular Parameters on the Dissolution Rate of Poly-(Methyl Methacrylate) Thin Films. *J. Electrochem. Soc.* **134,** 2003 (1987).

41. Miller-Chou, B. A. & Koenig, J. L. A review of polymer dissolution. *Prog. Polym. Sci.* **28,** 1223–1270 (2003).

42. Brochard & De Gennes. Kinetics of polymer dissolution. *Physicochemical Hydrodynamics* (1983).

43. Devanand, K. & Selser, J. C. Asymptotic behavior and long-range interactions in aqueous solutions of poly(ethylene oxide). *Macromolecules* **24,** 5943–5947 (1991).

44. Banerjee, P. *et al.* Sorption of Water Vapor, Hydration, and Viscosity of Carboxymethylhydroxypropyl Guar, Diutan, and Xanthan Gums, and Their Molecular Association with and without Salts (NaCl, CaCl2, HCOOK, CH3COONa, (NH4)(2)SO4 and MgSO4) in Aqueous Solution. *Langmuir* **25,** 11647–11656 (2009).

45. Navarrete, R. C., Seheult, J. M. & Coffey, M. D. New Biopolymers for Drilling, Drill-In, Completions, Spacer, and Coil-Tubing Fluids, Part II. in (Society of Petroleum Engineers, 2001). doi:10.2118/64982-MS

46. Oswald, P. & Saint-Jean, M. *Rhéophysique: Ou comment coule la matière*. (Belin, 2005).

47. Hermes, H. E., Sitta, C. E., Schillinger, B., Löwen, H. & Egelhaaf, S. U. Kinks in experimental diffusion profiles of a dissolving semi-crystalline polymer explained by a concentration-dependent diffusion coefficient. *Phys Chem Chem Phys* **17,** 15781–15787 (2015).

48. Aussillous, P. & Quéré, D. Liquid marbles. *Nature* **411,** 924–927 (2001).

49. Aussillous, P. & Quéré, D. Properties of liquid marbles. *Proc. R. Soc. Math. Phys. Eng. Sci.* **462,** 973–999 (2006).

50. McEleney, P., Walker, G. M., Larmour, I. A. & Bell, S. E. J. Liquid marble formation using hydrophobic powders. *Chem. Eng. J.* **147,** 373–382 (2009).

51. Dupas, J. *et al.* Dynamic Wetting on a Thin Film of Soluble Polymer: Effects of Nonlinearities in the Sorption Isotherm. *Langmuir* **29,** 12572–12578 (2013).

52. Tay, A., Lequeux, F., Bendejacq, D. & Monteux, C. Wetting properties of charged and uncharged polymeric coatings—effect of the osmotic pressure at the contact line. *Soft Matter* **7,** 4715 (2011).

53. Kajiya, T. *et al.* Advancing liquid contact line on visco-elastic gel substrates: stick-slip vs. continuous motions. *Soft Matter* **9,** 454–461 (2013).

54. Mráček, A. The Measurement of Polymer Swelling Processes by an Interferometric Method and Evaluation of Diffusion Coefficients. *Int. J. Mol. Sci.* **11,** 532–543 (2010).

55. Crank, J. *The mathematics of diffusion*. (Clarendon Press, 1975).

56. Doi, M. & Edwards, S. F. *The theory of polymer dynamics*. (Clarendon Press, 2009).

57. Barri�re, B. & Leibler, L. Kinetics of solvent absorption and permeation through a highly swellable elastomeric network. *J. Polym. Sci. Part B Polym. Phys.* **41,** 166–182 (2003).

58. Cabane, B. & Hénon, S. *Liquides: solutions, dispersions, émulsions, gels*. (Belin, 2007).

Contacts

Pauline Valois
SIMM Laboratory
UMR 7615 CNRS/UPMC/ESPCI
10 rue Vauquelin, 75231 Paris Cedex 05
pauline.valois@gmail.com
01 40 79 52 09

François Lequeux
SIMM Laboratory
UMR 7615 CNRS/UPMC/ESPCI
10 rue Vauquelin, 75231 Paris Cedex 05
francois.lequeux@espci.fr
01 40 79 45 16

Laurence Talini
SIMM Laboratory
UMR 7615 CNRS/UPMC/ESPCI
10 rue Vauquelin, 75231 Paris Cedex 05
laurence.talini@espci.fr
01 40 79 46 79

Emilie Verneuil
SIMM Laboratory
UMR 7615 CNRS/UPMC/ESPCI
10 rue Vauquelin, 75231 Paris Cedex 05
emilie.verneuil@espci.fr
01 40 79 47 42

Jean-Philippe Caritey
Schlumberger SRPC
1 rue Henri Becquerel, 92140 Clamart, France
caritey1@slb.com
01 45 37 29 32

Résumé : Les polymères de grande masse molaire sont couramment utilisés comme viscosifiants par l'industrie pétrolière. Ils se présentent sous la forme d'une poudre qui doit être dissoute dans l'eau le plus rapidement possible avant d'être pompée à l'intérieur du puits. Cette étude porte sur la compréhension des mécanismes qui entrent en jeu lors de la dissolution de la poudre d'un polyélectrolyte appelé GP. Bien qu'étant solubles dans l'eau, les grains de GP présentent un comportement hydrophobe lorsqu'ils sont mis en contact avec l'eau et le mouillage est défavorable. Une couche de gel viscoélastique gonfle et bouche les pores entre les grains, provoquant la formation de grumeaux qui augmentent le temps de dissolution. Nous avons montré que c'est la cinétique de gonflement du gel qui contrôle la cinétique de dissolution du GP. Le gonflement de ce gel est un processus diffusif gouverné par la pression osmotique due à la présence des contre-ions du GP dans la solution. La reptation ne joue aucun rôle dans le désenchevêtrement des chaines, qui survient uniquement lorsque la concentration en polymère dans le gel devient inférieure à la concentration critique de recouvrement c* du GP. La disparition du gel peut cependant être accélérée en imposant une vitesse d'agitation dans le mélange eau/GP qui génère un cisaillement à l'interface gel/solution. La couche de gel est alors érodée lorsque la concentration en polymère dans le gel devient inférieure, non plus à c*, mais à c_{er}, la concentration critique d'érosion, supérieure à c* et qui augmente avec la vitesse de mélange ω. Nous avons montré que la cinétique de dissolution du GP est alors contrôlée par l'érosion de la couche de gel et que le temps de dissolution varie comme ω à la puissance -1.2.

Mots-clefs : polyélectrolytes de grande masse molaire, dissolution, gel, gonflement, érosion

Abstract: Polymers of large molar mass are often used as viscosifiers for complex fluids in the oil industry. The polymer powder must mix with water and totally dissolve as fast as possible before being pumped in the well. This study focuses on the understanding of the mechanisms at stake during the dissolution of a polyelectrolyte called GP. Even if they are hydrosoluble, GP grains exhibit a hydrophobic behavior when they are put in contact with water, which is responsible for a poor wetting. A viscoelastic gel layer forms and clogs the pores between GP grains, leading to the formation of lumps which increases the dissolution time. We demonstrate that the GP dissolution kinetics is controlled by the gel swelling kinetics. Gel swelling is a diffusive process governed by GP counter-ions osmotic pressure. Gel dissolution is not controlled by a reptation process but occurs when the polymer concentration inside the gel reaches c*, the overlap concentration of the GP. Dissolution is accelerated by stirring the polymer/water mix. The shear at the gel/solvent interface is responsible for the gel erosion. Erosion occurs when the polymer concentration inside the gel reaches the critical erosion concentration $c_{er} > c^*$, which increases with the mixing velocity ω. We demonstrate that GP dissolution kinetics is thus controlled by the erosion of the gel layer and that the dissolution time varies as ω to the power -1.2.

Keywords: high molar mass polyelectrolytes, dissolution, gel, swelling, erosion